CALIFORNIA INSTITUTE OF TECHNOLOGY

EARTHQUAKE ENGINEERING RESEARCH LABORATORY

INVESTIGATION OF EARTHQUAKE AND MICROTREMOR GROUND MOTIONS

BY

F. E. UDWADIA

EERL 72-02

A REPORT ON RESEARCH CONDUCTED UNDER A GRANT FROM THE NATIONAL SCIENCE FOUNDATION

PASADENA, CALIFORNIA

SEPTEMBER, 1972

INVESTIGATION OF EARTHQUAKE AND MICROTREMOR GROUND MOTIONS

Thesis by

Firdaus Erach Udwadia

In Partial Fulfillment of the Requirements

for the Degree of

Doctor of Philosophy

California Institute of Technology
Pasadena, California

1972

(Submitted May 24, 1972)

ACKNOWLEDGMENTS

The author wishes to thank Professor D. E. Hudson for his guidance, assistance and encouragement throughout the investigation and in the preparation of this report. The time and effort devoted by Dr. M. D. Trifunac in making the field measurements and in data analysis and interpretation is sincerely appreciated. Mr. R. Dielman rendered very valuable assistance with the field tests. The author is thankful for the interesting discussions and various suggestions given by Professors G. W. Housner, T. K. Caughey, P. C. Jennings and R. F. Scott.

The earthquake accelerograms are the fruits of a program of field recording of strong earthquake ground motion carried out by the Seismological Field Survey of the National Oceanic and Atmospheric Administration (formerly the U. S. Coast and Geodetic Survey). The digitized accelerograms came from the special program of the Earthquake Engineering Research Laboratory at the California Institute of Technology to produce standardized data, under the directorship of Dr. A. G. Brady. Thanks are expressed to Dr. K. Kanai of Nihon University for kindly making available his original microtremor data collected in 1960 at many sites in California.

The author is grateful for the teaching and research assistantships and tuition scholarships granted by the California Institute of Technology during the course of this work. Major support from the National Science Foundation as well as important contributions from the Earthquake Research Affiliates of the California Institute of Technology are greatly appreciated.

ABSTRACT

The nature of strong earthquake ground shaking has been investigated based on a study of 15 accelerograms recorded at El Centro in southern California. It is concluded that the characteristics of the source mechanism and the transmission path play a dominant role in determining the details of strong ground shaking at the site. No local site periodicities could be clearly identified, which suggests that source and transmission path effects overshadow the influence of local site conditions.

The method of using microtremor measurements to determine local site characteristics has been tested by direct comparison with strong motion measurements. Microtremor ground motions were recorded at five sites in the El Centro area and measurements were repeated at three of these sites after a period of 24 hours. These low amplitude ground motions have been found to be widely different from the motions caused by strong earthquake ground shaking. Their non-stationary nature over a period of a day or so makes the interpretation of such data from a single microtremor measurement very unreliable. It has been concluded that these microtremor ground motions are forced oscillations of the ground caused by nearby sources of excitation. The microtremor acceleration spectra do not indicate prominent peaks that could be correlated with local site conditions. At this site the use of microtremor measurements to define local subsoil conditions would evidently not be feasible.

TABLE OF CONTENTS

I. INTRODUCTION

For many years engineers have been studying the nature of structural damage caused by large earthquakes with a view to improving the criteria for the aseismic design of structures. Studies of the distribution of damage caused by earthquakes indicate that large differences in the extent of damage often occur over relatively short distances. In fact, as observed from some recent earthquakes [1] the areas of intense damage can be highly localized, the amount of damage drastically changing over distances as short as a half to one kilometer. Some of these large variations in structural damage can be attributed to local foundation problems, especially when the soil is "soft". Damage arising from foundation failures caused by settlement, liquefaction [2] or failure [3] of the soil, especially when the ground water level is high, have been known to occur. In addition, soft soils may cause differential settlements prior to the earthquake leaving a structure in a weakened condition. However, even in the absence of such foundation problems, the intensity of ground shaking has been observed to be widely varying over short distances. This rather spotty distribution of structural damage has led some investigators to believe that it is the local subsoil conditions that are of primary importance in the assessment of damage to structures. Though the concept of site amplification may be important in the study of structural damage under certain special conditions, its general applicability as the prime criterion for the design of structures in seismic zones has not been established.

Damage to engineering structures caused by earthquakes is known to depend on the nature of the arriving seismic energy as well as on the characteristics of structures. For the purposes of engineering design, the characteristics of ground shaking that are of primary importance to earthquake engineers are the amplitude, the frequency content and the duration of ground shaking. These characteristics are dependent on various elements such as the earthquake source mechanism, the orientation of the site with respect to the source, the material properties of the earth media along which the waves propagate, the nature and orientation of various geologic discontinuities and the local subsoil conditions. The complex nature of the earthquake source mechanism and the irregular nature of the surface layers and that of the structure of the earth's upper mantle make it difficult to elucidate their actual influence on local ground shaking. The focus of a potentially destructive earthquake is not a point source but is a fault plane whose dimensions may range from several kilometers to several hundred kilometers. Due to the fact that engineers are interested in strong ground motions relatively close to the fault zone, energy cannot be considered to be emanating from a point source. When slippage occurs along a fault plane, a portion of the energy is released in the form of elastic wave emissions and a portion as heat energy. The elastic waves arrive at a site by various paths through the geologic strata. The seismic energy generated at the source is composed of both dilatational (P-waves) and shear (S-waves) body waves. In addition to this there are waves created at the interfaces of the different strata

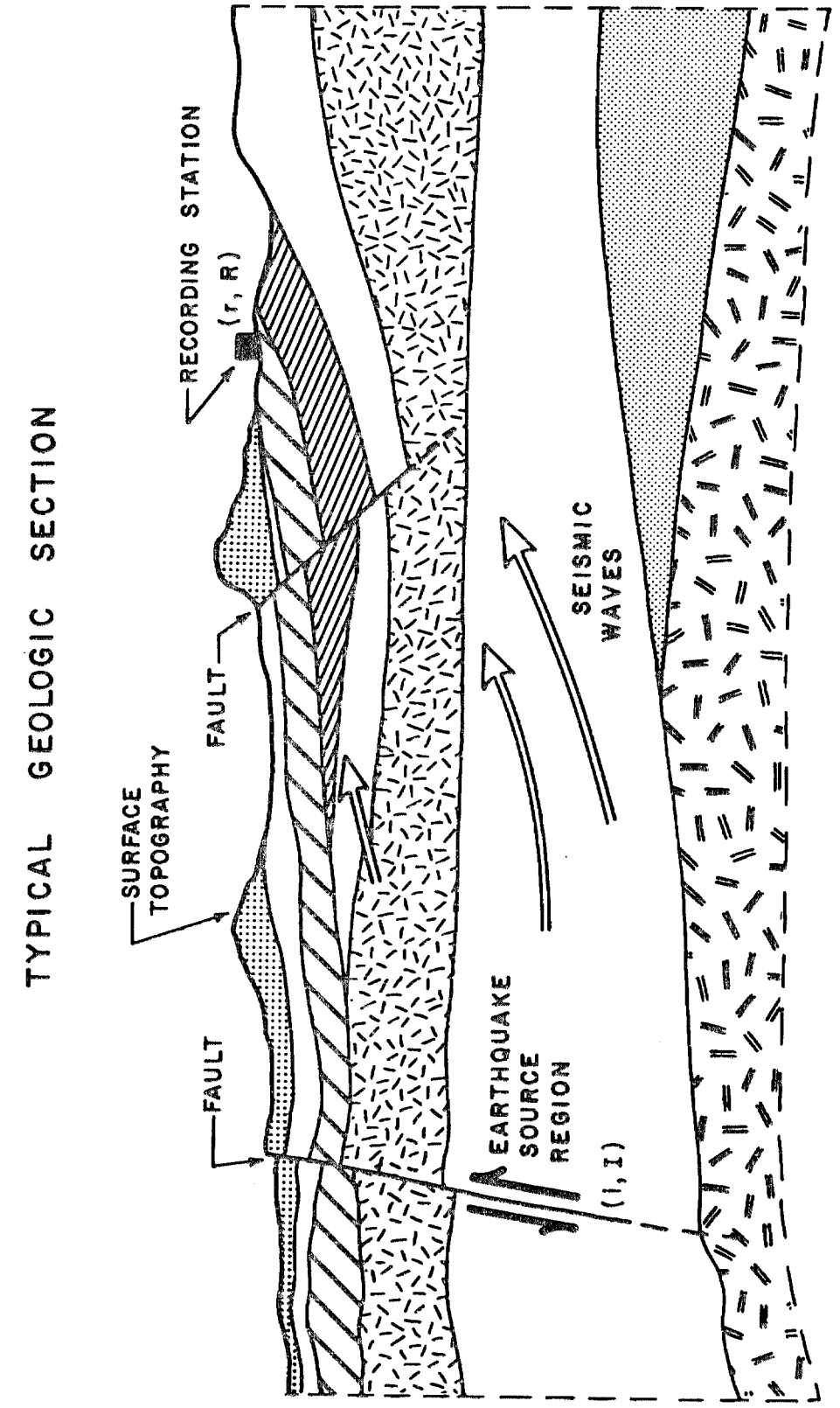
TYPICAL GEOLOGIC SECTION
RECORDING STATION
(r, R)
FAULT
SURFACE
TOPOGRAPHY
FAULT
SEISMIC
WAVES
EARTHQUAKE
SOURCE
REGION
(I, I)

FIGURE I. 1

and at the surface of the ground. The energy of such waves is concentrated near the ground surface or the particular interface. The relative contributions of these waves to the composite ground motion at a point is influenced by such factors as the focal depth, the epicentral distance of the site under consideration and the configuration of the surface layers. For shallow focus earthquakes, the nature of the surface layers may acquire added importance as a good portion of the energy gets trapped in them, these layers essentially acting as wave guides [4].

A simple schematic representation of the earthquake process is indicated in Figure I. 1. As seen from the figure, the nature of the recorded ground motions at a site are influenced by the nature of the energy released and by the modifications the seismic waves experience between source and receiver. Due to the lack of significant measurements obtained from strong ground shaking caused by close-in earthquakes and the complicated nature of the problem, very little is so far known about the effects on the ground motion at a site caused by factors such as source mechanism, epicentral distances, etc. We also note that local subsoil conditions form only a part of the total mechanism which modifies the seismic waves between source and receiver.

The large amount of interest in the study of the effects of local subsoil conditions has been principally due to two factors:

a) Local subsoil conditions can be obtained fairly simply with a reasonable degree of accuracy through seismic prospecting, boreholes, trenching, etc.; and

b) Simple modeling of soil conditions by parallel isotropic

homogeneous layers is easily amenable to theoretical study. Of course there may exist geologic sites that can be well represented by such a model which may modify the ground motions appreciably. However an application of such a simple theory to interpret strong earthquake ground motions might be insufficient in many instances. Sites with conditions that closely resemble the model composed of horizontal layers having strong velocity contrasts have been investigated in Japan [5] and some of the ground motions observed there have been satisfactorily interpreted through the concept of site amplification caused by vertically incident S waves. Site amplification studies were further encouraged when investigations of the motions of Mexico City during strong earthquakes indicated that the surface of the deep clay deposit there was oscillating essentially at the natural period of the layer as determined from a simple model [6]. However such simple models have at least two defects, namely, that in actuality it is unusual to have a parallel layering of homogeneous isotropic material, and that the study of close-in ground motions often necessitates the use of angles of incidence other than normal. In addition, waves other than body waves may play a dominant role in strong ground motion studies. [7].

Many investigators have studied the influence of local site conditions on the modification of seismic energy. Gutenberg [8] investigated small distant earthquakes with sensitive seismometers located on various thicknesses of alluvium and on bed rock. He concluded that large variations in ground shaking could occur under various site conditions. His data however indicated a wide variation in the

response at a given site caused by different earthquakes, suggesting that other variables should be considered in addition to local site conditions.

Byerly [9] examined data from a network of stations at different locations in California which had recorded small earthquakes. These low amplitude motions did not indicate the presence of any local site periodicities. Similar work done by Wiggins [10] indicates the lack of strongly prevalent "site periods".

Kanai and Sezawa [11] have studied the multiple reflection of S waves in layered media theoretically. They found that resonant oscillations of surface layers having uniform elastic properties can exist for steady harmonic wave inputs. In later studies they included the effects of soil viscosity. However, it may be noted that earthquake ground motions are transient excitations so that sharp amplification ratios at specific natural periods of the system may not appear during such shaking. As a check on their theoretical results [12], Kanai observed small vibrations from earthquakes in the basement and at the ground level of various buildings together with the nature of earthquake damage [13] to structures in Japan. By plotting the ratios of the maximum amplitudes in the basement of structures and at the ground surface, versus period, an attempt was made to correlate what was called "the predominant site frequencies" and the maximum amplitude ratios. In some cases clear correlations were obtained while in others more complex factors were evidently involved.

Later studies by Herrera, et al [14] extend the results of Kanai to the response of parallel homogeneous isotropic layers to random S wave excitation. Applications of the simplified model of a shear beam have been studied by Seed, et al [15] in order to compare theoretically computed and actually observed accelerograms from the San Francisco Earthquake of 1957. Past investigations of the horizontal layered vertical shear wave problem have recently been reviewed by Tsai and Housner [16].

The large amount of investigation into this field has led many engineers to believe that subsoil conditions must be of primary importance in the determination of the nature of ground shaking. If this is taken for granted, a simple method of determining these local site characteristics would appear to be a matter of considerable practical importance. It has been often suggested that these local site periods could be obtained economically and simply through the use of low amplitude ground motions called microtremors. A good deal of research effort has been devoted to their study in the hope that they might reveal "predominant site periods" thereby eliminating the need for seismic prospecting or more elaborate and time consuming methods of exploration.

In order to make quantitative studies of the extent to which local site conditions modify the nature of ground shaking, a region must be available where repeated measurements of strong ground shaking have been made. One such site is the El Centro strong motion accelerograph station in Imperial Valley, California, at which sixteen different close in events have been recorded since 1934.

The specific objectives of this thesis are (1) to study the set of strong motion accelerograms from El Centro in order to ascertain the extent to which common features possibly attributable to local subsoil conditions might exist, and, (2) to investigate the nature of micro-tremors so as to determine the amount of information they contain and to study the extent to which they resemble strong earthquake ground shaking.

II. EFFECTS OF GEOLOGIC CONDITIONS AND SURFACE TOPOGRAPHY ON STRONG EARTHQUAKE GROUND MOTIONS

II. 1 Introduction

The study of the effects of the transmission of energy from a seismic source to a receiving station can be looked at from the viewpoint of conventional systems analysis. The energy source causes an input to be fed into a 'black box' that represents the geologic formations and surface topography. The properties of this element will depend on the path taken by the waves through the transmitting medium between the recording station and the source. These waves then act as an input to the recording instrument whose response is obtained in the form of an analog trace. Depending on the nature of the instrument used, a trace that approximates ground acceleration, velocity or displacement can be obtained.

The nature of the input depends on the source mechanism that causes the energy release. A study of the actual nature of source mechanisms is extremely complex. Several idealized theories have been presented [17], [18] and [19]. All of them deal with rupture propagation in homogeneous isotropic media so that their validity in real life situations is limited. Broadly speaking, the nature of seismic energy generated is a function of the fault length, rupture velocity, the stress drop and the geometrical and temporal characteristics of the dislocation process. A more detailed discussion of the influence of some of these parameters on the nature of recorded ground motions,

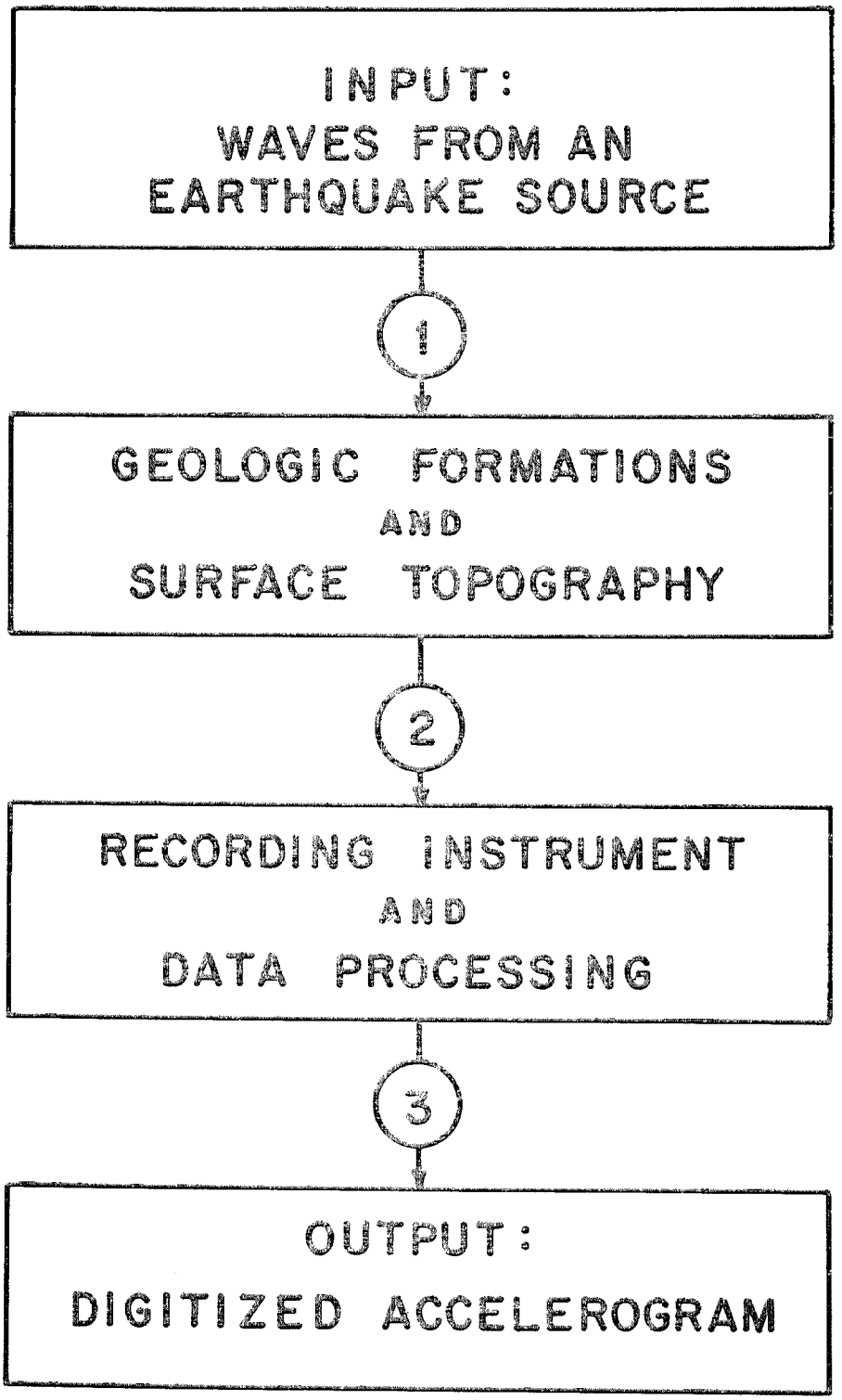
INPUT:
WAVES FROM AN
EARTHQUAKE SOURCE
1
GEOLOGIC FORMATIONS
AND
SURFACE TOPOGRAPHY
2
RECORDING INSTRUMENT
AND
DATA PROCESSING
3
OUTPUT:
DIGITIZED ACCELEROGRAM

FIGURE II. 1

as studied from some of the accelerograms considered in this thesis will be presented later. For the present purpose we shall simply replace the actual source by an element which generates elastic waves.

These waves travel through non-homogeneous, non-isotropic media and are reflected and refracted by the various geologic formations which they traverse on their way to the recording site. Though it is well known that the soil may behave nonlinearly when a sequence of stress pulses passes through it, as a first approximation, in order to get some physical insight into the problem, let us consider the black box representing the geologic formation to be a linear time invariant filter. This mode of looking at the problem makes available the whole body of mathematics related to linear operators for further analysis.

The most basic description of a linear time invariant system is through the unit impulse response function and the related convolution integral. If x(t) is the input time history and y(t) the result of the action of the linear system, the two are related through the equation

$$y(t) = \int_{-\infty}^{\infty} h(t)x(t-\tau)\, d\tau \qquad \text{(II. 1)}$$

where it has been assumed that $h(t) = 0$ for $t < 0$ and that it is the output of the system to a delta function input at $t = 0$.

Taking the Fourier transform on both sides of equation II. 1, we get

$$Y(\omega) = \overline{H}(\omega)X(\omega) \qquad \text{(II. 2)}$$

where $\overline{H}(\omega)$ is the transfer function of the element that modifies the input x(t) to give y(t).

The action of the physical systems comprising the geology and the surface topography can each be associated with a transfer function. The resultant transfer function $\overline{H}(\omega)$ can then be considered as a product of $H_1(\omega)$ and $H_2(\omega)$, $H_1(\omega)$ representing the effect of local geologic conditions and $H_2(\omega)$ the effect of surface topography. The recorded output can then be thought of as the application of the input i(t) through a succession of linear filters. Then,

$$O(\omega) = H_1(\omega)\, H_2(\omega)\, R(\omega)\, I(\omega)$$

$$= \overline{H}(\omega)\, I(\omega)$$

where $O(\omega)$ is the transform of the recorded output, $R(\omega)$ is the instrument response function and $I(\omega)$ is the transform of the source input.

A point to be noted here is that both $H_1(\omega)$ and $H_2(\omega)$ are not only dependent on the material properties of the transmitting media but also on spatial coordinates. Both $H_1(\omega)$ and $H_2(\omega)$ depend on the actual path of travel of the waves and are strongly influenced by the angle of incidence of these waves as they pass through various earth strata. Due to the large irregularities and anisotropic properties of the earth's crust, even this simplistic linear model is difficult to pursue. However, some idealized situations can be looked into in order to study the general effects of geologic formations and surface irregularities on the characteristics of ground motion.

II. 2 Effects of Interior Discontinuities on the Transfer Function $\overline{H}(\omega)$

The effects of interior discontinuities on the nature of ground motion has been studied by various investigators. Some of the basic work done in this field will be reviewed here, with a view to acquiring greater physical insight into some of the problems.

Figure II. 2(a) indicates a horizontally stratified geological profile having three layers each with shear and dilatational wave speeds β_n and α_n, and density ρ_n. Kanai [20] was among the first investigators to have studied the motion of such horizontally layered systems for vertically incident S waves. Later work carried out by Haskell [21] and Gupta [22] indicate that standing wave patterns can be set up for vertically propagating SH, SV and P waves in horizontally layered media. The idea of vertically propagating waves is well justifiable for earthquake focal zones which are distant from the recording site, in which case the P and S waves would come up almost vertically after refracting through media which becomes progressively softer towards the surface. Hence, such a model is useful for studies dealing with the effects of crustal layering on the recorded amplitudes of body waves. Earthquake engineers, on the other hand, are interested in strong motions generated close-by the epicenter. Here, the nature of ground motion is strongly influenced by such parameters as the depth of the focal region, its distance from the recording site and the size of dislocation surface. For a deep focus earthquake, the body waves will arrive almost at vertical incidence while for shallow and surface faulting most of the energy would arrive horizontally through the soft surface layers.

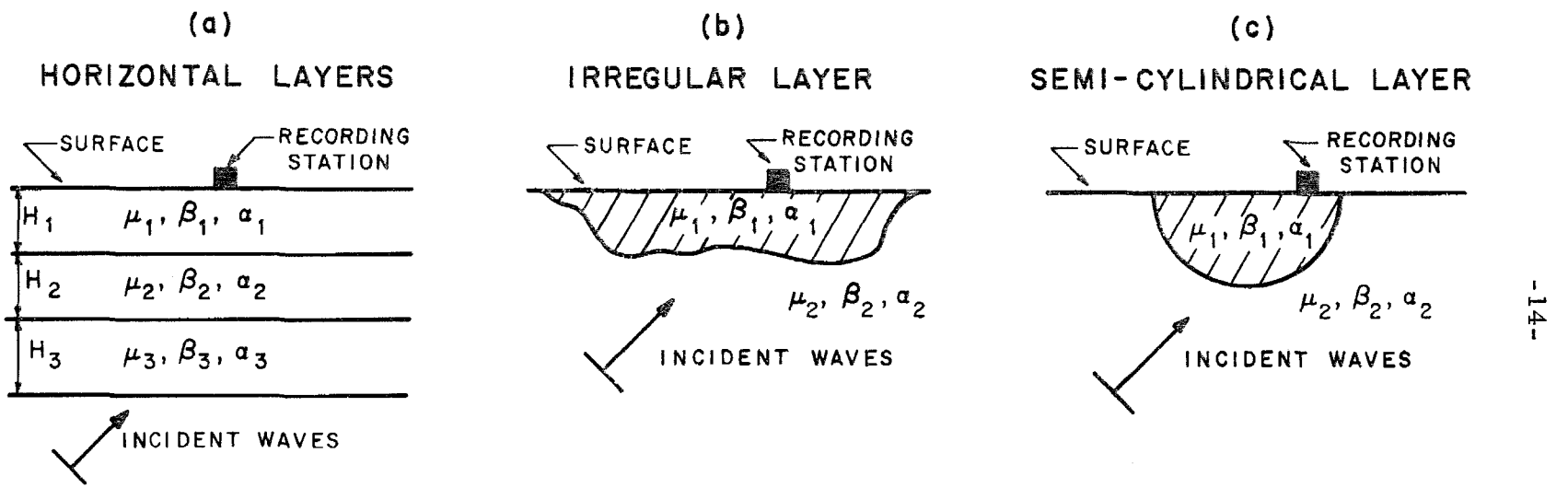
(a)
HORIZONTAL LAYERS
SURFACE
RECORDING STATION
H_1 μ_1, β_1, α_1
H_2 μ_2, β_2, α_2
H_3 μ_3, β_3, α_3
INCIDENT WAVES
(b)
IRREGULAR LAYER
SURFACE
RECORDING STATION
μ_1, β_1, α_1
μ_2, β_2, α_2
INCIDENT WAVES
(c)
SEMI-CYLINDRICAL LAYER
SURFACE
RECORDING STATION
μ_1, β_1, α_1
μ_2, β_2, α_2
INCIDENT WAVES

FIGURE II. 2

Among the first to realize that the angle of incidence of the arriving waves could drastically change the nature of ground motion were the Japanese investigators, Isikawa [23] and Suzuki [24]. They found that for shallow focus earthquakes, the angle of incidence of body waves at close to grazing incidence could be obtained. In the simple model of a soft layer resting on a semi-infinite half space, Haskell has also shown the dependence of the ground motion on the angle of incidence. For the study of close-in ground motions, then, it appears that the simplified model of vertically incident S waves may not be completely applicable in particular for shallow focus earthquakes. If the elastic energy originates in a surface layer which rests on another with higher impedance, a good portion of the energy is trapped in the layer, the layer essentially acting as a surface wave guide. The importance of these waves in surface wave guides becomes dominant due to their slow rate of decay in comparison to body waves. The dispersive Love and Rayleigh waves arriving at different times at a station are essentially responsible for the long duration of ground motions observed during some earthquakes.

These general qualitative ideas lead to the conclusion that even for the simplest idealized model of subsoil conditions at a site, the nature of earthquake ground motion may heavily depend on the depth of the focus, the distance of the recording station and the nature of the elastic energy generated at source.

The next step toward approaching a more realistic model, (Figure II.2 (b)), would be the inclusion of irregular interfaces at the

transition zone between layers and the two dimensional study of ground amplification. This problem has been examined by Aki and Larner [25]. With suitable restrictions on the nature of undulations of the boundary between the soft alluvial valley and the harder substratum, they study the nature of the ground amplifications of the surface. The nature of the ground motion is quite different from that predicted by the parallel layer model in that strong focusing effects can be observed. These effects are more prominent for high frequency waves which more readily diffract around the edges of the basin. We observe from their studies that short period, high frequency waves show a pronounced shadow zone at large angles of incidence.

Another example (Figure II. 2(c)) of the influence of geology on the nature of ground motion is the semi-cylindrical valley embedded in a half space. The closed form solution of this two dimensional problem obtained by Trifunac [26] shows complex wave interferences characterized by standing wave type patterns and rapid changes in ground amplification on the free surface of the valley. Again the angle of incidence and the frequency of excitation affect the nature of the ground motions heavily.

These three simple models qualitatively indicate that the nature of ground motions at a point can be strongly influenced by not only the geologic formation but also the angle of incidence of the incoming energy, the frequency content of the excitation, and the relative position of the site with respect to the energy source.

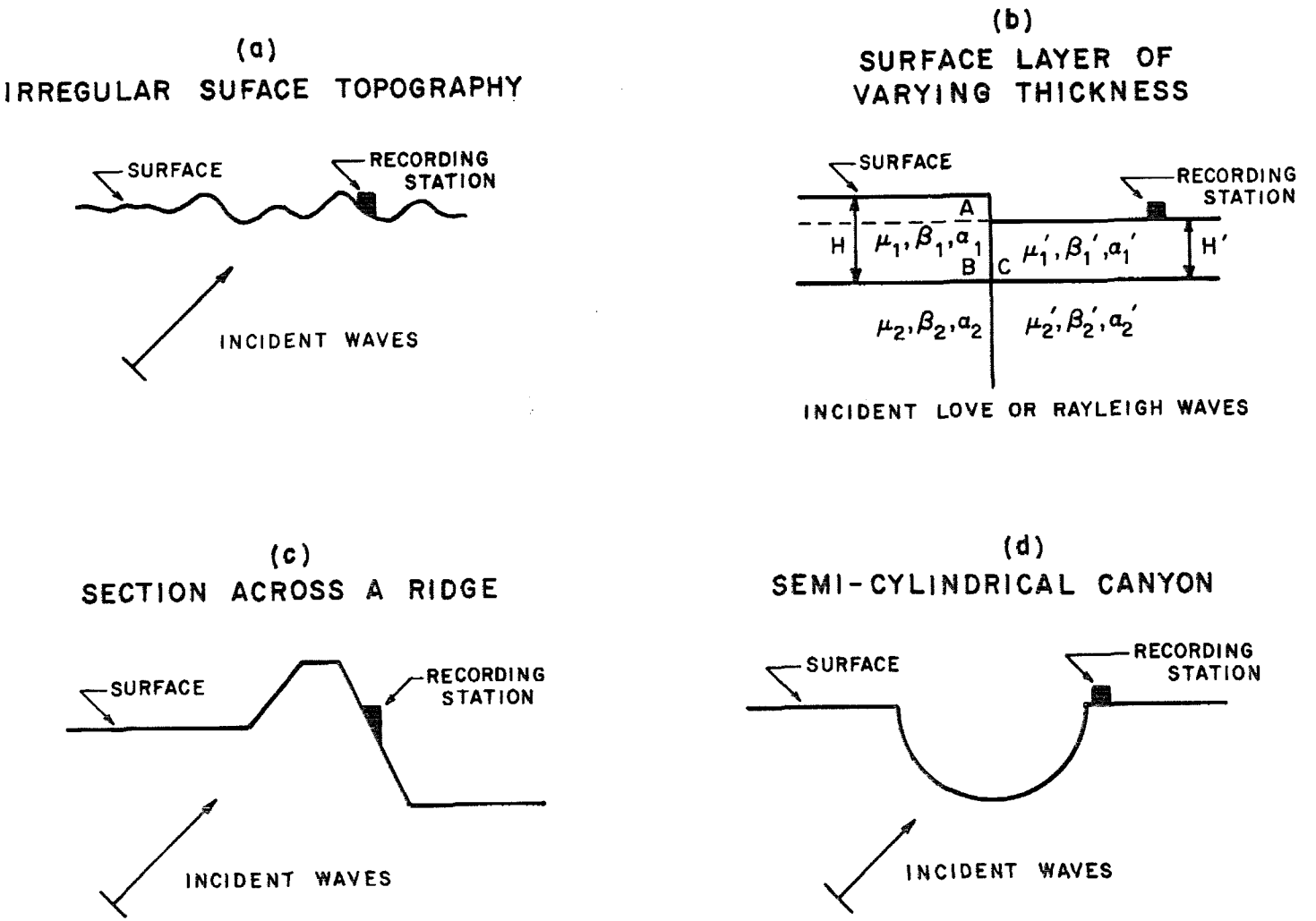
(a)
IRREGULAR SUFACE TOPOGRAPHY
SURFACE
RECORDING STATION
INCIDENT WAVES
(b)
SURFACE LAYER OF VARYING THICKNESS
SURFACE
RECORDING STATION
A
H
μ_1, β_1, α_1
B
C
$\mu_1', \beta_1', \alpha_1'$
H'
μ_2, β_2, α_2
$\mu_2', \beta_2', \alpha_2'$
INCIDENT LOVE OR RAYLEIGH WAVES
(c)
SECTION ACROSS A RIDGE
SURFACE
RECORDING STATION
INCIDENT WAVES
(d)
SEMI-CYLINDRICAL CANYON
SURFACE
RECORDING STATION
INCIDENT WAVES

FIGURE II. 3

II.3 Effect of Surface Topography on the Nature of $\overline{H}(\omega)$

The seismic waves on reaching the ground surface are scattered by surface irregularities. The nature of such scattering depends on the nature of the waves, the nature of the irregularities, the angle of incidence of the waves and their frequency content. The effect of surface topography may become more important for surface waves which travel close to the ground surface and thus feel the surface irregularities to a greater extent. Further, due to the low rate of attenuation of these surface wave amplitudes, the effect of surface topography may be important even at large distances from the focal zone.

Figure II.3 shows four examples of idealized surface conditions. Many investigators have studied these and similar problems. Abubakar [27] has worked on the reflections of SH waves from a harmonic boundary (Figure II.3(a)) by using a perturbation scheme assuming that the magnitude of the irregularities are small compared to the wavelengths of the incident waves. He finds from his approximate analysis that when the wavelength of the incident waves become comparable to that of the undulations, large scattering amplitudes are produced. The amplitudes and phases of the scattered field depend on the angle of incidence and the frequency content of the incident waves.

Another idealization of a surface irregularity is indicated in Figure II.3(b). Here a 'step' in the surface is illustrated. A complete analysis of the problem indicated is difficult. Sato [28] has worked with the nature of diffraction of plane SH waves when they hit a wedge.

From his analysis, one could study, though only qualitatively, the nature of transmission of small wavelength Love waves as they pass through a step discontinuity in a homogeneous isotropic medium, since such waves would have wave speeds close to the shear wave velocity of the medium, and hence, can be studied as small wavelength SH waves. The nature of surface ground motions for such a surface discontinuity can then be interpreted as follows. If the incident waves approach the transition zone from the thinner side, Sato's diffraction-around-a-corner studies show that the amplitudes of the diffracted waves appear only in Region B. In Region A, diffracted waves appear and may excite secondary Love wave characteristics for the thicker layer. The amplitudes of the diffracted waves decay inversely with the distance from the edge 0. Hence, one would suspect that the transmitted waves observed at points close to the transition zone would not be characteristic of the thicker layer but of the thinner layer. Reflected waves in Region C are not prominent because the diffracted waves that cause them are small in that region compared with those in other regions.

If, on the other hand, the incident Love wave energy arrives from the thicker side, a portion of it will be reflected in zone A and the edge 0 will cause large scattered fields in Region B. The energy of the waves contained in Region B is transferred to Region C. Hence, the transmitted wave characteristics of the thinner zone will be felt even at points close to the transition zone.

A further complication in the model could be introduced by placing a vertical line discontinuity at the transition zone. This

problem has been studied by Alsop [29]. He has considered the conversion of energy from one mode of Love waves to another, the vertical discontinuity bringing in this additional feature in a more pronounced way.

Figure II.3(d) shows a surface irregularity in the form of a cylindrical cavity. The two dimension problem of such a cylindrical cavity interacting with plane harmonic SH waves has been investigated by Trifunac [30]. For short period waves, and large angles of incidence, large shadow zones are involved. In the extreme case of high frequencies and grazing incidence, the cavity acts like a barrier reflecting a good portion of the energy and setting up almost stationary wave patterns. At smaller angles of incidence and small wavelengths compared to the radius of the cavity, the shadow zone is reduced in size, the motions becoming more and more symmetric about the center of the cavity as the angle of incidence is reduced.

Another simple form of a surface topography is indicated in Figure II.3(c) consisting of an inclined surface feature. The scattering caused by such surface topography is difficult to obtain for general types of wave motions. However finite difference schemes have been used to solve for the amplification ratios at different points along the irregularity for plane vertically ascending SH waves. The study done by Boore [31] indicates that such features may cause modifications in ground motion of the order of 75 - 100% when compared to ground motion in the absence of such a topography.

The effects of surface topography become more important for wavelengths which are comparable to a characteristic length of the

surface feature. For instance, assuming an S-wave velocity of 2 km/sec., we observe that surface features of the order of 200 m would influence local ground motions significantly for frequencies around 10 cps. Since the shorter wavelength motions are associated with higher frequency waves, which attenuate very rapidly with distance, the effects of such high frequency scattering by the surface features may become important in regions close by the focal zone. Though it is impossible to find out whether the effect of different surface topographies would be to amplify or deamplify the waves of a given frequency in any real life situation, one can estimate that the difference between the motions actually recorded and those that would have been recorded in the absence of topographic effects at the same site could be of the order of 25-30%.

III. ANALYSIS OF EL CENTRO ACCELEROGRAMS

III. 1 Introduction

As mentioned earlier, the large number of earthquakes that have been recorded at the El Centro standard strong motion accelerograph site makes this site unique for the study of strong ground motions created by earthquakes. A further advantage of this site is that the area has been reasonably well studied by geologists so that the subsoil conditions are relatively well known [32].

Sixteen strong motion records have been obtained at the U. S. C. G. S. station at El Centro. These records come from earthquakes whose assigned local magnitudes M_L range from 3 to 6.7, most of them being close-in to the recording station. These epicenters surrounding the strong motion site are mainly located on or near the major faults in the area as shown in Figure III. 1. Table I indicates their locations and assigned magnitudes. The code numbers in the table indicate the year in which the event occurred and the number of the event as catalogued by the Caltech library. The event numbers correspond to those indicated in Figure III. 1. The epicentral locations obtained independently by the seismological laboratory at Caltech [33] and by the U. S. C. G. S. [34] have been included. As seen from the table, most of the locations are in excellent agreement. These epicentral locations for most of the events can be assumed to be correct to within two to five kilometers of the exact locations [33].

TABLE 1

Event No.	Group No.	Code No.	Time	U.S.C.G.S. Location		C.I.T. Location		M_L	Δ-km*
				Latitude	Longitude	Latitude	Longitude		
1	III	34.2	Dec. 30, 1934	32°12'N	115°30'W	32°15'N	115°30'W	6.5	60
2	I	38.1	Apr. 12, 1938	32°53'N	115°35'W	32°53'N	115°35'W	3.0	16
3	—	38.3	June 5, 1938	32°15'N	115°10'W	32°54'N	115°13'W	5.0	35
4	III	38.4	June 6, 1938	32°15'N	115°10'W	32°15'N	115°10'W	4.0	71
5	III	40.1	May 18, 1940	32°44'N	115°27'W	32°46'N	115°29'W	6.5	15
6	II	42.1	Oct. 21, 1942	32°58'N	116°60'W	32°58'N	116°60'W	6.5	44
7	II	51.2	Jan. 23, 1951	33°07'N	115°34'W	32°59'N	115°44'W	5.6	25
8	II	53.1	Jan. 14, 1953	32°50'N	115°40'W	32°57'N	115°43'W	5.5	19
9	IV	54.5	Nov. 12, 1954	31°30'N	116°00'W	31°30'N	116°00'W	6.3	148
10	I	55.3	Dec. 16, 1955	33°00'N	115°30'W	33°00'N	115°30'W	4.3	27
11	I	55.4	Dec. 16, 1955	33°00'N	115°30'W	33°00'N	115°30'W	3.9	27
12	I	55.5	Dec. 16, 1955	33°00'N	115°30'W	33°00'N	115°30'W	5.5	27
13	IV	56.1	Feb. 9, 1956	31°45'N	115°55'W	31°45'N	115°55'W	6.8	119
14	IV	56.2	Feb. 9, 1956	31°45'N	115°55'W	31°45'N	115°55'W	6.1	119
15	III	66.9	Aug. 7, 1966	31°48'N	116°30'W	31°48'N	114°30'W	6.3	150
16	II	68.5	Apr. 8, 1968	33°12'N	116°06.9'W	31°58'N	116°49'W	6.4	72

*Distance from El Centro.

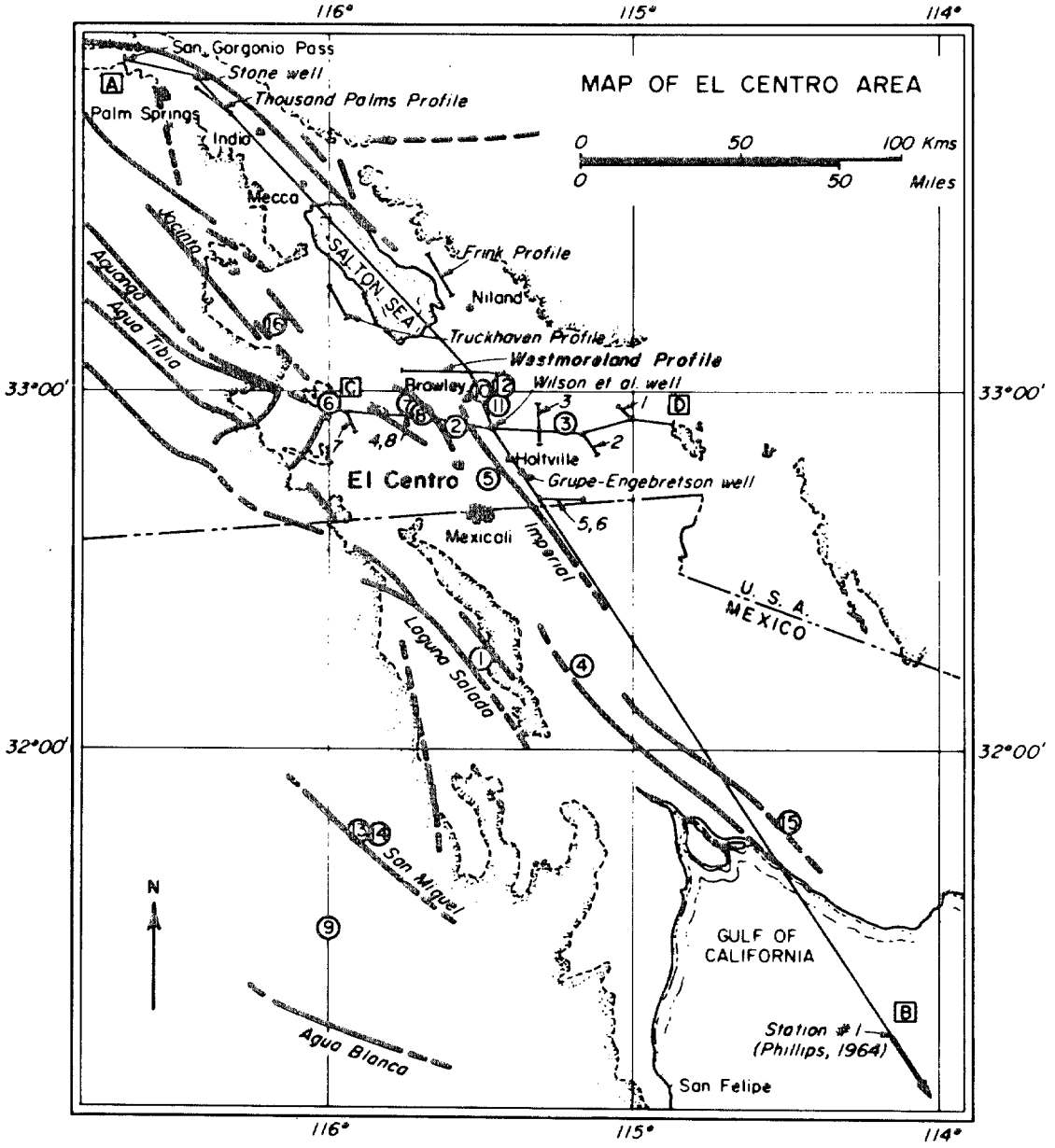
MAP OF EL CENTRO AREA
0 50 100 Kms
0 50 Miles
116°
115°
114°
33°00'
32°00'
San Gorgonio Pass
Stone well
Thousand Palms Profile
Palm Springs
Indio
Mecca
SALTON SEA
Frink Profile
Niland
Truckhaven Profile
Westmoreland Profile
Wilson et al well
Brawley
Holtville
Grupe-Engebretson well
El Centro
Mexicali
Imperial
Laguna Salada
San Miguel
Agua Blanca
Agua Tibia
Aguanga
U. S. A.
MEXICO
GULF OF CALIFORNIA
Station #1 (Phillips, 1964)
San Felipe
N

FIGURE III. 1

Since the installation of the strong motion instrument at El Centro in 1933, it has recorded numerous shocks. We shall outline here a brief history of the seismicity of the area since that time.

The first major earthquake recorded at the El Centro site was in 1934. Its epicenter was near the Laguna Salada fault, and was assigned a magnitude of 6.5. The next significant event was the Imperial Valley earthquake of 1940 (event 5, Figure III.1). It generated large ground accelerations, larger in magnitude than had been hitherto recorded. Due to the large amplitudes of motion and the long duration of strong ground shaking experienced at El Centro, this earthquake record has become of special interest to engineers. Its accelerogram (Figure III.6) has been used by many engineers for studies of earthquake resistant design. It is thus necessary to understand the significance of this accelerogram from two points of view. Firstly, to what extent does it represent a typical strong motion record obtained at a distance of about 15 km from the fault, and secondly, does it display some predominant characteristics which result from local site conditions? These and related questions on the general nature of earthquake processes represent the basic motivation for the study of these accelerograms, and will be discussed in the following sections dealing with their interpretations. The pattern of energy release during the Imperial Valley earthquake, its source mechanism and the nature of the recorded accelerograms for this event have already been studied in some detail [35].

Following the major activity in 1940, the seismicity of the Imperial Valley was low until 1950 when the activity resumed again

with two shocks of magnitude 5.4 [36]. A swarm of earthquakes of special interest in this investigation originated close to the town of Brawley on December 16-17, 1955 causing some minor damage. During this swarm, the El Centro accelerograph measured three shocks with magnitudes 4.3, 3.9 and 5.4 (events 10, 11 and 12 in Table I). These shocks have been assigned the same epicenter by both the Caltech and the U.S.C.G.S. networks. For these shocks both origin and receiving stations are the same, hence marked similarities in these records, if any, may tend to imply that the local station characteristics play an important role in strong ground shaking. These records also serve as a sample of close-in earthquake ground motions.

A similar swarm involving two distinct large events occurred later in 1956 (events 13 and 14, Table I). Both have been assigned the same epicenter. These two shocks differ from the group recorded in 1955 in their azimuthal orientation with respect to the recording station, their magnitude and their epicentral distances. Two later shocks, one in 1966 and one in 1968 have also been recorded, the 1968 event being the Borrego Mountain Earthquake.

Since the acceleration records have been obtained at the same point, having a particular set of local geologic conditions, from seismic waves arriving from different azimuths, it becomes possible to critically test various theories of ground amplification. The availability of such data has made it possible for the first time to investigate the relationships between ground motion on local geology so that the concept of local site characteristics based on simple models of vertically propagating shear waves can be tested from an engineering viewpoint.

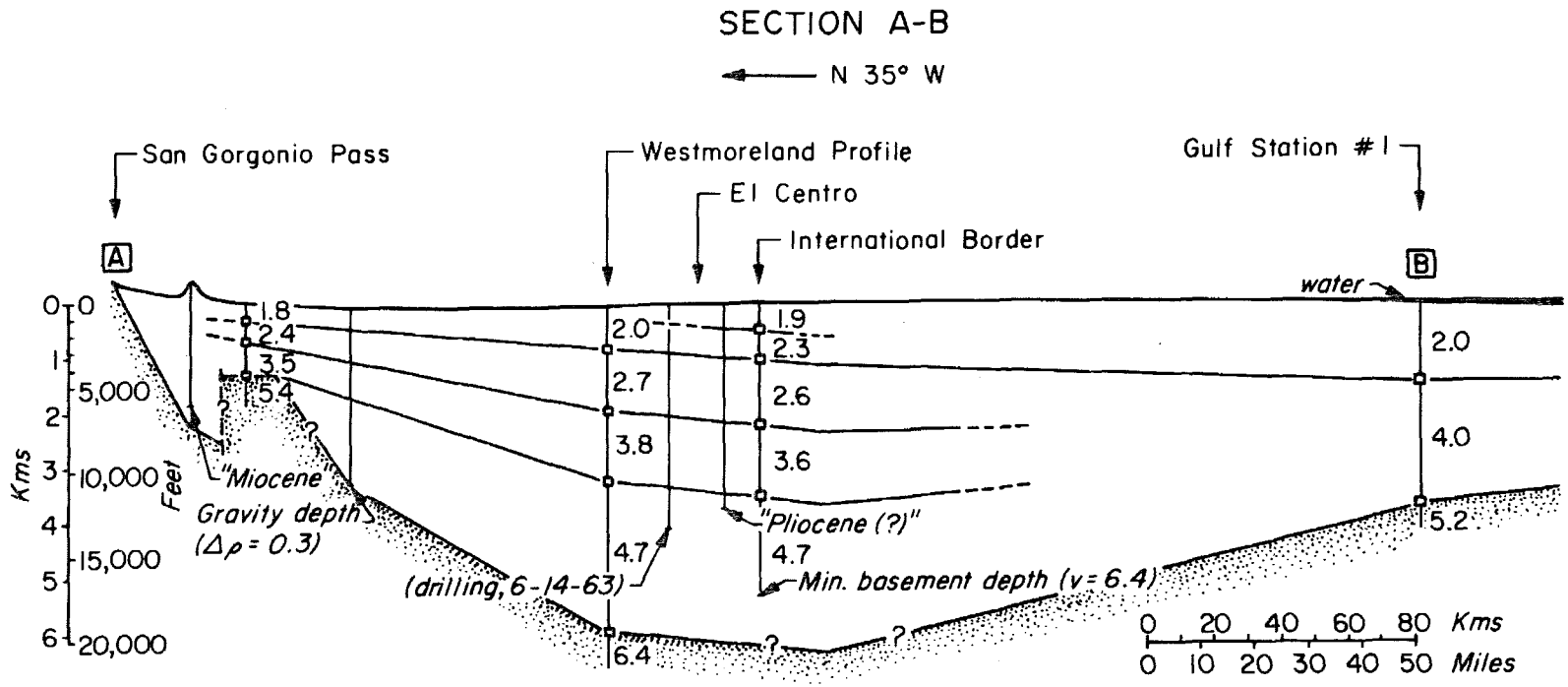

FIGURE III. 2 (After Biehler)

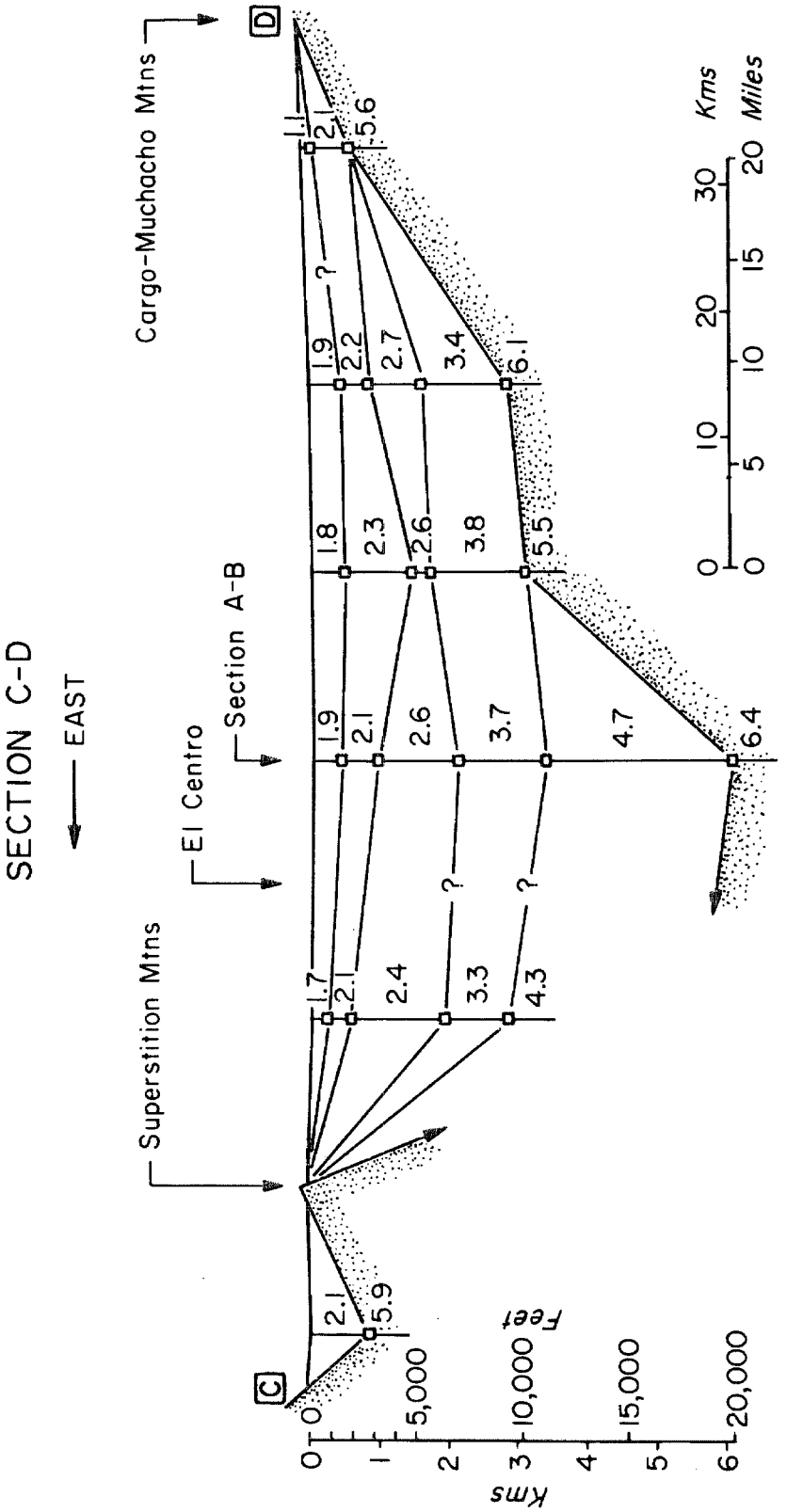

FIGURE III. 3 (After Biehler)

III. 2 Geology of the Imperial Valley

The Imperial Valley extends to the south of the Salton Sea (Figure III. 1) and is bounded by the Chocolate and Cargo Muchacho Mountains on the northeast, and by the Penninsular ranges of the southwest. Within the valley, along the southwest margin are several fault controlled hills of crystalline rock. The southeastern extent of the valley is poorly defined by mountains gradually decreasing in relief.

The valley is occupied by the sedimentary delta of the Colorado River filling a basin about 6 km deep (Figure III. 2 and III. 3). The sands, gravels, silts and clays of the delta appear to have been deposited primarily over the past four million years and in large parts consist of sediments eroded out of the Colorado plateau at the time of the cutting of the Grand Canyon and the uplift of the Kaibab Plateau [32].

As studied by Crowell [37], the predominant displacement along the faults cutting through the Imperial Valley is right lateral strike slip. The high velocity layer, having P-wave velocities in excess of 6. 4 km/sec (Figures III. 2 and III. 3), is interpreted as a basement complex composed of intrusive and metamorphic rocks [32]. The intermediate velocity layers (shear wave velocities between two and four kilometers/sec) are probably tertiary sediments having increasing velocity with increasing depth. The lower velocity layers are recent and have been classified as Pleistocene sediments [32].

III. 3 Grouping of Accelerograms

In order to study the dependence of ground motion on the azimuth of the epicenter with respect to the recording station, the different

events were divided into four distinct groups, each group containing events that have about the same epicentral azimuths with respect to the recording site (Table I). Group I consists of events that have azimuths roughly between N00E and N45E, Group II of events between N30W and N45W, Group III of events between S30E and S90E and Group IV of events between S00W and S30W. The first two groups which constitute earthquakes with epicenters north of El Centro have in general shorter epicentral distances than those on the south of the recording site. The record obtained at El Centro of Event 3 being very small, it has not been considered in our analysis.

A study of each group will now be taken up individually and the different groups will then be compared with each other.

III. 4 Processing of Accelerograms

The method used for processing the various accelerograms has been dealt with in detail in Appendix I. Problems such as the different sources and nature of "noise" in the data processing have also been considered. For the sake of completeness the data processing used will be briefly outlined here.

The earthquake records were obtained in the form of "uncorrected accelerograms" [38] from the Caltech earthquake library. These digital data are obtained by an optical digitization of the analog trace on the Benson-Lehner 099 digitizer. The digitization process introduces both high and low frequency [39], [40] errors in the data, which can be accounted for to some extent in the data processing. Since the data are used here in this thesis for the determination of the Fourier spectral

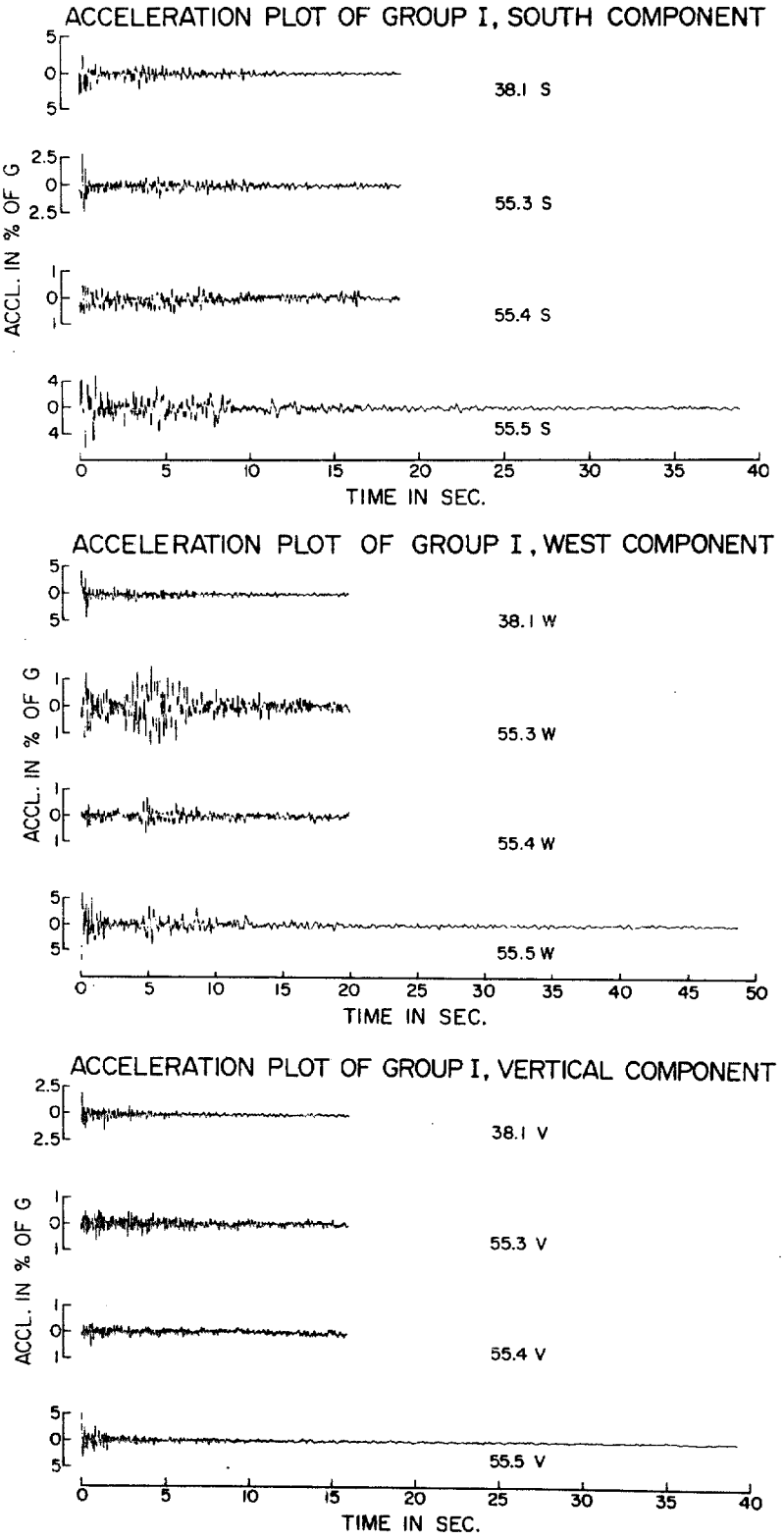
ACCELERATION PLOT OF GROUP I, SOUTH COMPONENT
38.1 S
55.3 S
55.4 S
55.5 S
ACCL. IN % OF G
TIME IN SEC.
ACCELERATION PLOT OF GROUP I, WEST COMPONENT
38.1 W
55.3 W
55.4 W
55.5 W
ACCL. IN % OF G
TIME IN SEC.
ACCELERATION PLOT OF GROUP I, VERTICAL COMPONENT
38.1 V
55.3 V
55.4 V
55.5 V
ACCL. IN % OF G
TIME IN SEC.

FIGURE III. 4

amplitudes, the usual procedure of "baseline correction" is not necessary (refer to Section B, Appendix I). Instead the data were reduced to have a mean of zero. The record was next considered as the output of a single degree of freedom oscillator of given period and damping, and the "true ground acceleration" was obtained using the standard instrument correction technique [40] (refer to Section B, Appendix I), after it was low pass filtered with a cutoff frequency of 25 cycles/sec. These accelerograms, that are now corrected for instrument response are shown in Figures III. 4, III. 5, III. 6 and III. 7.

III. 5 Interpretation of the Time Traces of Recorded Ground Motions

Group I. Accelerograms - (Events 2, 10, 11, 12)

This group consists of the three events 55. 3, 55. 4 and 55. 5 all of which have been assigned the same epicenter. Also included is event 38. 1, a smaller event that occurred at about half the distance from the recording station as the 1955 events (Figure III. 1).

The accelerograms of events 55. 3, 55. 4 and 55. 5 (Figure III.4) show some similarities particularly in the east-west components of ground motion, in that a predominant phase arrival about 4 sec after the instrument was triggered can be seen in all three records. This similarity in the phase arrivals together with the fact that all three events have the same epicenter indicates that the depths of the hypocenters for the three earthquakes may be quite similar. These depths are not determinable due to the lack of S-P times obtainable from the records. The phase arrival at about 4 sec is probably a surface wave,

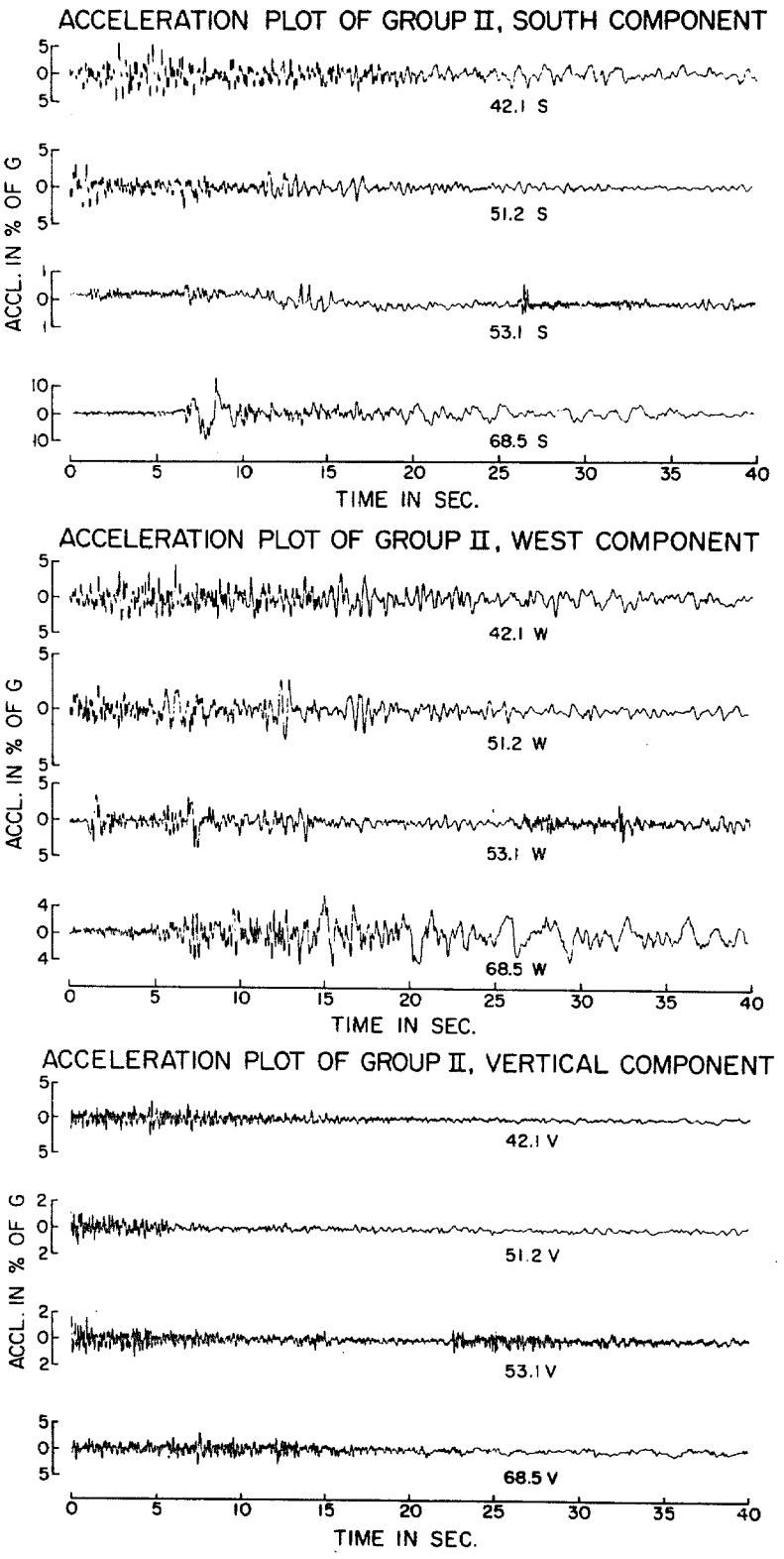
ACCELERATION PLOT OF GROUP II, SOUTH COMPONENT
42.1 S
51.2 S
53.1 S
68.5 S
ACCL. IN % OF G
TIME IN SEC.
ACCELERATION PLOT OF GROUP II, WEST COMPONENT
42.1 W
51.2 W
53.1 W
68.5 W
ACCL. IN % OF G
TIME IN SEC.
ACCELERATION PLOT OF GROUP II, VERTICAL COMPONENT
42.1 V
51.2 V
53.1 V
68.5 V
ACCL. IN % OF G
TIME IN SEC.

FIGURE III. 5

the beginning of each accelerogram being the latter portion of the S waves. These phase arrivals have been only approximately determined by considering the shear wave speeds and the dispersion curves [35] of the Westmoreland profile (Figure III. 1). Knowing the epicentral distances, the arrival time differences between the phases were computed. Despite the fact that the three events show similar phase arrivals, their frequency contents are quite different. The larger event (55. 5, $M_L = 5.5$) shows more long period components than the smaller ones. As seen from the horizontal and vertical component records the long period content in the accelerograms seems to increase for the larger events.

Event 38. 1, a much smaller earthquake compared to 55.5, shows prominent phase arrivals of surface waves despite the close location of the recording site to the epicenter. Similar features have been previously studied [7] for the aftershocks of the Imperial Valley Earthquake where surface waves were found to make an important contribution to the overall ground motion. The frequency content of this record seems to resemble more so that of the event 55. 5, in that it shows large contributions from long period components.

Group II Accelerograms -(Events 6, 7, 8, 16)

This group is composed of events 42. 1, 51. 2, 53. 1, and 68. 5 (Figure III. 5). The record of event 42. 1 indicates S wave arrivals at around 1 sec followed by higher surface modes, the fundamental Love and Rayleigh modes coming in at about 25 sec after the instrument was triggered. The long duration of strong shaking that is rich in both

high and low frequencies over a considerable time length (about 20 seconds) may indicate a large stress drop together with a long rupture length.

Event 53.1 is a multiple event showing S wave arrivals at about 2 sec and surface waves coming in between approximately 2 and 16 sec. Another event with a P wave arrival at 23 sec and an S wave arrival at about 26 sec is also indicated. Events 51.2 and 53.1 have almost the same epicenters. The various phase arrivals indeed do show some resemblances except for the fact that the instrument during event 51.2 seems to have started late. The beginning of this record shows probably the end of the S wave arrival, the higher frequency surface waves (corresponding to phase arrivals in event 53.1 at 6 - 7 sec) arriving at about 5-6 sec after the instrument was triggered followed by the fundamental surface waves between 10 and 16 sec.

Event 68.5 is a much more distant event than the previous three considered. We observe the S wave arrivals at about 6 - 7 sec followed by long period waves. These long periods probably consist of surface waves which appear to come in strongly 20 sec after the instrument was triggered.

In summary we observe from this group that the accelerograms from close-in large earthquakes (event 42.1) are rich in high and low frequencies over relatively large durations of time. The closeness of the recording site to the fault causes the different phases to be scrambled since the surface waves need some distance to properly establish themselves. The two events 51.2 and 53.1 though of about the

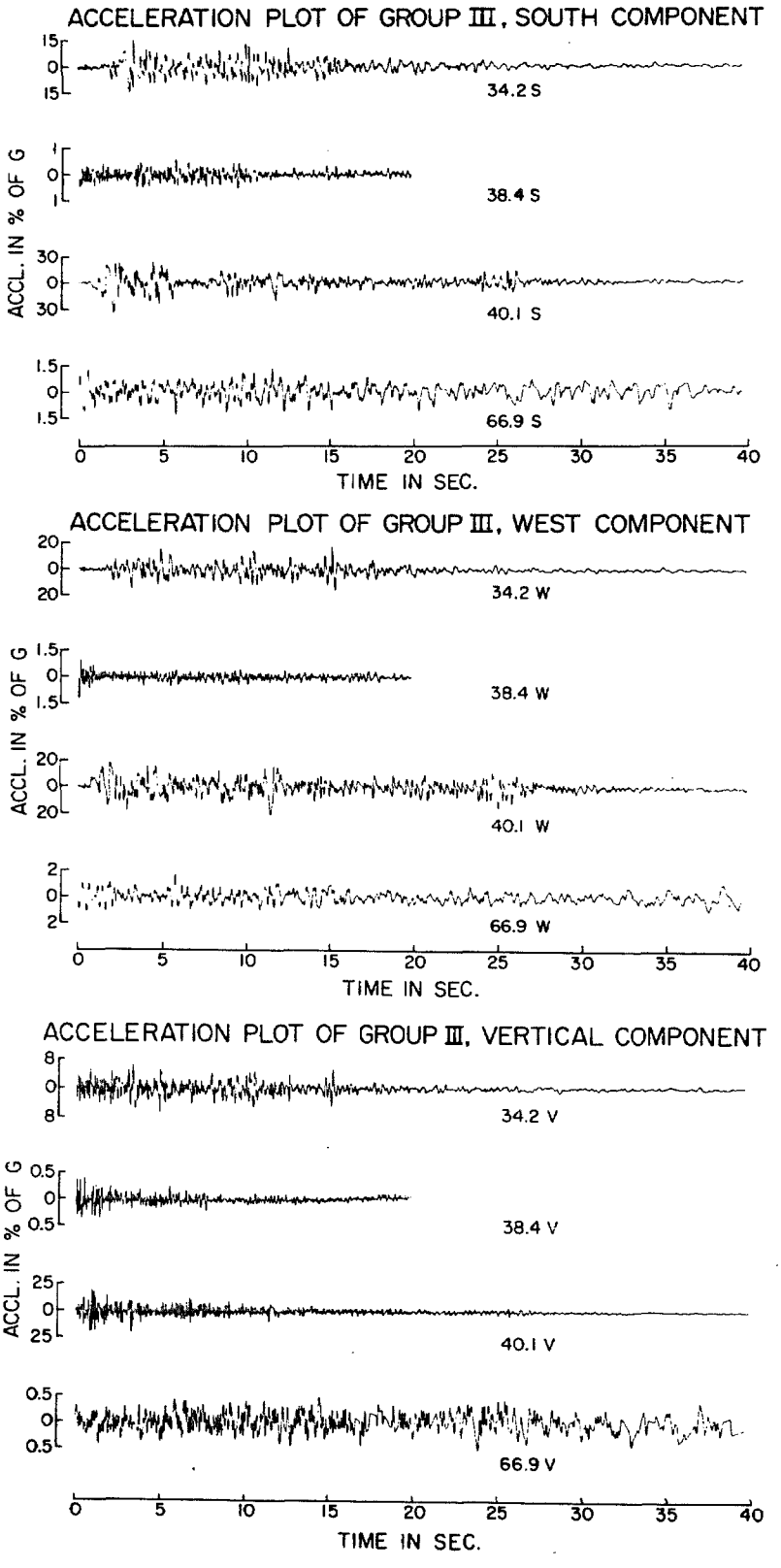
ACCELERATION PLOT OF GROUP III, SOUTH COMPONENT
34.2 S
38.4 S
40.1 S
66.9 S
ACCL. IN % OF G
TIME IN SEC.
ACCELERATION PLOT OF GROUP III, WEST COMPONENT
34.2 W
38.4 W
40.1 W
66.9 W
ACCL. IN % OF G
TIME IN SEC.
ACCELERATION PLOT OF GROUP III, VERTICAL COMPONENT
34.2 V
38.4 V
40.1 V
66.9 V
ACCL. IN % OF G
TIME IN SEC.

FIGURE III. 6

same magnitude ($M_L = 5.5, 5.6$), azimuths and epicentral distances show completely different natures of ground motion. One is a multiple event the other probably a single event. Events that occur far out from the recording site may (event 68.5) show larger relative contributions from surface waves their attenuation being less than that of body waves.

Group III Accelerograms - (Events 1, 5, 4, 15)

This group comprising events 34.2, 38.4, 40.1 and 66.9 includes the Imperial Valley Earthquake record (40.1). The accelerogram of this earthquake indicated that it is a multiple event. This record has been analyzed in some detail [35] earlier and the separate arrivals of S waves deciphered. Such multiple events would tend to have longer durations over which the ground motion is prevalent, as is clear from Figure III.6. Also one observes that such a record would show more high frequency components from the repeated impulses created by the successive P and S wave arrivals. This is more so brought out in the record of the vertical component of this event (Figure III.6).

The events of this group all consist of three large earthquakes (events 1, 5 and 15). Event 66.9 at an epicentral distance of 150 kms shows that the instrument was probably triggered by either the latter portion of the S waves or the larger amplitude surface waves that would be predominantly felt at such large distances. This record obtained at such a large distance reinforces the theory that surface waves might contribute significantly to the ground motions experienced at different

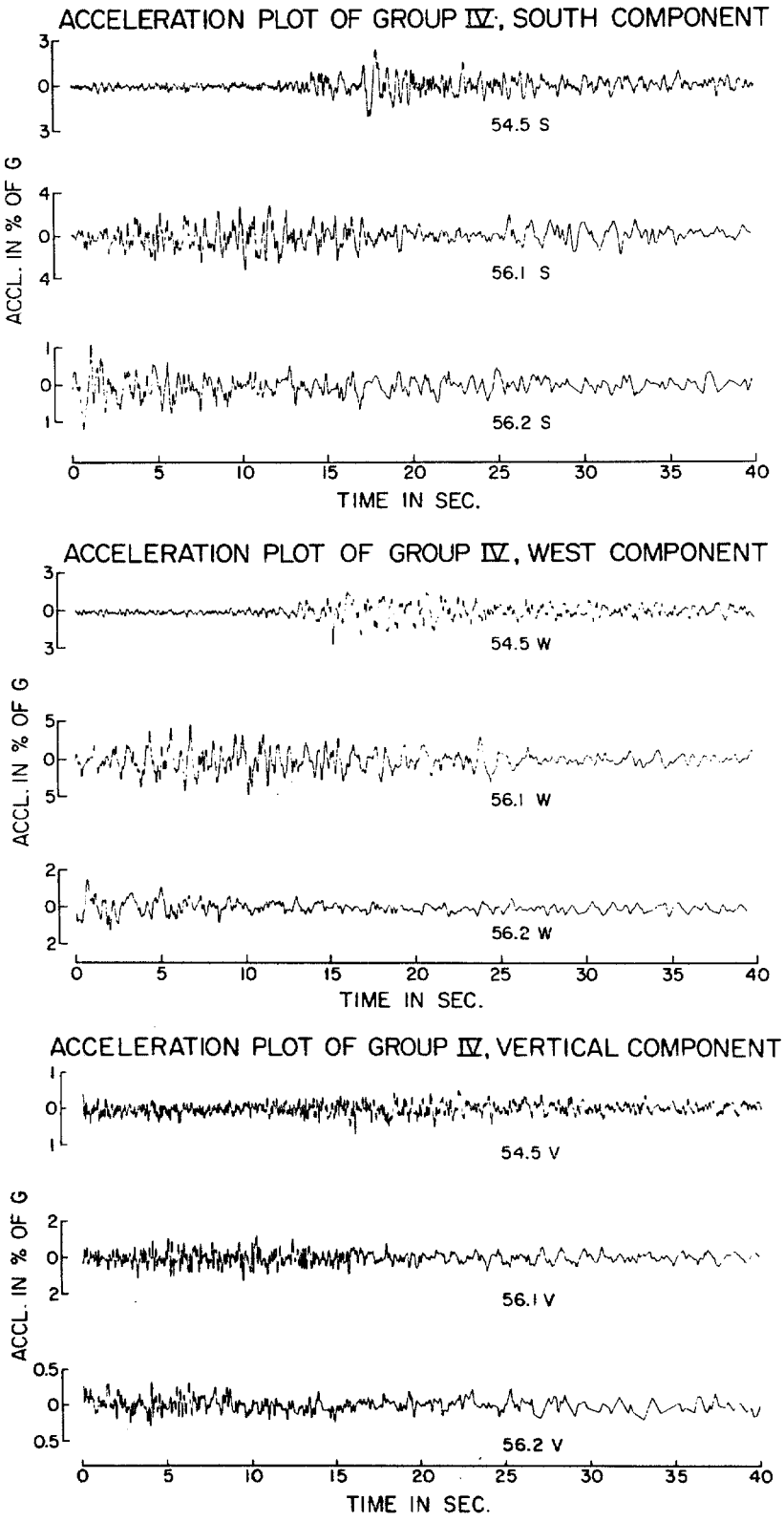
ACCELERATION PLOT OF GROUP IV, SOUTH COMPONENT
54.5 S
56.1 S
56.2 S
ACCL. IN % OF G
TIME IN SEC.
ACCELERATION PLOT OF GROUP IV, WEST COMPONENT
54.5 W
56.1 W
56.2 W
ACCL. IN % OF G
TIME IN SEC.
ACCELERATION PLOT OF GROUP IV, VERTICAL COMPONENT
54.5 V
56.1 V
56.2 V
ACCL. IN % OF G
TIME IN SEC.

FIGURE III. 7

distant points. Event 38.4 is a smaller event ($M_L = 4.0$) at about the same epicentral distance as event 34.2 ($M_L = 6.5$). One observes the accelerogram of this event as having relatively higher frequency contents than that compared to the record obtained from 34.2.

Group IV Accelerograms - (Events 9, 13, 14)

This group consists of three events 54.5, 56.1 and 56.2. The events 56.1 and 56.2 have been assigned the same epicenter. Their records do not indicate similarities in phase arrivals. The S wave arrival for the record of event 56.1 is a little before the accelerograph was triggered. We note the long period surface waves arriving at about 25 sec. A Rayleigh wave clearly can be discerned at 25 sec from the records of the N-S and vertical components of motion. The accelerogram of event 56.2 has clearly late-started, recording mainly the surface wave motions generated. Event 54.5 indicates that the P wave arrived a little before the instrument began recording. This could possibly be due to the conversion of the P waves to SV waves for distant earthquakes. The S wave arrival probably occurs at about 13 sec and is followed by surface waves.

In summary we observe from this group that large distant earthquakes may cause motions that are often quite different from close in motions. Large surface wave amplitudes can be obtained, the higher frequency S and P waves being suppressed by the geometrical scattering and attenuation along the path of energy transmission.

Summary of results obtained from the study of acceleration records at El Centro

1. The records tend to show that earthquake source processes cannot be correctly modelled as broad band processes. "White noise" - like source models may not be a correct representation of such mechanisms. It has been found that smaller earthquakes seem to have a relatively higher frequency content, factors such as the transmission path and the epicentral distance being maintained almost constant.

2. Multiple event earthquakes are quite different in character of energy release from single event earthquakes. Such earthquakes may also show in their records a relatively higher content of high frequency components than do single event earthquakes.

3. Surface wave energy is quite important for distant large earthquakes. The long duration of strong ground shaking observed in many of the records can be identified as caused by surface waves.

4. The nature of records obtained from different azimuths seems different. The phases do not arrive at the same relative times causing the response of a structure located at a site to be strongly dependent on the direction of approach of the waves.

III. 6 Spectral Analysis of Accelerograms

Introduction

The Fourier transform is a widely used mathematical tool in the study of earthquake processes. The frequency content of the

recorded signal can be used to study the source mechanism of earthquakes and the response of structures to strong ground shaking. In fact, the total energy acquired by an undamped single degree of freedom oscillator subjected to ground motions is directly proportional to the square of the Fourier spectral amplitude of the ground acceleration. Furthermore, the spectral amplitudes serve in the aseismic design of structures as they are often almost equal and always less than the velocity spectrum of an undamped oscillator. Further applications as in the study of vibration tests on structures are also becoming widespread. In comparison with other possible ways of representing functions the Fourier spectra have certain advantagaes of simplicity and ease of calculation.

(a) Computation of the Fourier Transform

In the process of optical digitization of accelerograms the operator imagines a straight line between two digitized points and is able to exercise his judgment as how to choose the unequally spaced points so that by joining the points by a number of straight segments a good representation of the function is obtained. There is thus in a sense more information in the digitized data than is given by the points themselves. An algorithm for the economical computation of the Fourier transform of a discrete sampled data system is the fast Fourier transform. Though computationally far superior [41] to a more straightforward procedure that computes the transform

of a piecewise linear continuous function [42], this algorithm only deals with sampled data. The loss of information on the function between the sampling points reduces somewhat the flexibility of the computations. With the sampled discrete data, problems such as aliasing arise. Such problems can be partially annulled by the use of prefiltering and by digitizing the data at a sufficiently high rate [42].

In the present work, the corrected accelerograms have already been low pass filtered. The sampling frequency used was 50 points/sec. The lengths of the signals Fourier analyzed were either 20 sec or 40 sec depending on the duration of the record containing significant ground motions. The Fourier analysis was carried out using the Cooley Tukey algorithm employing 2^{12} points [40]. The spectral estimates so obtained were smoothed with a 1/4, 1/2, 1/4 weighting function. These hanned spectra are shown in Appendix II.

(b) Smoothing of Fourier Amplitude Spectra

As observed from the nature of these spectra, the Fourier transform amplitude is a rapidly oscillating function. Since for engineering purposes we are interested in the general trend of the spectra rather than in individual peaks occurring at high frequencies in the amplitude spectra, these spectra need to be further smoothed.

Different smoothing techniques have been suggested by various investigators [43]. After trying out several types of smoothing windows, a simple smoothing technique using a triangular

window having a band width of 0.4 cps was chosen. The general trends in the spectra which are of engineering importance were found to be most clearly brought out by this simple smoothing procedure.

III. 7 Analysis of Fourier Amplitude Spectra

The extraction of information from the Fourier spectral curves of earthquakes is akin to the problem found in communication engineering wherein a noisy signal needs to be extracted from the "noise". The exact identification of significant peaks as being caused by a particular effect such as subsoil conditions, source mechanism or transmission path characteristics is almost impossible from the amount of data presently available in general. However one can extract useful information in certain favorable cases as will be discussed in this section.

(a) Predominant Periods in the Spectrum

In order to make quantitative studies on spectra, it is necessary to define a scheme for choosing spectral peaks having a special significance. Because of the large number of unknown parameters this is clearly not possible at a deterministic level in general and a statistical approach needs to be used. Following Nowroozi [44], one can estimate the significant spectral peaks obtained by harmonic analysis which are above a certain confidence level.

Since the scheme for revealing the periodic structure of a time series by means of harmonic analysis is based on the magnitude of the

amplitude corresponding to a particular frequency, any set of random numbers subject to harmonic analysis will yield harmonic amplitudes such that some are bigger than others by chance alone.

The decision as to the reliability of a spectral peak must then be based on a comparison with the magnitude of the amplitude which can be produced by harmonic analysis on the assumption that the time series are consequences of random fluctuation that have no physical meaning.

Consider the series x(i), $i = 1, 2, \cdots n$ constituting a random sample from a normally distributed population and its Fourier series representation

$$x(i) = \frac{a_o}{2} + \sum_{k=1}^{m} \left[a_k \cos \frac{2\pi ki}{n} + b_k \sin \frac{2\pi ki}{n} \right]$$

where

$$2m + 1 = n$$

The harmonic amplitude c_k of the kth harmonic is given by

$$c_k = \left[a_k^2 + b_k^2 \right]^{1/2}$$

Fisher [45] has shown that the probability P that the largest of the m ratios

$$\left(\frac{c_k^2}{\sum_{k=1}^{m} c_k^2} \right)$$

TABLE 2

Values of g for Hypothetical Probabilities

$m = 2^N$	N	P = 0.01 (-0.50%)	P = 0.02 (-1.0%)	P = 0.05 (-2.6%)	P = 0.10 (-4.8%)
8	3	0.615	0.575	0.516	0.465
16	4	0.389	0.360	0.319	0.287
32	5	0.229	0.212	0.188	0.170
64	6	0.130	0.120	0.107	0.0975
128	7	0.0717	0.0667	0.0599	0.0548
256	8	0.0390	0.0364	0.0329	0.0303
512	9	0.0210	0.0197	0.0179	0.0166
1024	10	0.0112	0.0105	0.00966	0.00899
2048	11	0.00596	0.00563	0.00517	0.00484
4096	12	0.00315	0.00298	0.00276	0.00259
8192	13	0.00166	0.00158	0.00146	0.00138

exceeds a parameter g is given by

$$P = m(1-g)^{m-1} - \frac{m(m-1)}{2}(1-2g)^{m-1} + \ldots \frac{(-1)^{L-1} m!}{L!\,(m-L)!}(1-Lg)^{m-1} \quad \text{(III. 1)}$$

where L is the largest integer less than $1/g$. It has been stated by Nowroozi [44] that the error in calculating g from only the first term in Equation III. 1 is very small. Values of g for hypothetical probabilities $P = 0.01,\ 0.02,\ 0.05$ and 0.10 calculated from the first term only of Equation III. 1 for values of $m = 2^N$ where $N = 3, 4, 5, \ldots 13$ are given in Table 2.

In order to examine the accuracy of the first term approximation for a given P the value of g obtained by the first approximation was used again in Equation III. 1 [42]. The new value of P, P_0 was obtained by using all the terms in Equation III. 1 and the errors

$$\epsilon = \left(\frac{P_o - P}{P}\right) 100$$

were calculated for each N. For small values of N the errors ϵ are negligible but increase uniformly with increasing N. For the largest value of $m = 8192$, given in Table 2, the errors ϵ for the various assumed P values are given in brackets. We note the negative sign which indicates that the error in calculating g by neglecting the higher order terms is in the direction of decreasing the probability P. This would mean that we would err on the safe side by using the first term approximation to calculate g.

In practical applications it is necessary to calculate Σc_k^2. Noting however that

$$\sum_{k=1}^{m} c_k^2 = \frac{2}{n} \sum_{i=1}^{n} \left(x(i) - \frac{a_0}{2} \right)^2$$

and using the first term approximation

$$g_\alpha = \left[1 - \left(\frac{P_\alpha}{m} \right)^{1/m-1} \right]$$

the maximum significant amplitude Z, based on the assumption that the data are random, is calculated as

$$z = \left\{ \frac{2 g_\alpha}{n} \sum_{i=1}^{n} \left[x(i) - \frac{a_0}{2} \right]^2 \right\}^{1/2} = c$$

where g_α is the maximum ratio, g, corresponding to the probability $P = P_\alpha$. It may be noted here that the determination of the value of Z does not necessitate the calculation of the c_k's $k = 1, \cdots m$. A convenient way of applying this test [42] is to plot a line $c = z$ across the plot of the Fourier spectrum so that all the peaks above the line could be identified as significant at the "95% confidence level". This level has been indicated by the dashed line in the spectra shown in Appendix II.

(b) Interpretation of the Spectra

A direct comparison of the actual spectra to reveal the predominant recurring frequencies is difficult due to the large oscillations present in them. A more meaningful engineering comparison can be obtained by a study of the smoothed curves shown in Figure III.8 and Figure III.9. On them are also indicated the epicentral distances of these events and their assigned magnitudes.

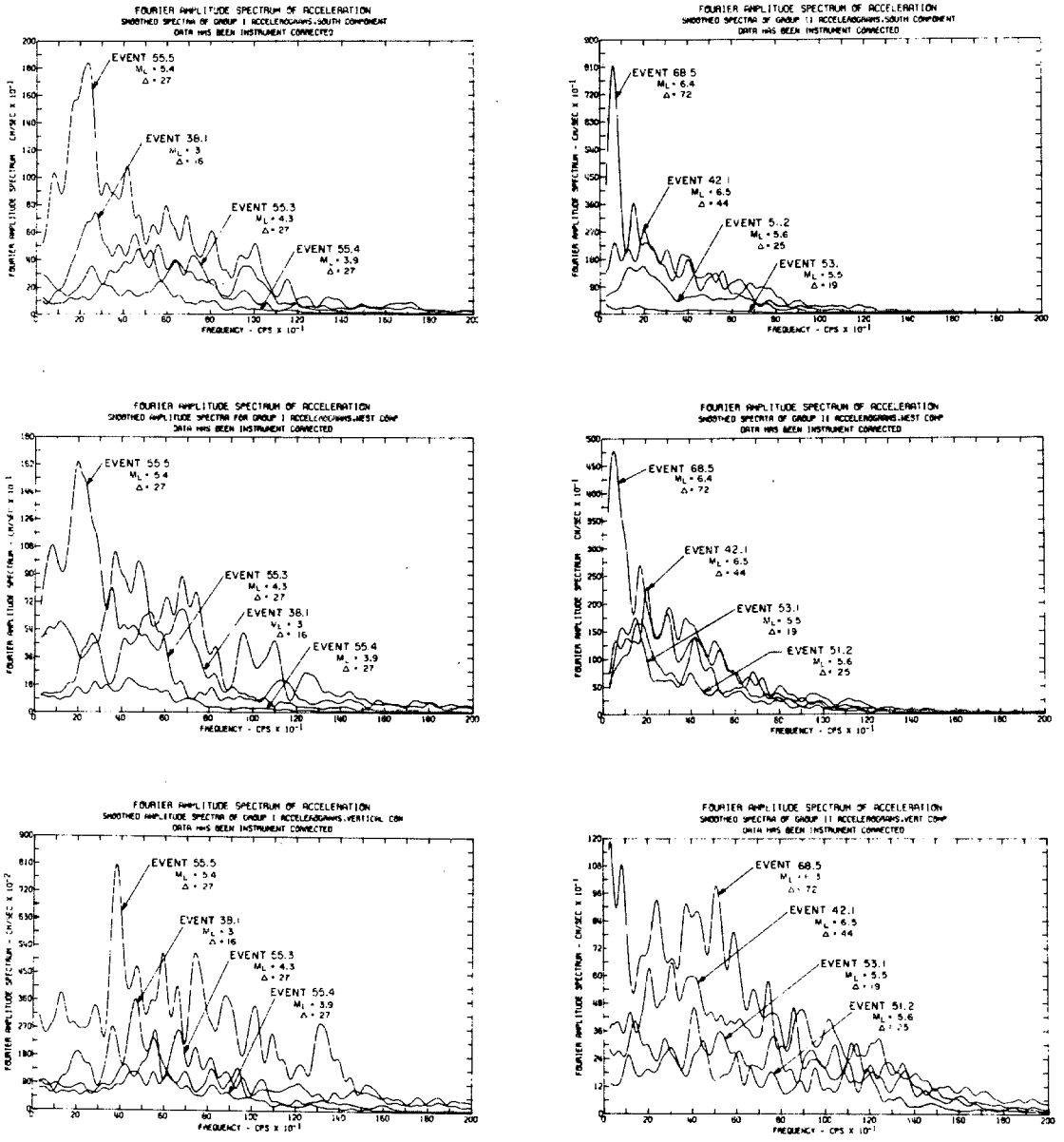
FOURIER AMPLITUDE SPECTRUM OF ACCELERATION
SMOOTHED SPECTRA OF GROUP I ACCELEROGRAMS.SOUTH COMPONENT
DATA HAS BEEN INSTRUMENT CORRECTED
EVENT 55.5
EVENT 38.1
EVENT 55.3
EVENT 55.4
FOURIER AMPLITUDE SPECTRUM - CM/SEC X 10⁻¹
FREQUENCY - CPS X 10⁻¹
FOURIER AMPLITUDE SPECTRUM OF ACCELERATION
SMOOTHED SPECTRA OF GROUP II ACCELEROGRAMS.SOUTH COMPONENT
DATA HAS BEEN INSTRUMENT CORRECTED
EVENT 68.5
EVENT 42.1
EVENT 51.2
EVENT 53.
FOURIER AMPLITUDE SPECTRUM OF ACCELERATION
SMOOTHED AMPLITUDE SPECTRA FOR GROUP I ACCELEROGRAMS.WEST COMP
DATA HAS BEEN INSTRUMENT CORRECTED
EVENT 55.5
EVENT 55.3
EVENT 38.1
EVENT 55.4
FOURIER AMPLITUDE SPECTRUM OF ACCELERATION
SMOOTHED SPECTRA OF GROUP II ACCELEROGRAMS.WEST COMP
DATA HAS BEEN INSTRUMENT CORRECTED
EVENT 68.5
EVENT 42.1
EVENT 53.1
EVENT 51.2
FOURIER AMPLITUDE SPECTRUM OF ACCELERATION
SMOOTHED AMPLITUDE SPECTRA OF GROUP I ACCELEROGRAMS.VERTICAL COM
DATA HAS BEEN INSTRUMENT CORRECTED
EVENT 55.5
EVENT 38.1
EVENT 55.3
EVENT 55.4
FOURIER AMPLITUDE SPECTRUM OF ACCELERATION
SMOOTHED SPECTRA OF GROUP II ACCELEROGRAMS.VERT COMP
DATA HAS BEEN INSTRUMENT CORRECTED
EVENT 68.5
EVENT 42.1
EVENT 53.1
EVENT 51.2

FIGURE III. 8

The local magnitude M_L is defined as the maximum response in microns of a standard Wood-Anderson instrument with a natural frequency of 1.25 cps and 80% critical damping and a maximum amplification of 2800 located at a distance of 100 km from the disturbance. An inherent deficiency in characterizing the earthquake process by the response of such an instrument lies in the fact that the instrument amplifies certain frequencies and filters out other frequency components. From the point of view of acquiring information on the earthquake mechanism the local magnitude might be interpreted in the following way.

A simplified model of an earthquake source can be thought of as a plane discontinuity involving an instantaneous stress drop. Such a model has been studied by Brune [17], Aki [18] and Haskell [19]. They conclude that the nature of the source spectrum under such assumptions should be flat up to a certain frequency falling off as ω^{-1} to ω^{-3} beyond what is called the "corner frequency". The nature of the spectrum at frequencies higher than the corner frequency is related to the short time dynamic aspects of the problem, the long time processes (static) being characterized by the level of the flat zone in the spectrum. This level is generally related to the seismic moment created by the earthquake. The Wood-Anderson instrument may be thought of as a linear filter that filters the source spectrum. Hence, depending on the nature of the source spectrum, this filter will characterize to a greater or lesser degree the dynamic phenomena related to stress drop if the corner frequency is very low or the static phenomena

related to the earthquake moment. The larger the earthquake, the lower the corner frequency and the greater the extent to which the instrument represents the dynamic effects at the source; the smaller the event, the higher the characterization of the seismic moment. Thus we observe that although the local magnitude of an earthquake gives a simple numerical characterization of the process it may be hard to interpret this number in terms of the actual physical processes concerned.

(1) Group Characteristics of Earthquake Spectra from El Centro Group I Accelerograms

Figure III.8 shows the smoothed spectra of Group I accelerograms plotted to the same scale. The special significance of this group lies in events 55.3, 55.4 and 55.5. The spectra of these three events show that the smaller events have a relatively increasing contribution of higher frequencies in them. The spectra of the larger events show a greater concentration towards the low frequency end of the spectrum. The different general characteristics of these three spectra indicate that the three events have different source mechanisms. Of significant importance is the attenuation of the waves with distance. The smaller event 38.1 ($M_L = 3.0$) has caused roughly the same energy input at the recording site as seen from the area under the spectral curves as the more distant event 55.3 ($M_L = 4.3$). Thus from an engineering standpoint the destructive nature of an earthquake is related to many factors such as epicentral distance and orientation

of the site with respect to the fault in addition to its local magnitude Also, the local magnitude may not give a correct representation of the energy generated at the source for reasons discussed earlier. The vertical components of ground motion indicate that the energy of the signal is mainly concentrated in the high frequency zone between 4 and 14 cps.

Group II Accelerograms

Another indication of the inadequacy of the local magnitude scale for engineering purposes is shown in Figure III. 8. Considering the spectra of the horizontal components of events 68.5 and 42.1 whose local magnitudes [M_L] are 6.5 and 6.4 respectively and which have the same azimuths with respect to the recording site, it may be observed that the total energy received at the station from the nearer larger event is less than that from the smaller more distant event. The concentration observed in event 68.5 near the low frequency end may be attributable to the establishment of surface waves (see accelerogram Figure III.4) which require some distance before constructive interference occurs. Event 53.1, which has been considered earlier as a possible multiple event, shows a spectral behavior different from the others of this group in that the E-W component shows a marked two banded spectrum. The higher frequency band may be attributed to the presence of higher frequencies caused by the multiple nature of the source mechanism. This is more so brought out in the vertical component which shows an almost broad band spectrum all the way to 12 cps.

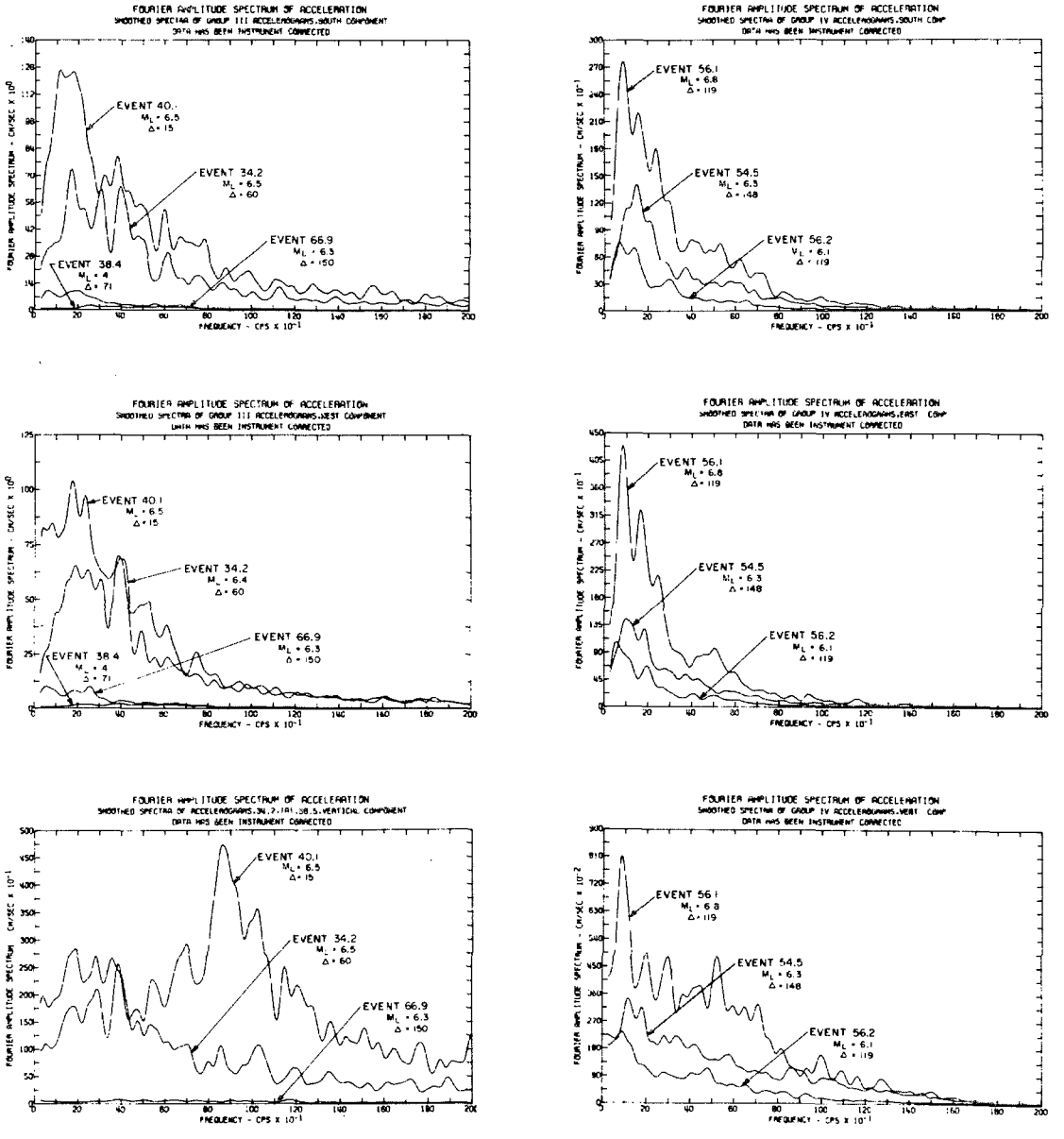
FOURIER AMPLITUDE SPECTRUM OF ACCELERATION
SMOOTHED SPECTRA OF GROUP III ACCELEROGRAMS.SOUTH COMPONENT
DATA HAS BEEN INSTRUMENT CORRECTED
EVENT 40.1
ML = 6.5
Δ = 15
EVENT 34.2
ML = 6.5
Δ = 60
EVENT 66.9
ML = 6.3
Δ = 150
EVENT 38.4
ML = 4
Δ = 71
FOURIER AMPLITUDE SPECTRUM - CM/SEC x 10^0
FREQUENCY - CPS x 10^-1
FOURIER AMPLITUDE SPECTRUM OF ACCELERATION
SMOOTHED SPECTRA OF GROUP IV ACCELEROGRAMS.SOUTH COMP
DATA HAS BEEN INSTRUMENT CORRECTED
EVENT 56.1
ML = 6.8
Δ = 119
EVENT 54.5
ML = 6.3
Δ = 148
EVENT 56.2
ML = 6.1
Δ = 119
FOURIER AMPLITUDE SPECTRUM - CM/SEC x 10^-1
FREQUENCY - CPS x 10^-1
FOURIER AMPLITUDE SPECTRUM OF ACCELERATION
SMOOTHED SPECTRA OF GROUP III ACCELEROGRAMS.WEST COMPONENT
DATA HAS BEEN INSTRUMENT CORRECTED
EVENT 40.1
ML = 6.5
Δ = 15
EVENT 34.2
ML = 6.4
Δ = 60
EVENT 66.9
ML = 6.3
Δ = 150
EVENT 38.4
ML = 4
Δ = 71
FOURIER AMPLITUDE SPECTRUM - CM/SEC x 10^0
FREQUENCY - CPS x 10^-1
FOURIER AMPLITUDE SPECTRUM OF ACCELERATION
SMOOTHED SPECTRA OF GROUP IV ACCELEROGRAMS.EAST COMP
DATA HAS BEEN INSTRUMENT CORRECTED
EVENT 56.1
ML = 6.8
Δ = 119
EVENT 54.5
ML = 6.3
Δ = 148
EVENT 56.2
ML = 6.1
Δ = 119
FOURIER AMPLITUDE SPECTRUM - CM/SEC x 10^-1
FREQUENCY - CPS x 10^-1
FOURIER AMPLITUDE SPECTRUM OF ACCELERATION
SMOOTHED SPECTRA OF ACCELEROGRAMS.3N,7-181,38.5,VERTICAL COMPONENT
DATA HAS BEEN INSTRUMENT CORRECTED
EVENT 40.1
ML = 6.5
Δ = 15
EVENT 34.2
ML = 6.5
Δ = 60
EVENT 66.9
ML = 6.3
Δ = 150
FOURIER AMPLITUDE SPECTRUM - CM/SEC x 10^-1
FREQUENCY - CPS x 10^-1
FOURIER AMPLITUDE SPECTRUM OF ACCELERATION
SMOOTHED SPECTRA OF GROUP IV ACCELEROGRAMS.VERT COMP
DATA HAS BEEN INSTRUMENT CORRECTED
EVENT 56.1
ML = 6.8
Δ = 119
EVENT 54.5
ML = 6.3
Δ = 148
EVENT 56.2
ML = 6.1
Δ = 119
FOURIER AMPLITUDE SPECTRUM - CM/SEC x 10^-2
FREQUENCY - CPS x 10^-1

FIGURE III. 9

Group III Accelerograms

The spectrum of the Imperial Valley Earthquake of 1940 has been shown in Figure III. 9. It was a multiple event [35] earthquake at a distance of 15 km from the recording station. The large peak in the spectrum of the vertical component at around 8.8 cps may be attributed to the "multiple event" nature of the source mechanism, to the nearness of the source from the recording station and possibly due to ground amplification characteristics.

Group IV Accelerograms

Group IV consists of three relatively distant (>60 km) earthquakes. Events 56.1 and 56.2 have been assigned the same epicenter and show resemblances in the general spectral appearance. The dissimilarities between these spectra (Figure III. 9) can then be attributed to differences in the nature of the energy release. The larger event once again has a greater peakedness toward the low frequency zone, the spectral amplitudes falling off much more rapidly than for the smaller event (56.2). This indicates that the nature of the fall-off of the spectrum may be attributable to both the earthquake size and the ground attenuation phenomenon.

It may be of interest to compare the spectra of events 55.3, 55.4 and 55.5 (all of which have the same epicenter), which show distinctly dissimilar general features, with those of events 56.1 and 56.2, which do show distinctly similar characteristics. One might deduce from the similar trends observed in these latter spectra that at distances far out from the epicenter the effect of differences in the

short time details of source mechanism get wiped out, the site feeling the effect of the transmission path and local topography more predominantly. Another comparison can be made between events 66.9 and 54.5. Despite the fact that both events have been assigned the same local magnitude ($M_L = 6.3$) and have about the same epicentral distances, the time histories and the spectra of the events are quite different, indicating again the importance of the source mechanism and the transmission path between source and receiver on strong ground shaking.

(2) Summary of Results from the Interpretation of General Characteristics of Earthquake Spectra

(a) The spectral characteristics of ground motion as observed from these records depend strongly on the direction of arrival of the incoming seismic waves.

(b) We noted that the local magnitude may not be a consistent characterization of the earthquake source process, the response of the Standard Wood-Anderson Instrument at times portraying more predominantly the long time source characteristics related to the seismic moment, and at others portraying more the short time or dynamic source characteristics related to stress drop. Also, from an engineering viewpoint, factors such as distance and relative site location with respect to the fault may become important parameters for assessing the destructive capacity of an earthquake in a given area. The engineer is basically interested in a broader spectral range than is characterized by the Standard Wood-Anderson instrument with which is associated the local magnitude scale.

BAR CHART SHOWING NUMBER OF MATCHINGS

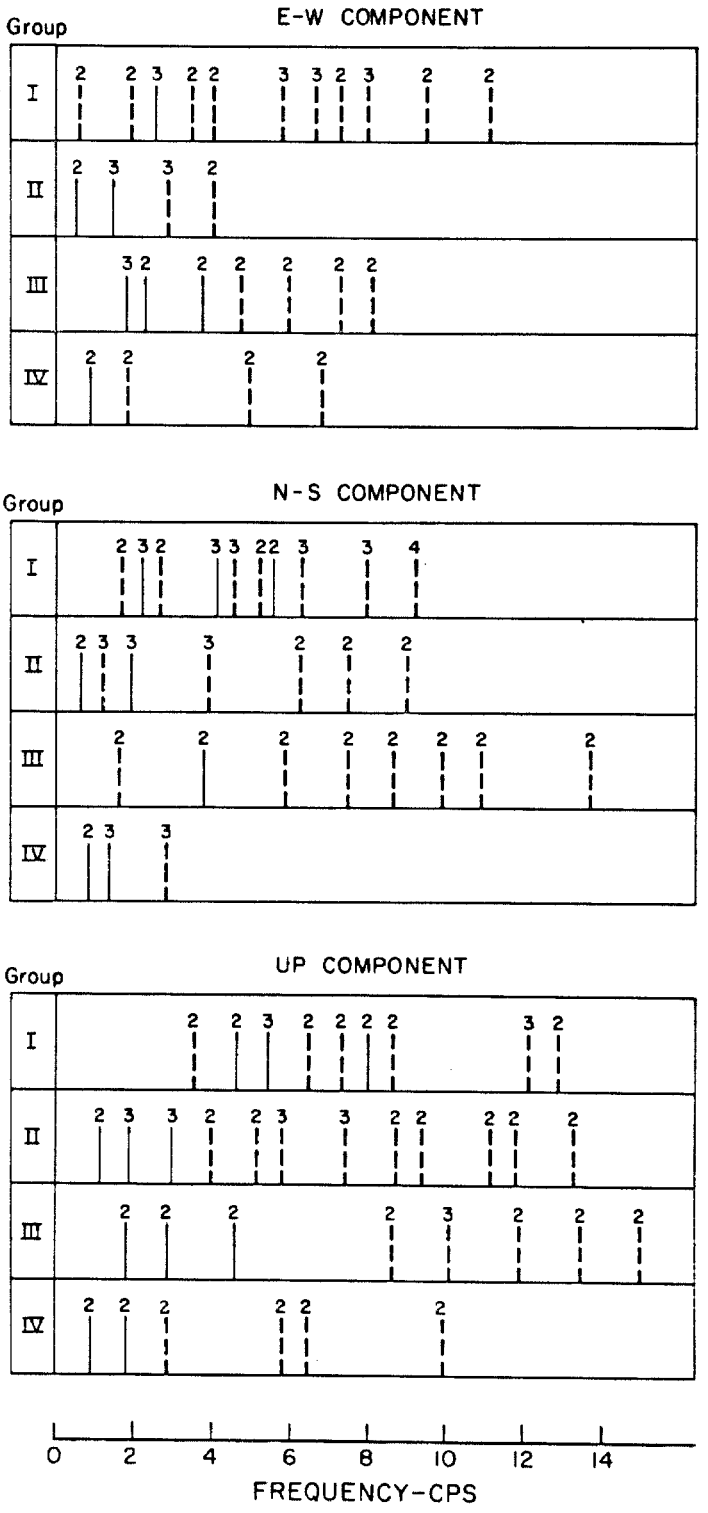

FIGURE III. 10

(c) Many tall structures have fundamental periods of motion in the horizontal direction of the order of one second. Surface wave motions observed during strong ground shaking show significant amplitudes in this period range. When such motions occur over long durations they may excite damaging resonant vibrations in tall structures.

(d) The spectra of the vertical components show that they are of a more basic broad band nature than the corresponding spectra for the horizontal components. The spectral amplitudes fall off more slowly than for horizontal motions.

(e) The fall-off in the amplitudes of horizontal components of the spectra is related to both the magnitude of the earthquake and to the ground attenuation.

(3) Analysis of Spectral Peaks in Ground Motion Accelerograms

In order to search for periodicities that appear recurrently for all different azimuths the matching of spectral peaks can be studied. For this purpose the different peaks have been picked by eye and their positions indicated in the bar chart shown in Fig. III.10. As the resolution of our smoothing window is 0.2 cps two peaks more than 0.2 cps apart shall be considered distinctly different from each other and two peaks closer than 0.2 cps from each other coincident. The thick bars correspond to peaks above the 95% confidence level, while the dotted bars indicate peaks below that confidence level. The numbers above each bar indicate the number of peaks that match at the frequency in question. As seen from the chart it appears that no recurrent peaks are prevalent in the horizontal components of ground

motion. The location of the bars varies widely from group to group for the horizontal components of ground motion and does not indicate any frequencies that might be construed as being characteristic of the local site conditions. The same kind of general scatter is found in the vertical components of ground motions except perhaps for the line-up at a frequency of 1.8 cps, 2.8 cps and a weaker possibility at 4.6 cps. The vertically ascending S-wave model [56] does not identify with any of these frequencies.

An attempt was made to improve the above matching process by the use of quantitative statistical criteria. In view of the numerous judgmental factors involved, it was concluded that the above approach results in a more meaningful picture.

IV. ANALYSIS OF MICROTREMOR GROUND MOTIONS AT EL CENTRO

IV.1 Introduction

Two basic approaches have hitherto been used in the study of the vibrational characteristics of subsoil layers. The first involves field exploration either through seismic prospecting, trenching or bore hole studies. The second approach instituted chiefly by Kanai [46] involves the application of microtremors. Microtremors as the word suggests are low amplitude (1~5 microns) oscillations of the ground surface produced by natural sources such as the wind and the sea breaking on nearby shores, and by artificial ones such as vehicular traffic and other cultural noise. The measured microtremor motions may be modified by local soil and geological conditions and hence the recorded signal may contain information on these local conditions.

The study of naturally occurring microtremors, usually called microseisms, started soon after seismology was established as a branch of science. However little research was done on the subject for a long time since it was considered to have little basic scientific value. Microseismic studies have been used to assist in the tracking of hurricanes. Such studies are also commonly used in the selection of low-noise sites for the location of high-magnification seismological instruments. In recent years, a revived interest has been generated in this field because of its possible applicability in the study of soil vibrational characteristics [46].

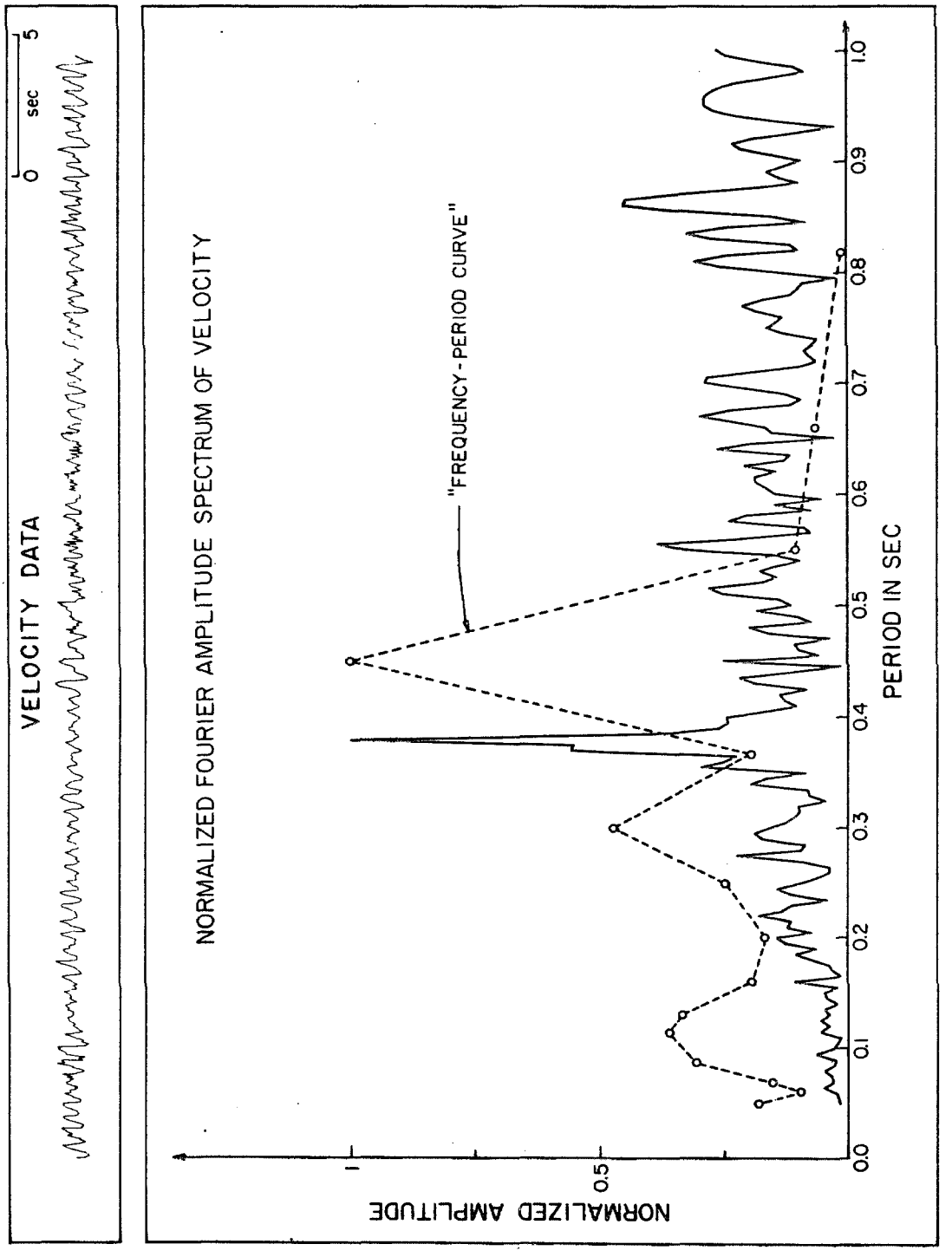
VELOCITY DATA
0
sec
5
NORMALIZED FOURIER AMPLITUDE SPECTRUM OF VELOCITY
"FREQUENCY-PERIOD CURVE"
NORMALIZED AMPLITUDE
1
0.5
0.0
0.1
0.2
0.3
0.4
0.5
0.6
0.7
0.8
0.9
1.0
PERIOD IN SEC

FIGURE IV. 1

Kanai and his colleagues made several studies on the analysis of microtremors [47]. Their investigations typically made use of a two minute length of record from one horizontal component of ground motion and involved measuring the intervals between successive zeros. The periods of ground motion were taken to be twice the time interval. An automatic analyzer was used to count the number of waves of each period. By plotting the periods versus the number of waves of each period they obtained a "frequency period curve". From their study they suggested [46] that for a given site such curves had some correlation with similar plots obtained from those of strong earthquake ground motions. They categorized sites in Japan on the basis of the general appearance of these "frequency-period" curves into four classes for use in assigning lateral force coefficients in the aseismic design of structures. However, a review of Kanai's data [48] suggests that a direct correlation between strong earthquakes and microtremor processes has yet to be established. It is the purpose of this section to study the extent and nature of such a correlation so that the rationale behind the "microregionalization" of an area on the basis of variations in the nature of microtremor ground motions for the purposes of assessing damage susceptibility during strong earthquake ground motions can be critically viewed.

Kanai, et al [48] have also suggested that "site periodicities" can be defined by microtremor measurements and that these same periodicities show up in the much larger ground motions created by destructive earthquakes. As has been observed clearly in the previous

Sections III.5 and III.7 the frequency content in earthquake ground motions depend on many factors. The nature of ground motions experienced at a site would be the composite effect of all these. Factors such as the azimuth, the focal mechanism, the distance of the source from the recording site, the nature of the geologic media between the source and the receiver and the local surface topography play an important part in earthquake ground motion studies. Such factors might well offset or overshadow the effect of a local soil or geologic condition as has been indicated in this particular study. This strongly suggests that the importance of local ground amplifications in similar geologic settings should not be taken for granted. The frequency-period curve in the form used initially by Kanai as a measure of the harmonic content of the ground signal has certain inherent difficulties. Allam [49] has pointed out that such a statistic is suspect for data that have more than one predominant period. To independently verify this, a 30 sec segment of data recorded by Kanai [50] was Fourier analyzed. The "frequency-period curve" and the numerically computed frequency spectrum are shown in Fig. IV.1 where both spectra are normalized to have the same peak values. The comparison indicates that the two curves are distinctly dissimilar both in the general trends and in their matching of different peaks.

Before a comparative study of earthquake and microtremor observations can be made, it is necessary to study the nature of microtremors and earthquake processes, and how they differ from one another. The following is a very brief review of the physical characteristics of microtremor ground motions.

Kanai [46] has interpreted microtremors as being chiefly multiple reflections of SH waves in parallel subsoil layers. If such a theory were totally applicable microtremor ground motions ought not to show significant components in the vertical direction. The present study (Figs. IV. 5-9) indicates that significant vertical components of ground motion can occur in such a process. Wilson [51] studied microtremors in the frequency range 4 - 100 cps and found the main sources to be heavy traffic, machinery, aircraft, wind and other cultural noise. Aki [52] found that microtremors at a particular site had a uniform intensity with respect to azimuth. He found that these waves had a definite velocity at a given frequency and identified them as Love waves. Akamatsu [53] on studying particle orbits arrived at the conclusion that they are mainly combinations of Love and Rayleigh waves. Recordings made at the surface and at depth by Douze [54] indicated that microtremors may be both P and Rayleigh waves while Allam [55] in his recent study in Tokyo concludes that microtremors are combinations of body and/or surface waves, which leaves open the possibility of just about any type of motion.

The above brief outline indicates the diversity of opinion prevalent on the basic nature of microtremors. The source of microtremors has been considered by most investigators who subscribe to the idea of microregionalization to be a process that leads to a white noise input into "bed rock". The validity of such an argument is questionable in view of the strong possibility that their source often comprises close-in surface excitations caused by operating machinery

such as pumps and compressors and by nearby traffic. As the nature of these ground inputs is usually unknown, deductions from microtremor ground measurements need to be made with caution. One plausible reason for the wide variety of opinions expressed by various investigators on the nature of microtremor processes is the uncertain nature of this input ground motion.

It would be instructive at this point to consider some obvious similarities and dissimilarities between microtremor and earthquake processes. Microtremor motions have been found by various investigators [55] to be stationary over periods of time of the order of 40 sec to 2 - 3 minutes. Though this point will be considered again in greater detail in Section IV.3 it will suffice to say at this stage that earthquake processes are not stationary in nature and hence ground response to the two processes may be quite different. The nature of the input ground motions at the sorce are unknown in both cases. The ground input in earthquake processes has a determinable spatial relation to the receiver. However, large uncertainties exist regarding the modification of these unknown inputs as they pass through the complicated intervening medium between the source and the receiver. The receiver of course feels the integrated effect of all these modifications that the waves experience along their travel path from the source. Microtremors on the other hand are more or less locally created by close-in sources whose spatial distribution is ordinarily unknown.

One way of studying in greater detail correlations between the two processes would be to make microtremor measurements at or near

a site where a large number of strong earthquake ground motions had been recorded. This is the main objective of this present investigation. The area chosen was El Centro because of the large number of strong earthquakes recorded there, and because the local site conditions there are relatively well known. Microtremor field measurements have been made at five different sites in the El Centro area so as to throw some light on their nature and ascertain the extent to which possible correlations with the strong motion measurements exist.

IV.2 Field Measurements of Microtremor Ground Motions

(a) Description of the Measuring Equipment

Three Earth Sciences - Teledyne Ranger seismometers were used to measure the three components of ground motion at five different sites in the El Centro area. Each seismometer essentially consists of a permanent magnet which is allowed to move within a stationary coil. The voltage generated in the coil is proportional to the velocity of the moving magnet. Permanent rod magnets, which provide a destabilizing force, are attached to the case in order to lengthen the natural period of the spring mass system. This results in a natural period of around one second. Damping during all the tests was maintained to be about 0.7 of its critical value, by an adequate adjustment of the coil resistance and that of the external amplification circuits. The amplification of all frequencies beyond 1 cps was nearly a constant.

The three outputs from the seismometers were fed into an Earth Sciences - Teledyne SC-210A Signal Conditioner which amplified the signals. Each channel on the signal conditioner has an amplification of up to 350,000 times and an attenuation from 0 to 82 db. The

power for the signal conditioner is provided by internal rechargeable batteries with a nominal 25-hour operation between charges. When used with a velocity transducer each channel can provide output voltages proportional to displacement, velocity and acceleration. Depending on the level of ground motion, different attenuations from 24 to 64 db were used. The recorded signals were kept within 1 volt in amplitude corresponding to ground velocities of the order of 1 - 5 microns/sec. This voltage output was next recorded on an Ampex SP-300 tape recorder. Before each recording the recorder was adjusted to have no d. c. bias and the ratio of output to input voltages adjusted to unity. A direct visual display of the ground motions was obtained by simultaneously recording the three signals on two Mark 220 Brush Recorders. On the fourth channel of the tape recorder was fed a 10 cps sine wave from a function generator in order to record time accurately.

(b) Measurement Procedures

Figure IV.2 shows a map of El Centro and the five different sites at which the microtremor measurements were made. Three of them are close to (within 2 - 3 km) the strong motion accelerograph site, the other two being nearer the Imperial fault zone. Microtremor measurements could not be made exactly at the strong motion accelerograph site which is located in a steam turbine electric generating plant with a very high level of background noise. All measurements were made during the night in order to eliminate as far as possible the effects of close-by local disturbances. To establish the stationarity of the process three of the sites were revisited the following night and

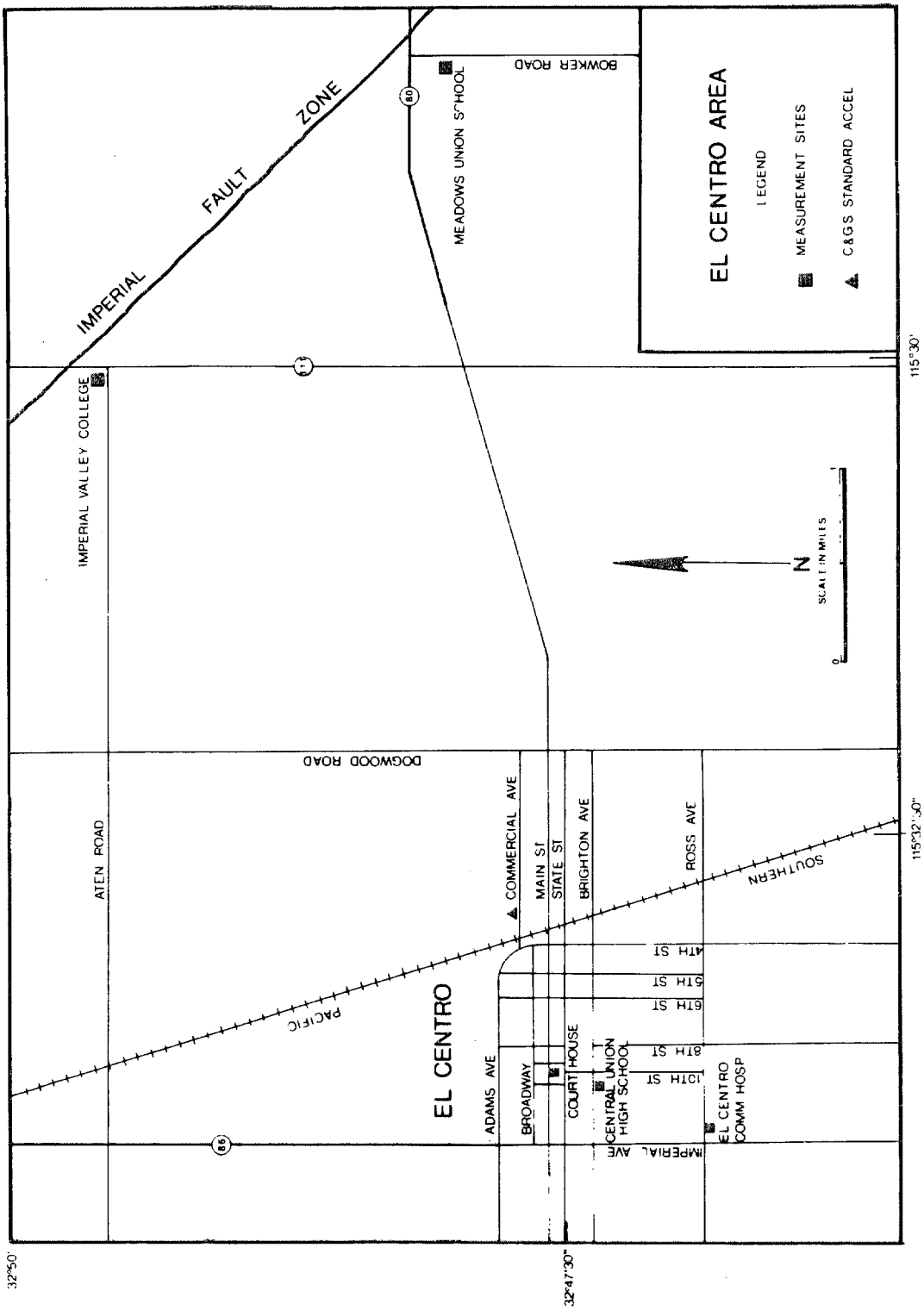
EL CENTRO AREA
LEGEND
MEASUREMENT SITES
C&GS STANDARD ACCEL
IMPERIAL FAULT ZONE
MEADOWS UNION SCHOOL
BOWKER ROAD
IMPERIAL VALLEY COLLEGE
ATEN ROAD
DOGWOOD ROAD
EL CENTRO
ADAMS AVE
BROADWAY
COURT HOUSE
CENTRAL UNION HIGH SCHOOL
EL CENTRO COMM HOSP
COMMERCIAL AVE
MAIN ST
STATE ST
BRIGHTON AVE
ROSS AVE
IMPERIAL AVE
13TH ST
8TH ST
6TH ST
5TH ST
4TH ST
PACIFIC
SOUTHERN
N
SCALE IN MILES
0
1
115°30'
115°32'30"
32°50'
32°47'30"

FIGURE IV. 2

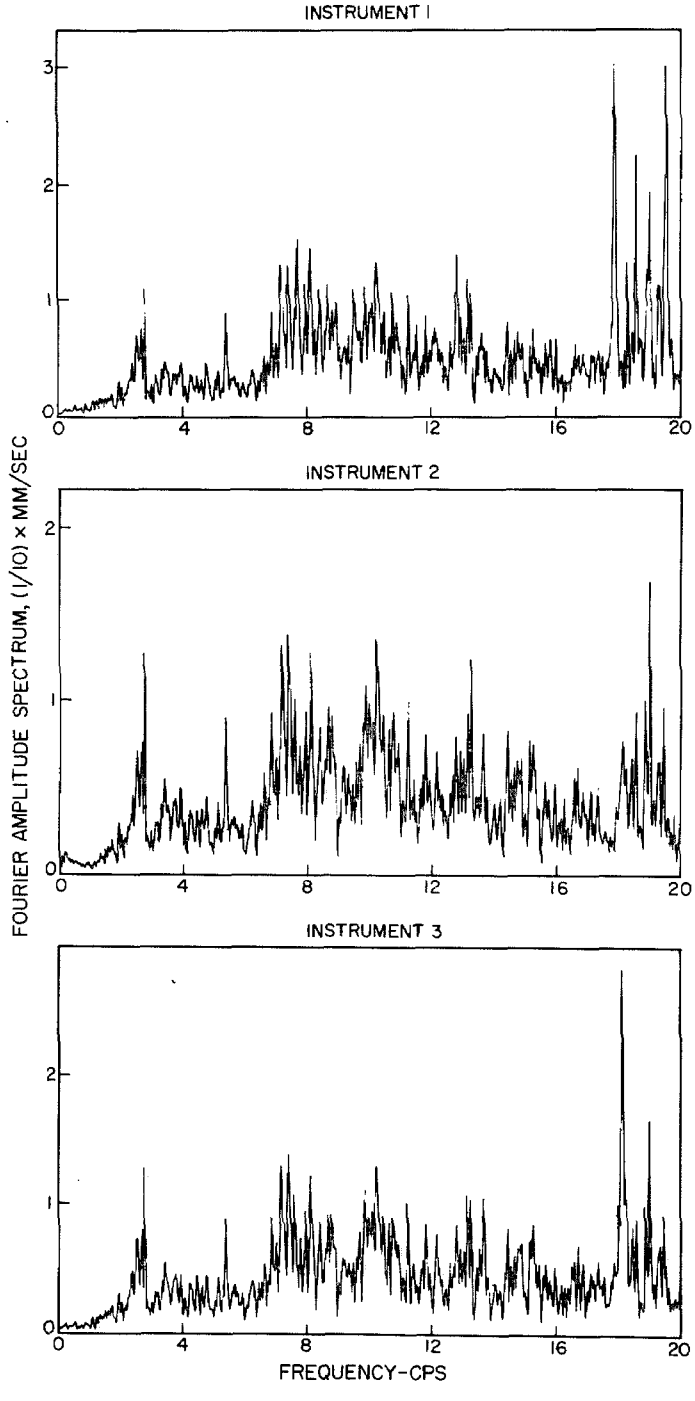
FOURIER AMPLITUDE SPECTRUM OF ACCELERATION
MICROTREMOR MEASUREMENTS AT CITY HALL, EL CENTRO
AUGUST 4, 1970, 11 PM
CALIBRATION — EAST-WEST COMP.
INSTRUMENT 1
INSTRUMENT 2
INSTRUMENT 3
FOURIER AMPLITUDE SPECTRUM, (1/10) x MM/SEC
FREQUENCY-CPS
0
1
2
3
4
8
12
16
20

FIGURE IV. 3

measurements once more were taken. Before each set of recordings, which lasted about 4 to 5 minutes, a calibration run was made wherein each of the three seismometers was oriented in an EW direction. This gave an idea of the reliability of the instruments and the total error bounds on the experimental procedures coupled with the numerical processing. Figure IV.3 shows a typical set of spectra obtained from the calibration run. The spectral peaks are correct to within 2 to 5%, the variance in the spectra being less than 2-3 radians/sec.

(c) Data Analysis

The three simultaneous analog signals recorded on magnetic tape were converted to digital form on a Digital Data Systems Model 1103 Analog-Digital Converter. The digitized record contained the scanned signal with 200 pt/sec. Only a portion of each digitally converted 3 min record was used in the spectral analysis. Two data blocks were selected in each run, each lasting forty seconds, after visually editing the seismometer readings on the brush recorders to ensure that the samples were representative and not contaminated by undesirable short term disturbances, such as might be caused by passing vehicular traffic.

This signal was next passed through a low pass filter with a cutoff frequency at 100 cps. This was done in order to maintain a reasonably high power level in the filtered signal up to 50 cps or so. This digital filter was an equally weighted running mean type filter having three weights each of one-third. The filtering process basically consisted of smoothing out the original signal so that the i^{th} data point

was replaced by the smoothed function calculated as

$$v_s = (v_i + v_{i+1} + v_{i-1})/3$$

The smoothed function was next decimated, taking every second point, hence reducing the number of points to 100 pts/sec corresponding to a Nyquist frequency of 50 cps. This led to a considerable saving in the cost of subsequent analysis without altering the accuracy of the spectra measurably [42].

The actual ground acceleration was next obtained by considering the output of the seismometers to represent the relative velocity between the coil and the magnet. The differential equation describing a single degree of freedom oscillator, viscously damped, is

$$\ddot{x} + 2\omega_n \xi \dot{x} + \omega_n^2 x = -\ddot{a} \qquad \text{(IV.1)}$$

where $\dot{x}$ is the relative velocity

a is the absolute ground acceleration

ω_n is the natural frequency of the oscillator

ξ is the fraction of critical damping

The different terms of the left-hand side of Equation (IV.1) were assembled by differentiating the velocity signal to obtain relative acceleration and integrating the velocity signal to get the displacement. Long period drifts were next eliminated from the displacement by fitting a "least-square-fit" baseline to the displacements calculated. Knowing ω_n and ξ, the ground acceleration was next computed. Further processing of this ground acceleration resulting in the calculation of the Fourier spectral amplitudes (Figs. IV.4 - 8) proceeded in a way similar to that for the earthquake accelerograms.

In order to ascertain the confidence with which the spectral peaks were computed, a 95% confidence level line has been drawn on each spectrum.

IV.3 Spectral Analysis of Microtremor Motions

The hanned microtremor spectra smoothed with $\frac{1}{4}, \frac{1}{2}, \frac{1}{4}$ weights were obtained from the five sites at which the readings were made by visually editing a forty second length of microtremor recording. In order to determine whether or not the time length of record analyzed was sufficiently long to portray the characteristic features of ground motion, two typical forty second blocks were selected from the recordings at each site and their spectra compared. Figure IV.4 indicates a typical comparison. The figure shows that so far as short time periods (of the order of 2 - 3 minutes) are concerned, a 40 sec length of record is long enough to permit the extraction of information representative of the process. Over such short time intervals the process is fairly stationary judging from the appearance of the spectra. To see if this stationarity persists over relatively longer periods (of the order of a day or so) measurements were made at three of the sites after a lapse of about 24 hours. These spectra are shown in Figs. IV. 5 - 7. The spectra on the right show the nature of ground motions about 24 hours after the first measurements were made. From these figures, we observe that the nature of the spectral content can change drastically over a period of about a day. This clearly implies that the determination of any common patterns presented by microtremor spectra would require extended measurements

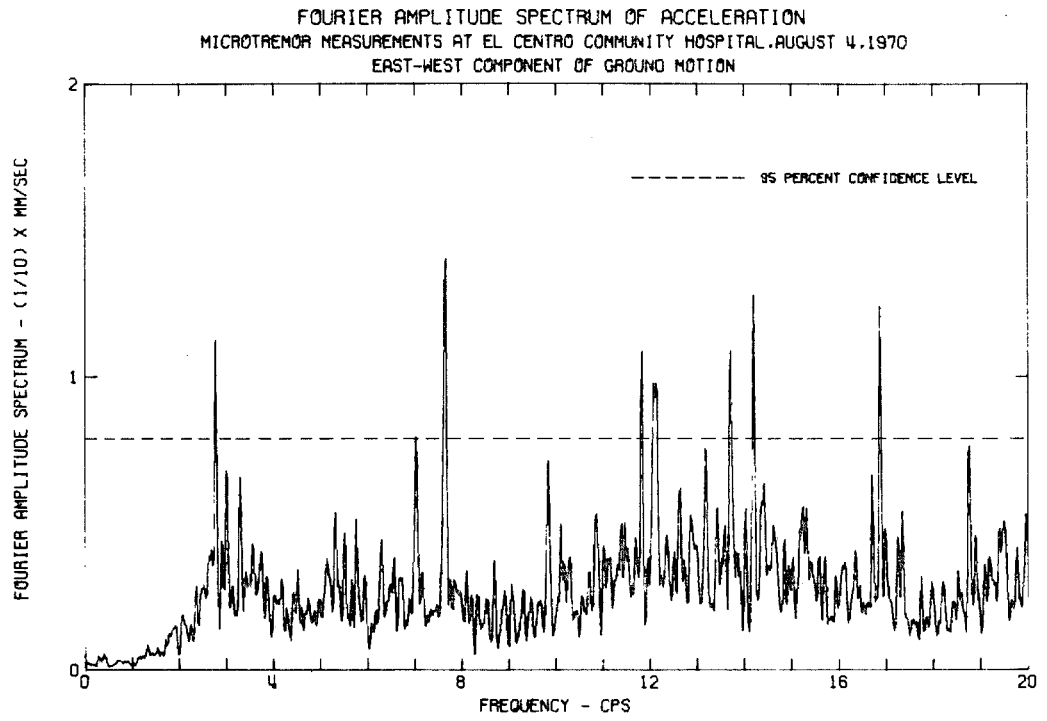
FOURIER AMPLITUDE SPECTRUM OF ACCELERATION
MICROTREMOR MEASUREMENTS AT EL CENTRO COMMUNITY HOSPITAL.AUGUST 4.1970
EAST-WEST COMPONENT OF GROUND MOTION
95 PERCENT CONFIDENCE LEVEL
FOURIER AMPLITUDE SPECTRUM - (1/10) X MM/SEC
FREQUENCY - CPS
0
1
2
0
4
8
12
16
20

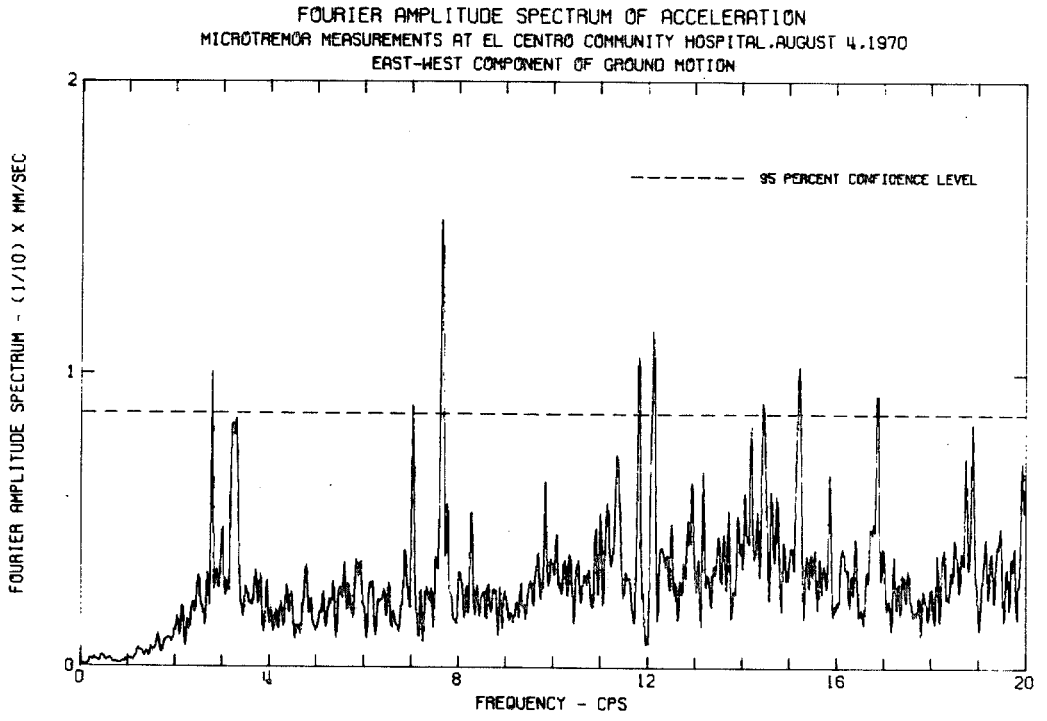
FOURIER AMPLITUDE SPECTRUM OF ACCELERATION
MICROTREMOR MEASUREMENTS AT EL CENTRO COMMUNITY HOSPITAL.AUGUST 4.1970
EAST-WEST COMPONENT OF GROUND MOTION
95 PERCENT CONFIDENCE LEVEL
FOURIER AMPLITUDE SPECTRUM - (1/10) X MM/SEC
FREQUENCY - CPS
0
1
2
0
4
8
12
16
20

FIGURE IV. 4

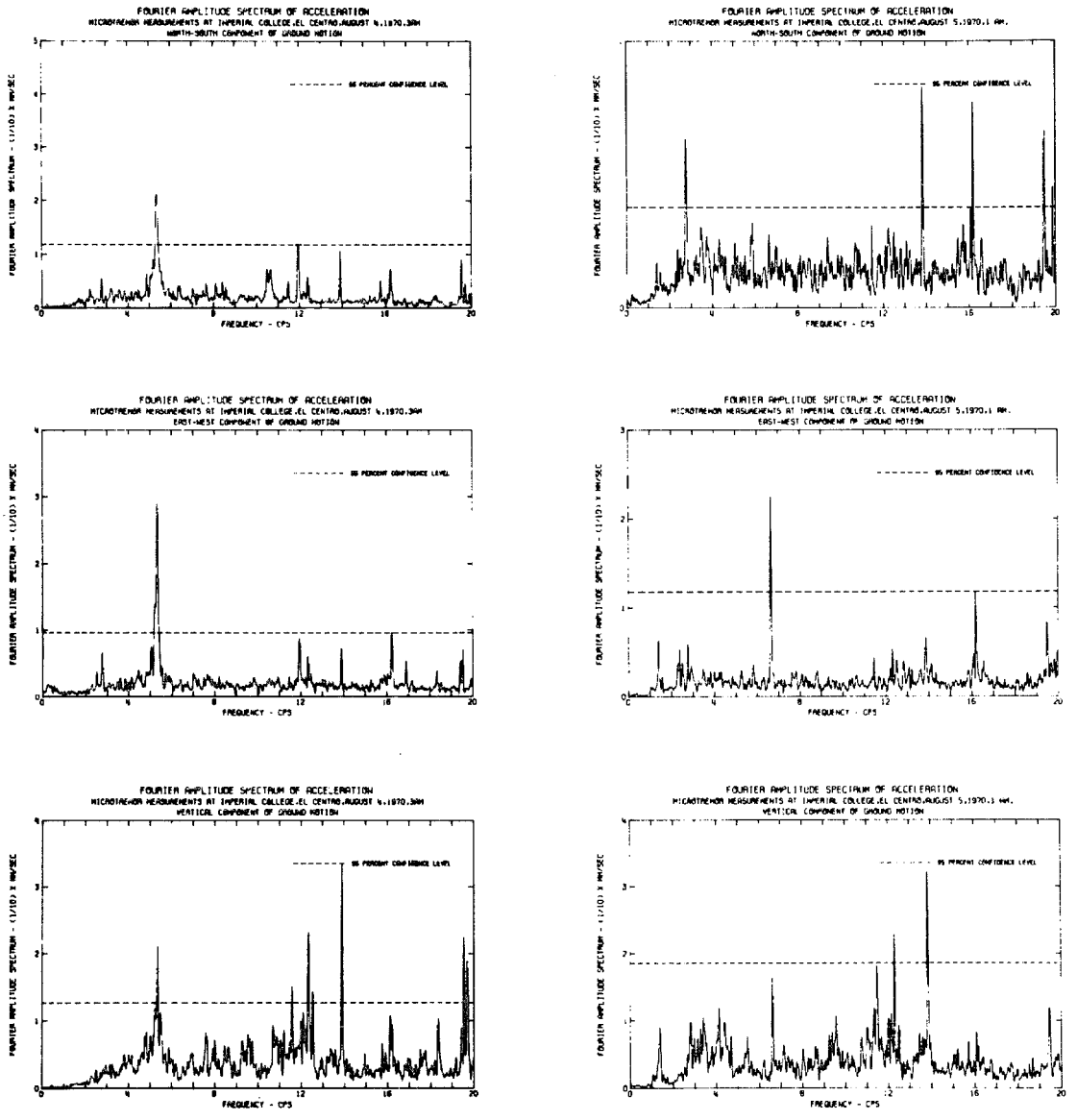
FOURIER AMPLITUDE SPECTRUM OF ACCELERATION
MICROTREMOR MEASUREMENTS AT IMPERIAL COLLEGE,EL CENTRO,AUGUST 4,1970,3PM
NORTH-SOUTH COMPONENT OF GROUND MOTION
95 PERCENT CONFIDENCE LEVEL
FOURIER AMPLITUDE SPECTRUM - (1/10) X MM/SEC
FREQUENCY - CPS
FOURIER AMPLITUDE SPECTRUM OF ACCELERATION
MICROTREMOR MEASUREMENTS AT IMPERIAL COLLEGE,EL CENTRO,AUGUST 5,1970,1 AM.
NORTH-SOUTH COMPONENT OF GROUND MOTION
95 PERCENT CONFIDENCE LEVEL
FOURIER AMPLITUDE SPECTRUM - (1/10) X MM/SEC
FREQUENCY - CPS
FOURIER AMPLITUDE SPECTRUM OF ACCELERATION
MICROTREMOR MEASUREMENTS AT IMPERIAL COLLEGE,EL CENTRO,AUGUST 4,1970,3PM
EAST-WEST COMPONENT OF GROUND MOTION
95 PERCENT CONFIDENCE LEVEL
FOURIER AMPLITUDE SPECTRUM - (1/10) X MM/SEC
FREQUENCY - CPS
FOURIER AMPLITUDE SPECTRUM OF ACCELERATION
MICROTREMOR MEASUREMENTS AT IMPERIAL COLLEGE,EL CENTRO,AUGUST 5,1970,1 AM.
EAST-WEST COMPONENT OF GROUND MOTION
95 PERCENT CONFIDENCE LEVEL
FOURIER AMPLITUDE SPECTRUM - (1/10) X MM/SEC
FREQUENCY - CPS
FOURIER AMPLITUDE SPECTRUM OF ACCELERATION
MICROTREMOR MEASUREMENTS AT IMPERIAL COLLEGE,EL CENTRO,AUGUST 4,1970,3PM
VERTICAL COMPONENT OF GROUND MOTION
95 PERCENT CONFIDENCE LEVEL
FOURIER AMPLITUDE SPECTRUM - (1/10) X MM/SEC
FREQUENCY - CPS
FOURIER AMPLITUDE SPECTRUM OF ACCELERATION
MICROTREMOR MEASUREMENTS AT IMPERIAL COLLEGE,EL CENTRO,AUGUST 5,1970,1 AM.
VERTICAL COMPONENT OF GROUND MOTION
95 PERCENT CONFIDENCE LEVEL
FOURIER AMPLITUDE SPECTRUM - (1/10) X MM/SEC
FREQUENCY - CPS

FIGURE IV. 5

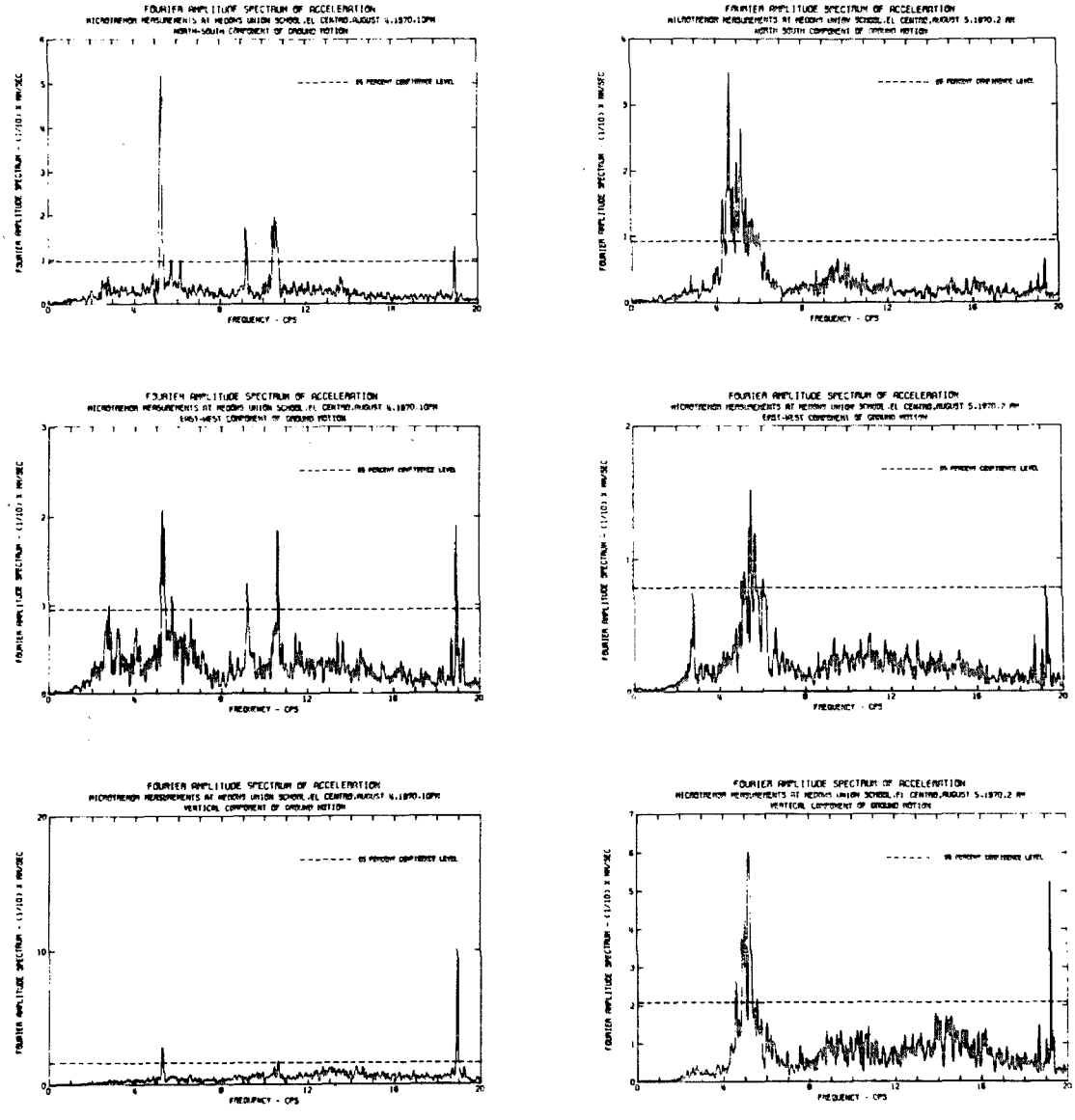

FIGURE IV. 6

over a several day period. The large changes in the spectra (Fig. IV.5-7) over time lengths of a day or so indicate that the process is not truly stationary and that considerable care needs to be exercised in interpreting spectral peaks obtained through the analysis of one particular record obtained at a site.

General Spectral Patterns and Analysis of Spectral Peaks

In comparison to earthquake spectra which are relatively narrow band the relative frequency content beyond 15 cps being very small (Fig. III.8-9), microtremor spectra cover a wider frequency range. The higher frequency components which are characteristic of the microtremor process can be attributed to two main causes. First, since the microtremor source areas are local in nature there is little opportunity for attenuation of the high frequencies with distance, as in the case for more distant earthquakes. Secondly, the microtremors are believed to be largely the result of excitations from rotating machinery, many of which undoubtedly are operating in this higher frequency range.

The microtremor spectra show a gradual increase in spectral amplitude with frequency. This is more noticeable in the vertical components which seem to have relatively low spectral contents at frequencies below 8 cps.

Of the three recording sites closest to the standard accelerograph site, one was revisited after an interval of 24 hours. Figures IV. 7, 8 and 9 indicate the Fourier amplitude spectra of the recorded motion. A comparison of these three figures which represent

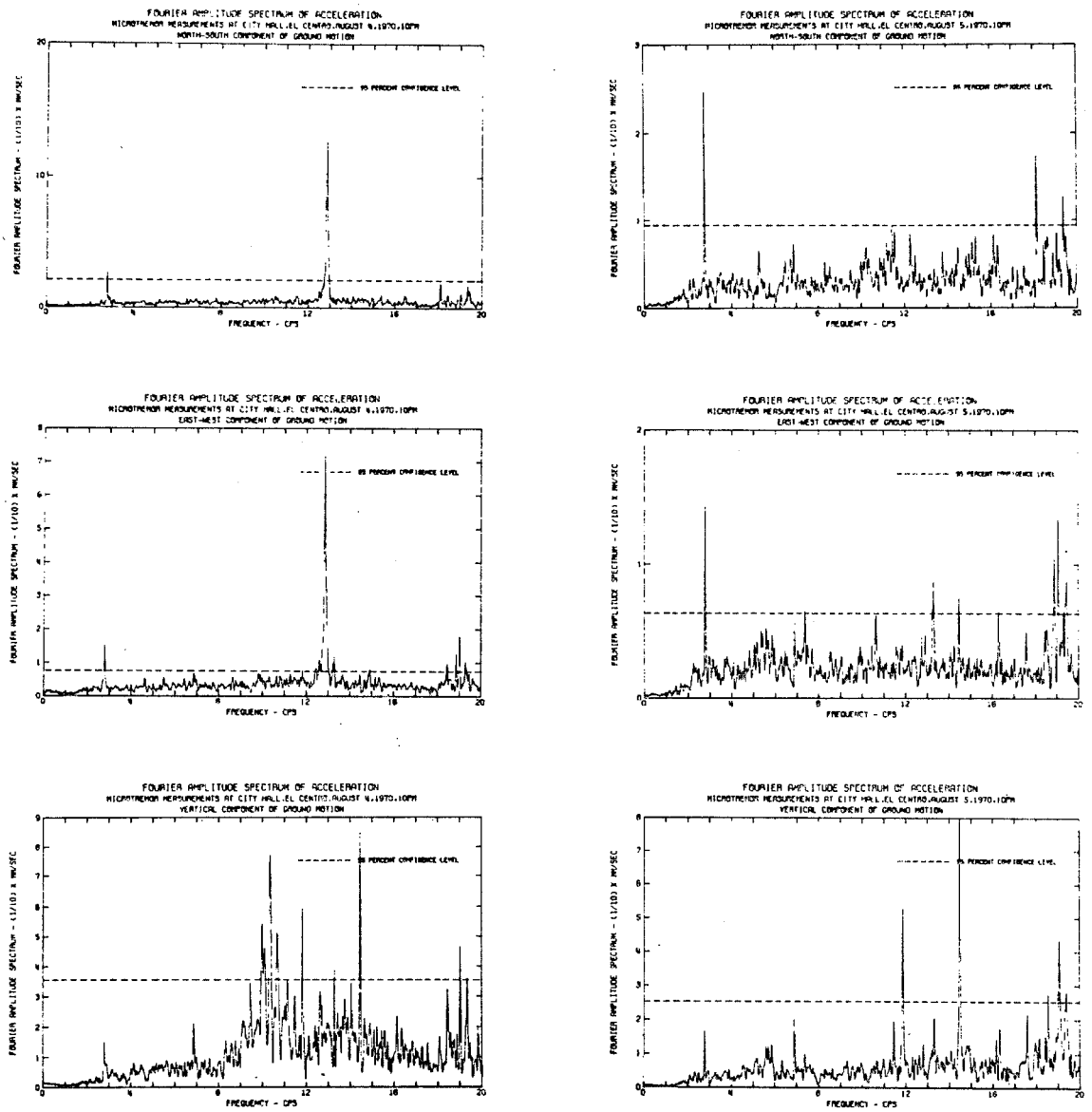
FOURIER AMPLITUDE SPECTRUM OF ACCELERATION
MICROTREMOR MEASUREMENTS AT CITY HALL,EL CENTRO,AUGUST 4,1970,10PM
NORTH-SOUTH COMPONENT OF GROUND MOTION
95 PERCENT CONFIDENCE LEVEL
FOURIER AMPLITUDE SPECTRUM - (1/10) X MM/SEC
FREQUENCY - CPS
FOURIER AMPLITUDE SPECTRUM OF ACCELERATION
MICROTREMOR MEASUREMENTS AT CITY HALL,EL CENTRO,AUGUST 5,1970,10PM
NORTH-SOUTH COMPONENT OF GROUND MOTION
95 PERCENT CONFIDENCE LEVEL
FOURIER AMPLITUDE SPECTRUM - (1/10) X MM/SEC
FREQUENCY - CPS
FOURIER AMPLITUDE SPECTRUM OF ACCELERATION
MICROTREMOR MEASUREMENTS AT CITY HALL,EL CENTRO,AUGUST 4,1970,10PM
EAST-WEST COMPONENT OF GROUND MOTION
95 PERCENT CONFIDENCE LEVEL
FOURIER AMPLITUDE SPECTRUM - (1/10) X MM/SEC
FREQUENCY - CPS
FOURIER AMPLITUDE SPECTRUM OF ACCELERATION
MICROTREMOR MEASUREMENTS AT CITY HALL,EL CENTRO,AUGUST 5,1970,10PM
EAST-WEST COMPONENT OF GROUND MOTION
95 PERCENT CONFIDENCE LEVEL
FOURIER AMPLITUDE SPECTRUM - (1/10) X MM/SEC
FREQUENCY - CPS
FOURIER AMPLITUDE SPECTRUM OF ACCELERATION
MICROTREMOR MEASUREMENTS AT CITY HALL,EL CENTRO,AUGUST 4,1970,10PM
VERTICAL COMPONENT OF GROUND MOTION
95 PERCENT CONFIDENCE LEVEL
FOURIER AMPLITUDE SPECTRUM - (1/10) X MM/SEC
FREQUENCY - CPS
FOURIER AMPLITUDE SPECTRUM OF ACCELERATION
MICROTREMOR MEASUREMENTS AT CITY HALL,EL CENTRO,AUGUST 5,1970,10PM
VERTICAL COMPONENT OF GROUND MOTION
95 PERCENT CONFIDENCE LEVEL
FOURIER AMPLITUDE SPECTRUM - (1/10) X MM/SEC
FREQUENCY - CPS

FIGURE IV. 7

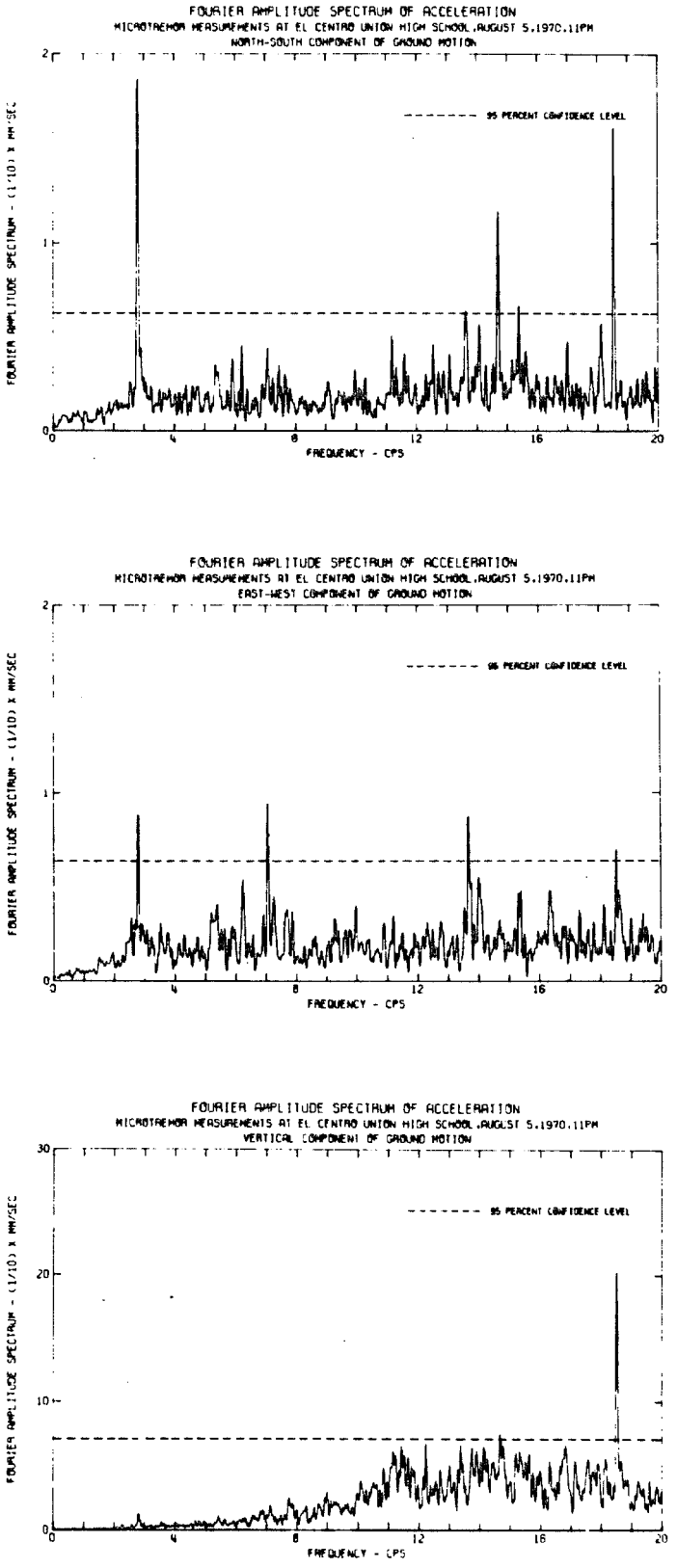
FOURIER AMPLITUDE SPECTRUM OF ACCELERATION
MICROTREMOR MEASUREMENTS AT EL CENTRO UNION HIGH SCHOOL,AUGUST 5,1970,11PM
NORTH-SOUTH COMPONENT OF GROUND MOTION
95 PERCENT CONFIDENCE LEVEL
FOURIER AMPLITUDE SPECTRUM - (1/10) X MM/SEC
FREQUENCY - CPS
FOURIER AMPLITUDE SPECTRUM OF ACCELERATION
MICROTREMOR MEASUREMENTS AT EL CENTRO UNION HIGH SCHOOL,AUGUST 5,1970,11PM
EAST-WEST COMPONENT OF GROUND MOTION
95 PERCENT CONFIDENCE LEVEL
FOURIER AMPLITUDE SPECTRUM - (1/10) X MM/SEC
FREQUENCY - CPS
FOURIER AMPLITUDE SPECTRUM OF ACCELERATION
MICROTREMOR MEASUREMENTS AT EL CENTRO UNION HIGH SCHOOL,AUGUST 5,1970,11PM
VERTICAL COMPONENT OF GROUND MOTION
95 PERCENT CONFIDENCE LEVEL
FOURIER AMPLITUDE SPECTRUM - (1/10) X MM/SEC
FREQUENCY - CPS

FIGURE IV. 8

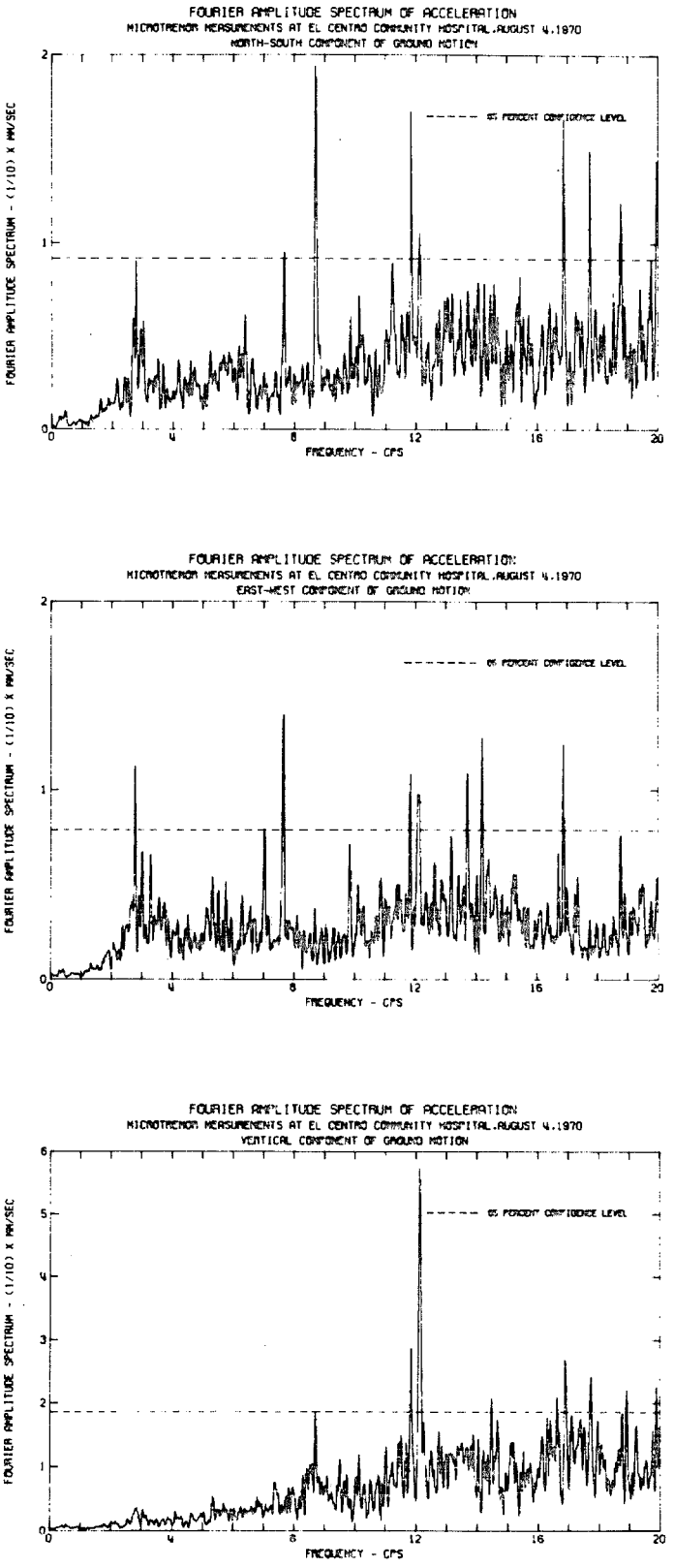
FOURIER AMPLITUDE SPECTRUM OF ACCELERATION
MICROTREMOR MEASUREMENTS AT EL CENTRO COMMUNITY HOSPITAL.AUGUST 4.1970
NORTH-SOUTH COMPONENT OF GROUND MOTION
95 PERCENT CONFIDENCE LEVEL
FOURIER AMPLITUDE SPECTRUM - (1/10) X MM/SEC
FREQUENCY - CPS
FOURIER AMPLITUDE SPECTRUM OF ACCELERATION
MICROTREMOR MEASUREMENTS AT EL CENTRO COMMUNITY HOSPITAL.AUGUST 4.1970
EAST-WEST COMPONENT OF GROUND MOTION
95 PERCENT CONFIDENCE LEVEL
FOURIER AMPLITUDE SPECTRUM - (1/10) X MM/SEC
FREQUENCY - CPS
FOURIER AMPLITUDE SPECTRUM OF ACCELERATION
MICROTREMOR MEASUREMENTS AT EL CENTRO COMMUNITY HOSPITAL.AUGUST 4.1970
VERTICAL COMPONENT OF GROUND MOTION
95 PERCENT CONFIDENCE LEVEL
FOURIER AMPLITUDE SPECTRUM - (1/10) X MM/SEC
FREQUENCY - CPS

FIGURE IV. 9

recordings in the urbanized zone of El Centro indicate little to no resemblances in their general trends. From an engineering viewpoint one would expect microregionalization to be an effective tool in the study of damage susceptibility if areas close to one another with similar subsoil conditions gave similar spectral characteristics of microtremor ground motions. As seen from the three figures, it would be difficult to attach any special significance to a particular spectral peak, since such peaks might simply be the result of an excitation marking what happened to be operating at the time the recording was made. For instance had the two recordings (Fig. IV.7) on August 4 and 5 not been made one might have concluded from the spectra obtained on August 4 that a sharp resonant ground frequency corresponding to 12.9 cps exists. The complete absence of such a peak after a lapse of 24 hours strongly indicates that it has been caused by some close-in rotating machinery. Another significant peak observed from the three figures is the one around 2.8 cps. The bar chart indicating the peaks that were above the 95% confidence level shown in Fig. IV.10 shows that a peak in this region generally occurs in all three components of ground motion. On further inspection of the spectra we observe that the form of the spectral peaks in this region for each particular site is identical but is different from site to site. One cannot, however, rule out the possibility of a site periodicity at this frequency. The nature of the three components of the spectra indicate comparable amplitudes in the two horizontal and the vertical directions. Considering the transfer function curves obtained by

Matthiesen, et al [56] for the El Centro site under the assumption of vertically propagating S waves, we note that this frequency of 2.8 cps is nowhere near any of the peaks of this numerically ascertained ground response function. Due to the difficulty in numerically computing the dispersion curves for such a frequency one cannot be sure of the interpretation of the wave nature associated with this frequency, though it seems quite likely that it may be caused by ground response to forced excitations originating close to the station. The subdued peak in the vertical component in Fig. IV.5 and general likeness in the spectra of the horizontal components at any one site seems to lend weight to the latter interpretation.

The last two sites chosen were both very close to the Imperial Fault. The spectra computed at the Imperial College site (Fig. IV.5) at intervals of 24 hours indicate that the two sets of spectra have distinctly dissimilar natures. The marked spectral peak at 5.5 cps observed in the spectra of August 4 has disappeared in the spectra of August 5 indicating that these peaks were possibly a result of forced oscillations of the ground surface caused by local sources. We also generally observe that the spectra of all three components look very similar giving a further indication that such a ground motion may be generated by the forced oscillations created by specific sources hence reflecting the nature of the source spectrum rather than the characteristic ground behavior. Also large differences in the amplitude levels in the NS direction are observed in the spectra (Fig. IV.5) clearly indicating the nonstationary nature of the source functions in the microtremor process.

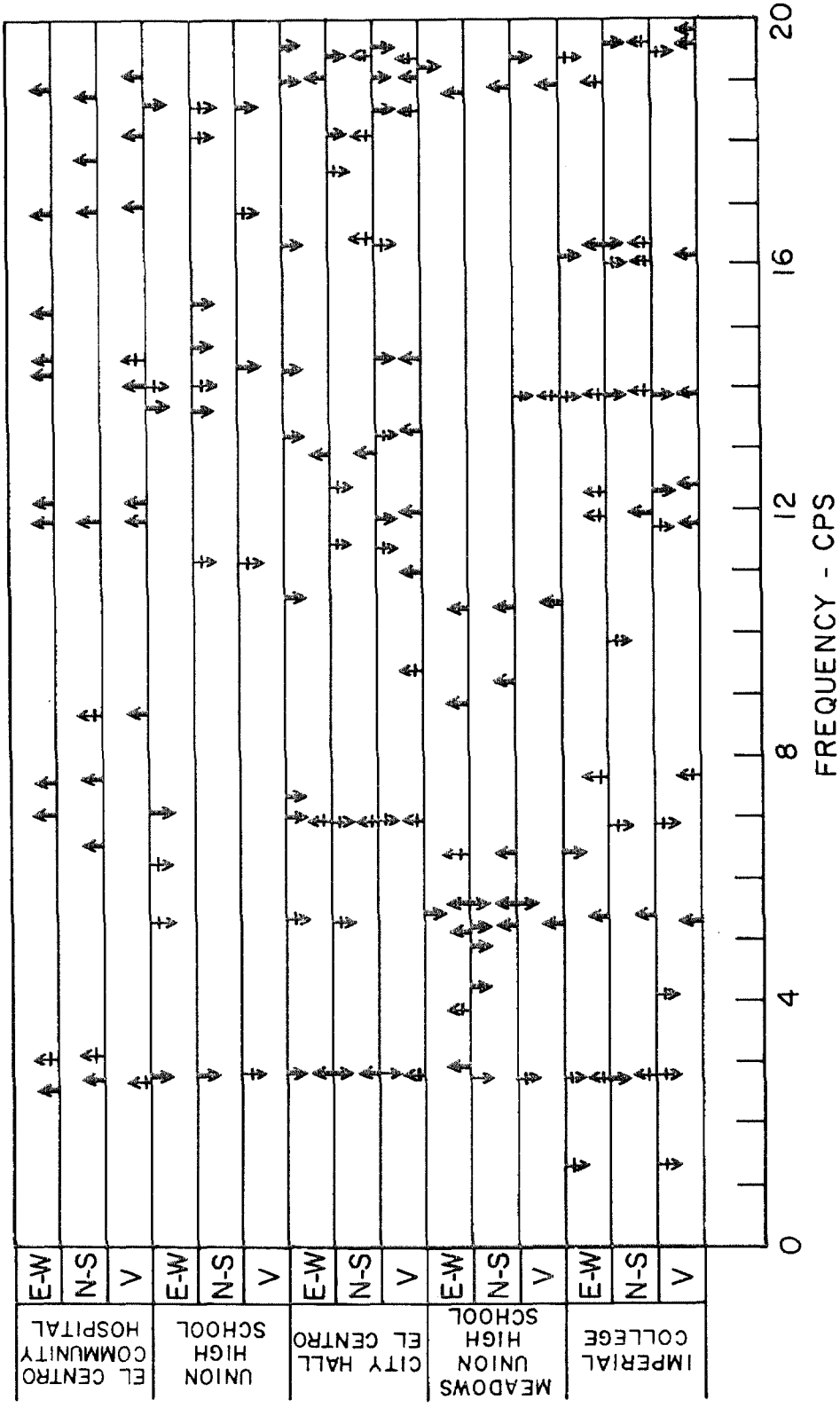
IMPERIAL COLLEGE
MEADOWS UNION HIGH SCHOOL
CITY HALL EL CENTRO
UNION HIGH SCHOOL
EL CENTRO COMMUNITY HOSPITAL
E-W
N-S
V
0
4
8
12
16
20
FREQUENCY - CPS

FIGURE IV. 10

The spectra observed at Meadows Union High School (Fig. IV.6) indicate similar features. The spectral peak around 5.3 cps could be interpreted as a possible site periodicity. However, the similar character of all three components of the spectrum seem to indicate some kind of a forced response of the ground to sources in the neighborhood.

The presence of marked spectral peaks caused by machinery, etc. tends to raise the 95% confidence levels and hence tends to hide the peaks of more significance to this study. In order to make a more thorough investigation it was decided to pick out by eye what might be significant peaks below the 95% confidence level and include them in the bar chart (Fig. IV.10). These are shown by crossed arrows on the chart. Since the detection of these peaks is a subjective process, the choices were independently made by two investigators and similar results were obtained. The scatter of the bars on the chart indicates that predominant frequencies if present are very difficult to spot. The bar chart however strongly indicates that a frequency of about 2.8 cps may have some special significance. The fact that it always seems to occur in all three components suggests that it might be the consequence of a forced oscillation. One cannot however rule out the possibility of a surface mode [58] at this frequency, as discussed above.

IV. 4 Conclusions from Microtremor Analysis

1. It has been illustrated that microtremor source processes are not stationary broad band processes with a flat spectrum making the interpretation of the spectra of these low amplitude ground motions

difficult from a single microtremor recording at a site. To obtain information on ground periodicity one would need to repeatedly take measurements at a site in the hope that each time the excitation patterns are so different that common spectral features can be attributed to "site conditions". This may make the study of soil vibrational characteristics through the application of microtremors a time consuming process, more uneconomical and less reliable than it would seem at first sight.

2. The examples above show that the general nature of microtremor ground motions are very different from those in strong ground shaking. The microtremor spectra show a gradual increase in amplitudes up to about 4-6 cps, leveling off somewhat beyond that frequency. Earthquake spectra seem to show larger energy concentrations in the 0 - 6 cps range dropping off sharply beyond that, primarily due to the attenuation of the high frequency components of earthquake ground motions.

3. The vertical components of ground motion have been found to be comparable to the horizontal components in microtremor processes. This would seem to refute the idea that microtremors are mainly multiple reflections of vertically incident SH waves. However these vertical components show little resemblance to the earthquake spectra.

4. The drastic differences in the spectra obtained over time intervals of a day at a site indicate wide variations in the nature of source excitations. Since these source excitations are unknown,

predominant frequencies associated with site conditions are difficult to pick out. The process that we record, then, seems to give details of the exciting function rather than the transfer function of the ground. The general trends in the spectra also seem to be quite different for sites close by each other that have similar subsoil conditions and also for recordings made at the same site at different times.

5. A repeated frequency of about 2.8 cps shows up in the data. This could be interpreted as being associated with a local soil condition. Other interpretations such as the effect of forced excitations are also possible. No other dominant frequencies in the 0 - 3 cps range were observed. Further, the parallel modeling of the soil with vertically incident SH waves does not satisfactorily interpret this frequency of 2.8 cps.

V. CONCLUSIONS

The major results reported in the previous sections may be summarized in the following way:

a) Analysis of El Centro accelerograms.

1) Strong ground shaking caused by close-in earthquakes depends strongly on the nature of the source. Accelerograms of smaller events show a relatively higher frequency content compared to those of larger events, other parameters like azimuth and epicentral distance being constant.

2) The motions recorded from large distant earthquakes indicate that surface waves play an important role in strong ground shaking.

3) The records obtained from different azimuths vary widely both in the relative arrival times of the different phases and in their spectral contents indicating that variations in travel path characteristics are important for this site.

4) The local magnitude scale may not be a consistent characterization of the nature of damaging motions at a site. Such factors as the location of the site with respect to faults and the character of the source mechanism may become important for close-in ground shaking.

5) As commonly observed for strong motion records, the spectra of the vertical components of earthquake ground motion show a broader band character as compared to the horizontal components indicating significant higher frequency components.

6) No distinctly identifiable site periodicities have been observed at the El Centro site. The effect of any local site condition seems to be

overshadowed by such factors as the nature of the source and the transmission path characteristics.

b) Analysis of microtremor ground motions at El Centro

1) Microtremor processes have been found to be nonstationary over periods of time of the order of a day.

2) Microtremor ground motions are distinctly different from strong earthquake ground motions. The spectral characteristics of microtremors indicate that a significant portion of their energy is in the higher (> 4 cps.) frequency range in which the earthquake spectra show markedly decreasing amplitudes.

3) The microtremors at El Centro have been interpreted to be largely forced oscillations of the ground caused by close-in excitations. Their spectral characteristics are thus more representative of the nature of the source input rather than of local subsoil characteristics. Their nonstationary nature makes the extraction of useful information on site characteristics very time consuming, difficult and highly unreliable.

4) No prominent peaks that could be directly related to site conditions were found in the microtremor spectra at El Centro. The peak found in the spectra at about 2. 8 cps. may be related to a site condition though there is strong evidence to believe that it is a consequence of forced ground oscillations.

5) The characteristics of microtremors and earthquake motions are so widely different that microregionalization based on microtremors may not be a meaningful approach to the evaluation of earthquake risk in the El Centro area.

Appendix I

SOME ASPECTS OF THE ANALYSIS OF EARTHQUAKE ACCELEROGRAMS AND MICROTREMOR DATA

Introduction

Information on the detailed time history of strong motion comes from accelerographs. These instruments usually record one vertical and two horizontal components of ground acceleration. Accelerograph records are used by earthquake engineers to study the design of earthquake-resistant structures, and by seismologists to study the nature of earthquake source mechanisms. Since these recorded ground accelerations represent the main source of basic data, it is essential to retrieve the maximum available information contained in them through the use of adequate data processing.

In order to decide on the nature of the data processing to be used and the accuracy of the final result obtained it is essential to understand the different errors that arise in the process of data acquisition, together with the instrumental limitations involved in recording the data.

To record ground accelerations, the relative response of a viscously-damped single degree of freedom oscillator is usually employed. The natural frequency of such a transducer is between 10 and 30 cps, while the equivalent viscous damping is about 60 - 70% of critical. The recorded relative instrument response approximates

accurately the ground acceleration up to about 1/2 or 3/4 of the natural frequency of the transducer. Thus, the direct instrument output can be used to represent ground accelerations up to about 5 to 15 cps, depending on the instrument. If higher frequency information is required, instrument correction of the accelerograms must be performed. This involves a calculation to recover the actual ground motion from a knowledge of the instrument characteristics and the response of the accelerograph.

The recovery of the high frequency content contained in a record has considerable importance in earthquake engineering. Modern computational methods in the dynamics of structures require an adequate representation of these high frequency components to study the response of special equipment and higher modes of building vibration. Also the nature of the source mechanism can be studied through the high frequency characteristics of earthquake spectra. Low frequency response is equally important since tall buildings may have fundamental frequencies as low as .2 to 1 cps and bodies of fluid may be excited with damaging motions at even longer periods.

The two basic steps involved in the processing of recorded strong-motion accelerograms are (a) a baseline correction in which frequency components less than 0.07 cps are removed from the data because they are indistinguishable from digitization noise, and (b) instrument correction in order to extend the validity of the data to higher frequencies.

The following sections review some of the aspects of data processing studied by the Caltech Earthquake Engineering group [39], [40] which are of special relevance for the present thesis. Section A deals with the nature of high frequency errors involved in uncorrected hand digitized paper accelerograms with particular reference to the different sources of high frequency errors. Section B deals with a method for instrument correction of the output obtained from a velocity transducer. The double differentiation scheme [40] used earlier has been further developed to include analog records obtained from velocity transducers during microtremor measurements. Section C deals with the use of the Fourier Transform in microtremor studies. A more detailed study of Fourier Transforms as used in the analysis of strong earthquake ground motions is presented in the EERL Report 71-100 [42].

A. Analysis of High-Frequency Errors

A.1 High-Frequency Errors in Digitization of Analog Traces

To determine the high-frequency domain in which uncorrected digitized accelerogram and microtremor noise data may be used, and to generate corrected accelerograms, a study has been made of errors present in the raw digitized data. These errors come from various sources and are in many cases dependent on the properties of each particular instrument.

Most high-frequency errors can be divided into several groups:

1. Modifications of the harmonic amplitudes and phase shifts caused by the finite natural frequency ω_n of the acceleration transducer.

2. The errors resulting from imperfections in the transducer design.
3. Random digitization errors.
4. Low pass filtering effects in the mechanical-optical digitization process.

There are also other types of errors present in analog record traces. Examples are errors caused by the transverse play of recording paper or film in the drive mechanism, warping of records from photographic processing and aging, the imperfect mechanical traverse mechanism of the cross-hair system on the digitizing table [40] and electronic noise from FM modulation-demodulation in tape recording. Although all these errors may contain some high-frequency components in the frequency range investigated here, experience with typical accelerograms recorded mainly on light-sensitive media indicates that these errors are negligible compared to the four main sources of errors listed above. We shall now consider each of these errors and describe how they affect the accuracy of the digitized accelerograms in the high-frequency domain.

1. Transducer Distortions of Amplitude and Phase. Modifications of harmonic amplitudes and phases of original input signals may be caused by the relatively low natural frequency of a transducer element. The relative motion x of the transducer mass is given by the differential equation

$$\ddot{x} + 2\omega_n \xi \dot{x} + \omega_n^2 x = -a(t) \qquad (A.1)$$

where ξ is a fraction of critical damping, ω_n is the natural frequency ($\omega_n = 2\pi F$) and a is the absolute ground acceleration. For acceleration transducers the largest possible ω_n is chosen so that the term $\omega_n^2 x$ dominates on the left-hand side of the equation. For input frequencies ω that are several times smaller than ω_n, $\ddot{x}$ and $2\omega_n \xi \dot{x}$ are small, and $\omega_n^2 x$ is nearly the same as -a(t). Therefore the transducer response is proportional to the absolute ground acceleration. For the higher input frequencies, both amplitudes and phases are modified and the correction terms involving $\ddot{x}$ and $2\omega_n \xi x$ may not be neglected.

2. Imperfections in the Transducer Design. To simplify instrument response interpretation, the strong motion acceleration transducers are designed to act as single degree of freedom viscously damped oscillators. Unfortunately, it is not always feasible to design an ideal single-degree-of-freedom oscillator, so that most of the transducers presently existing are essentially multi-degree-of-freedom systems. Their design is aimed at using only the fundamental mode of vibration so that the higher modes will not be excited to the extent that the simplified theory based on a single-degree-of-freedom oscillator cannot be approximately applied. Since most accelerometers are used for frequencies lower than the fundamental frequency of the transducer, these simplifying assumptions are quite justified in most cases. However, for a correct characterization of higher frequency components one would need to consider the higher modes of vibration of the transducer element. The frequencies corresponding to the higher modes of vibration of the transducers used in this particular

ENLARGED PORTION OF A TYPICAL
OPTICALLY RECORDED ACCELEROGRAPH RECORD

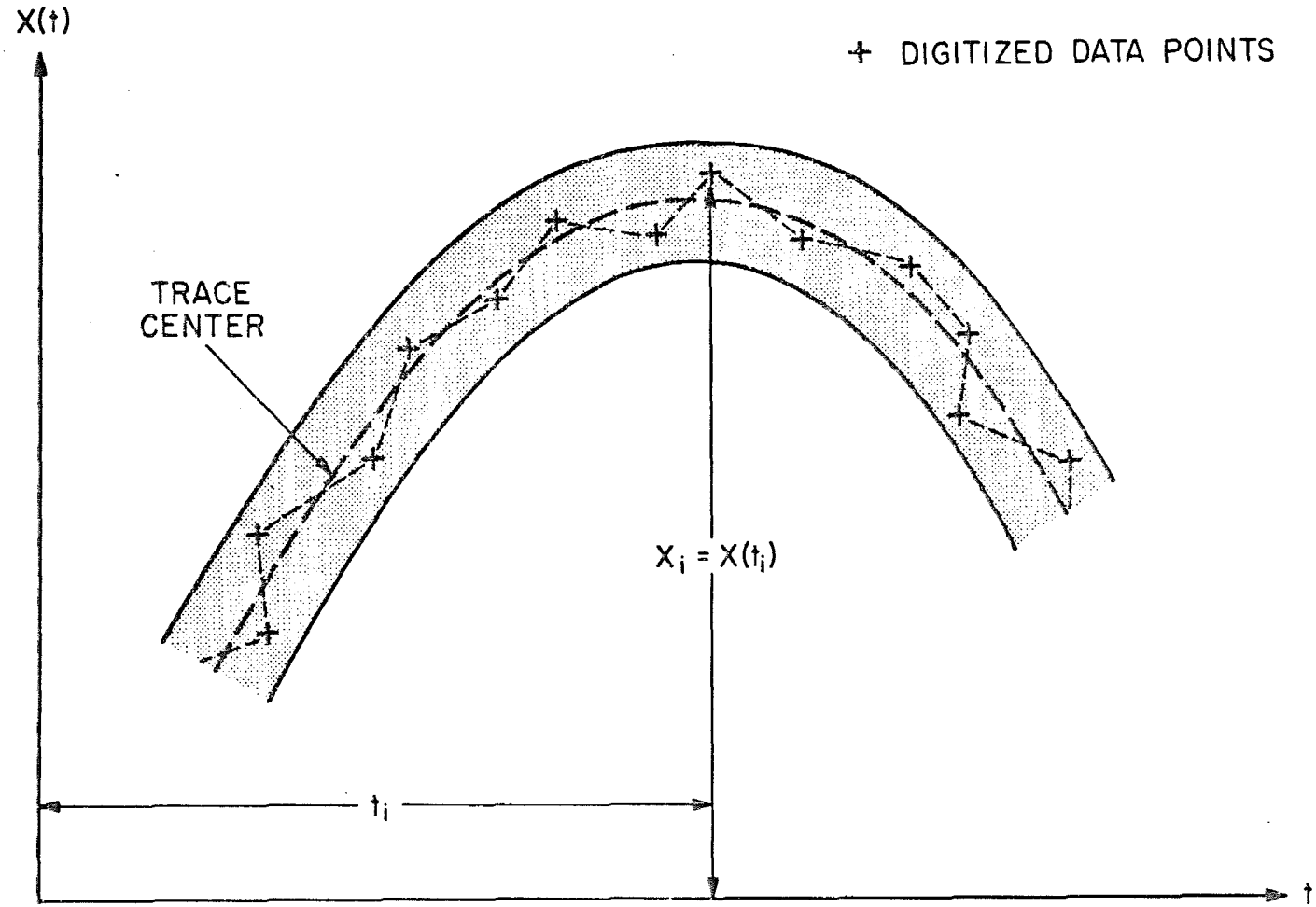

Figure A. 1

study exceed the frequency limit (≈ 25 cps) set by other factors, as will be shown later, so that this effect does not need further consideration here.

3. Random Digitization Errors. The process of optical digitization introduces errors which are of three basic kinds:

(a) "Human Error", because of the inability of the operator to pick out the centerline of the analog trace.

(b) "Discretization Error", because the accuracy of the digital data is limited to one digitizer unit, and

(c) "Systematic Error" built into the optical digitizing system.

The first two will be collectively referred to as random digitization errors.

Figure A.1 shows part of a typical photographically recorded trace. During the digitization process the operator attempts to align the cross-hair with the center of the trace as indicated by the dashed line in Figure A.1. It has been demonstrated [39] that if the operator is careful, is not biased in choosing the points, and the digitization of every point is independent of the previous ones the errors are nearly normally distributed with zero mean and the average standard deviation $\sigma \approx 1/300$ cm. This standard deviation may be affected by the equipment used for this particular study (Benson Lehner 099D Data Reducer) but is probably a good estimate of many sets of random digitization errors on other equipment as well. These errors are the main reason why one cannot differentiate the digitized data without a serious high-frequency noise problem.

To analyze the properties of high-frequency errors in digitized accelerograms a sloping straight line [40] was digitized five times by four operators. One operator repeated the digitization and used a magnifying glass to see whether there was a significant improvement in the accuracy of the digitization. Since it was taken under essentially the same conditions as the other four, and there was only a slight improvement, that digitization was taken as another independent trial. After five digitizations were completed, a sloping straight line was least-square fitted to each set of data, translating and rotating it to a horizontal line. The five sets of data obtained in this way are shown in Fig. A.2. In order to maintain the generality of these results, the straight lines (Fig. A.2), here treated as accelerograms, are given in units of pts/cm^2, where one point corresponds to a unit of the vertical digitized scale equal to 1/312 cm and the horizontal axis is measured in centimeters.

Since the digitizing errors are nearly normally distributed, with zero mean, across the ensemble of five sequences, by averaging the five digitizations one can approximately eliminate random errors and by subtraction obtain systematic errors caused by imperfect digitizing equipment. The average of the digitizations is also shown in Fig. A.2. Differences between each individual digitization Z_i and the average $\overline{Z}$ then approximately represent the random digitization errors.

Predominant frequencies in random digitization errors were obtained by averaging the five Fourier amplitude spectra computed for each $Z_i - \overline{Z}$. The average of the five spectra is given in Fig. A.3.

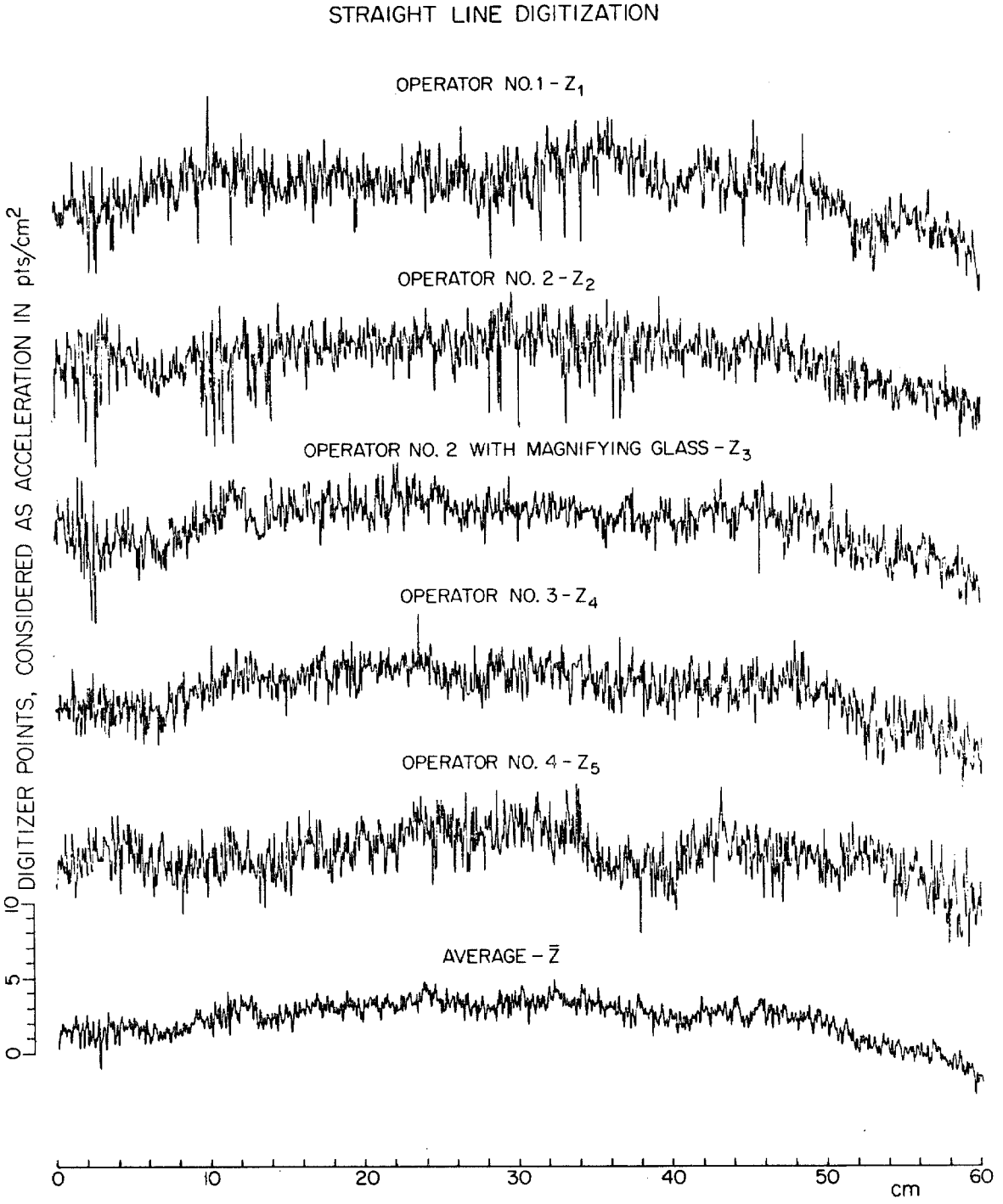
STRAIGHT LINE DIGITIZATION
OPERATOR NO.1 - Z_1
OPERATOR NO. 2 - Z_2
OPERATOR NO. 2 WITH MAGNIFYING GLASS - Z_3
OPERATOR NO. 3 - Z_4
OPERATOR NO. 4 - Z_5
AVERAGE - $\bar{Z}$
DIGITIZER POINTS, CONSIDERED AS ACCELERATION IN pts/cm²
0
5
10
0
10
20
30
40
50
60
cm

Figure A.2

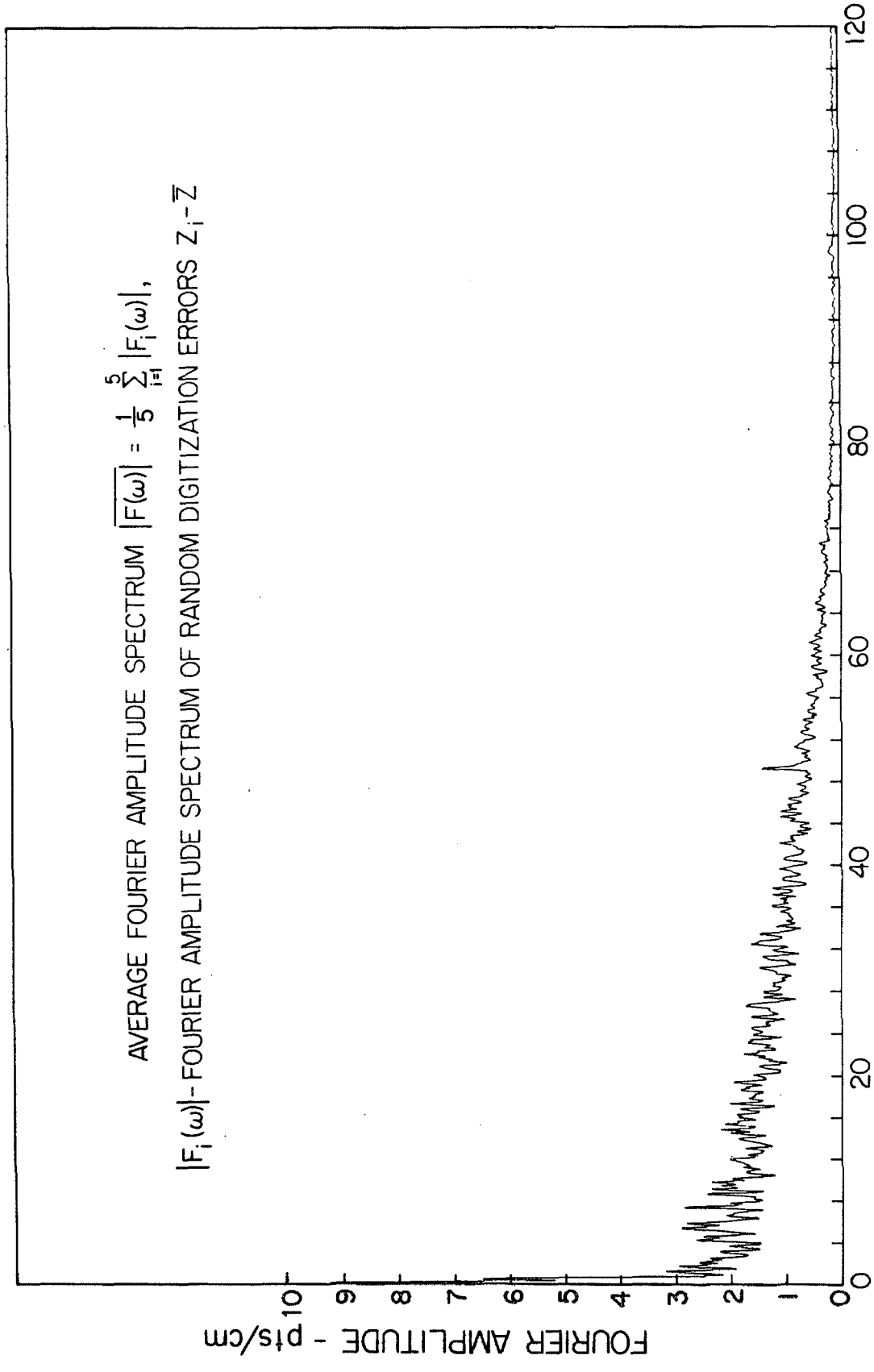
AVERAGE FOURIER AMPLITUDE SPECTRUM $\overline{|F(\omega)|} = \frac{1}{5}\sum_{i=1}^{5}|F_i(\omega)|$,
$|F_i(\omega)|$- FOURIER AMPLITUDE SPECTRUM OF RANDOM DIGITIZATION ERRORS $Z_i - \overline{Z}$
FOURIER AMPLITUDE - pts/cm
FREQUENCY - rad/cm
0
1
2
3
4
5
6
7
8
9
10
0
20
40
60
80
100
120

Figure A.3

For instrument correction it is necessary to differentiate the digitized function twice. As already mentioned, such a process amplifies high-frequency random digitization errors. To show the Fourier amplitude spectrum of these errors, five Fourier spectra calculated for five differences $Z_i - \overline{Z}$ were multiplied by ω^2 and averaged. The result is shown in Figure A.4.

The resolution during the digitization process is reduced because of the thickness of the digitizer cross-hair and the parallax. The parallax on the 099D Benson Lehner data reducer amounts to one to two digitizer points (1 point = 1/312 cm) and is treated here as part of the random digitization errors.

The relative importance of the two main constituents of the random digitization error, namely the human error and the discretizing error, can be studied in further detail as far as their effect on the final probability distribution of the total error is concerned.

(a) Human error: Denoting the human error in choosing the centerline of the trace by ϵ, its probability distribution can be approximated by one of those shown in Fig. A.5 (a) and (b), where 2n indicates the thickness of the line in digitizer units.

When the trace is thin (n lying between say 2 and 5) the distribution would be relatively constant across the thickness of the line. As the thickness of the line increases, the distribution will have a larger spread but will be more peaked towards the center. From the above distribution it may be noted that the variance of the distribution does not necessarily keep increasing with line thickness.

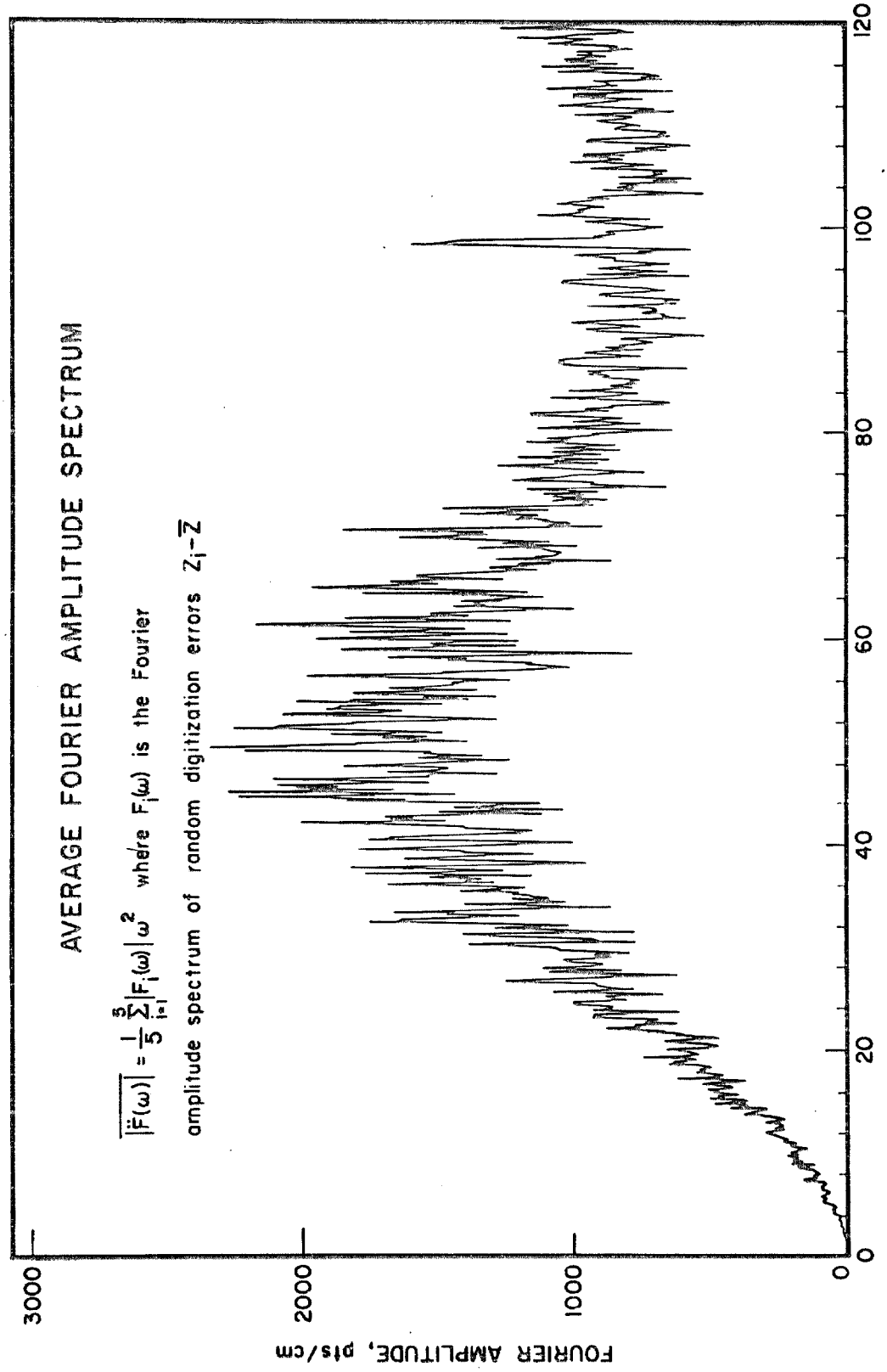
AVERAGE FOURIER AMPLITUDE SPECTRUM
$\overline{|F(\omega)|} = \frac{1}{5}\sum_{i=1}^{5}|F_i(\omega)|\omega^2$ where $F_i(\omega)$ is the Fourier
amplitude spectrum of random digitization errors $Z_i - \bar{Z}$
FOURIER AMPLITUDE, pts/cm
3000
2000
1000
0
0
20
40
60
80
100
120
FREQUENCY, RAD/CM

Figure A. 4

SIMPLIFIED PROBABILITY DENSITY FUNCTIONS FOR THE DIGITIZING ERROR ϵ

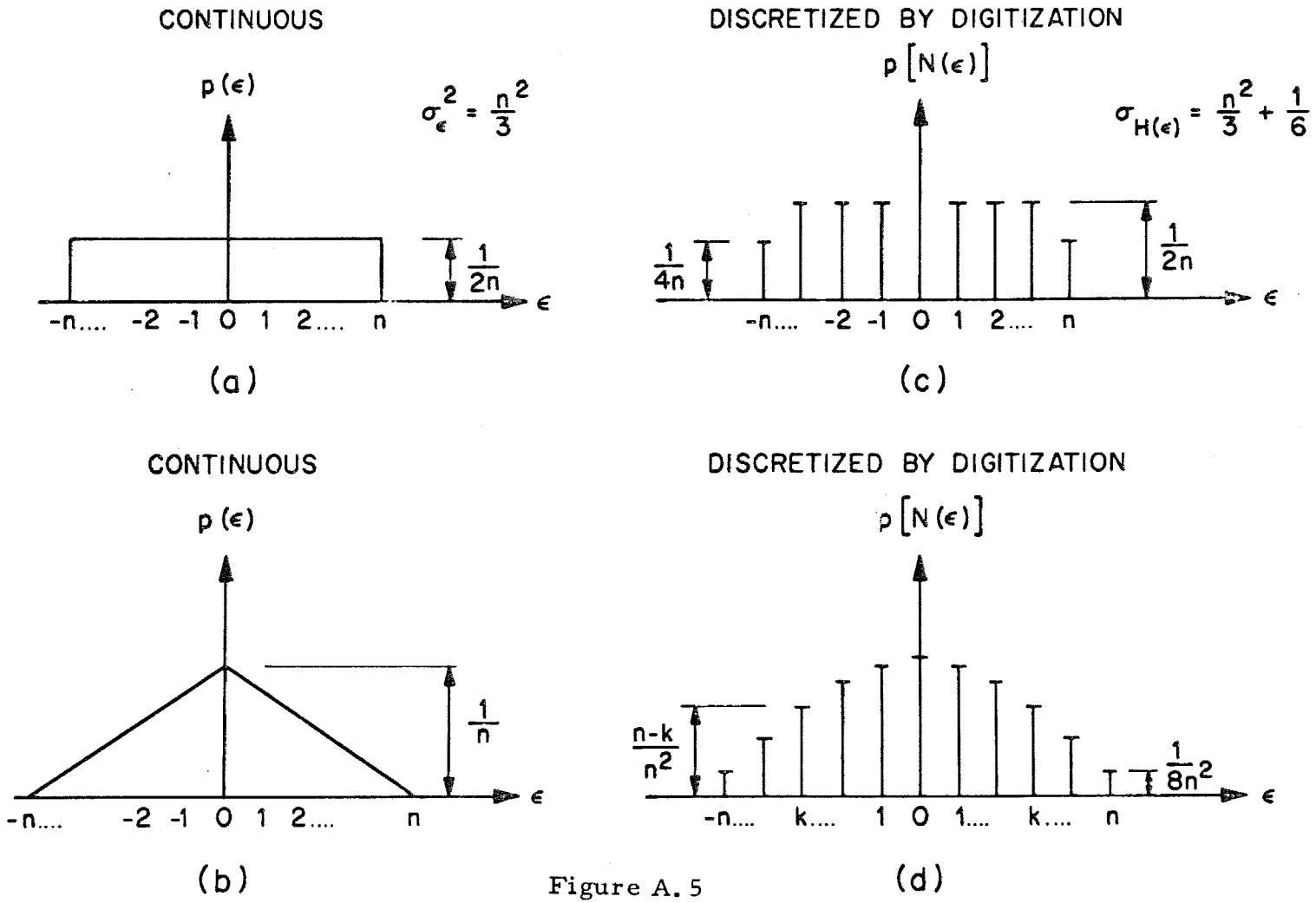

Figure A.5

(b) Discretization error: The digitizer can be described mathematically as a nonlinear operator N, such that

$$N(y) = \text{int}[y] + H\Big(2(y - \text{int}[y]) - 1\Big) \qquad (A.2)$$

where int[y] denotes the integer part of y and H is the unit step operator.

Figure A.7 a indicates the process of digitization. The dashed line indicates the centerline of a segment of a typical acceleration trace being digitized. The operator attempts to place the cross hair of the digitizer exactly on the centerline of the trace. It may be noted that even if he were capable of doing this, the digitized output would still be in error by an amount δ here referred to as the truncation error. However, since the operator cannot pick out the centerline of the trace exactly, he creates an error ϵ in picking it out. Hence, the cross hair instead of being placed at a distance y from the zero level of the digitizer is set at a distance $y+\epsilon$ from the t axis (Fig. A.7 a). This quantity is then discretized by the digitizer through the operator N so that the recorded ordinate of the point becomes $N(y+\epsilon)$. The digitizer discretization operator can be further studied by dividing the discretization process into two cases.

In the first case, y coincides with a certain discretization level of the digitizer, implying that $\delta \equiv 0$ (Fig. A.7 a). This situation is shown schematically in Fig. A.6(a). The probability distribution of $N(\epsilon)$ corresponding to the assumed distribution of ϵ given in Fig. 5(a) and (b) can then be obtained. It may be noted that the new distribution is discrete, has a somewhat larger variance than that of $p(\epsilon)$ and is

DIGITIZER DISCRETIZATION OPERATOR N

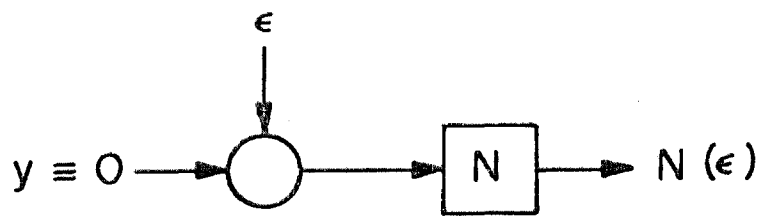

(a)

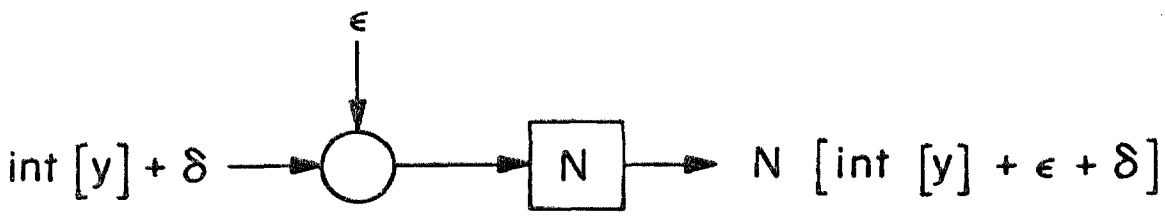

(b)

Figure A.6

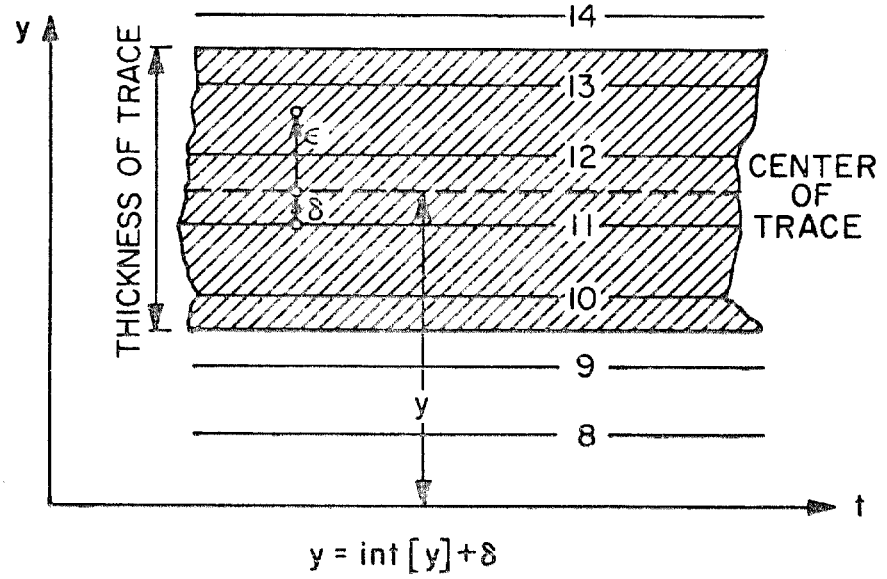

Figure A.7a Enlarged portion of a typical optically digitized record showing the true ordinate y and the recorded ordinate N(int[y] + e + δ).

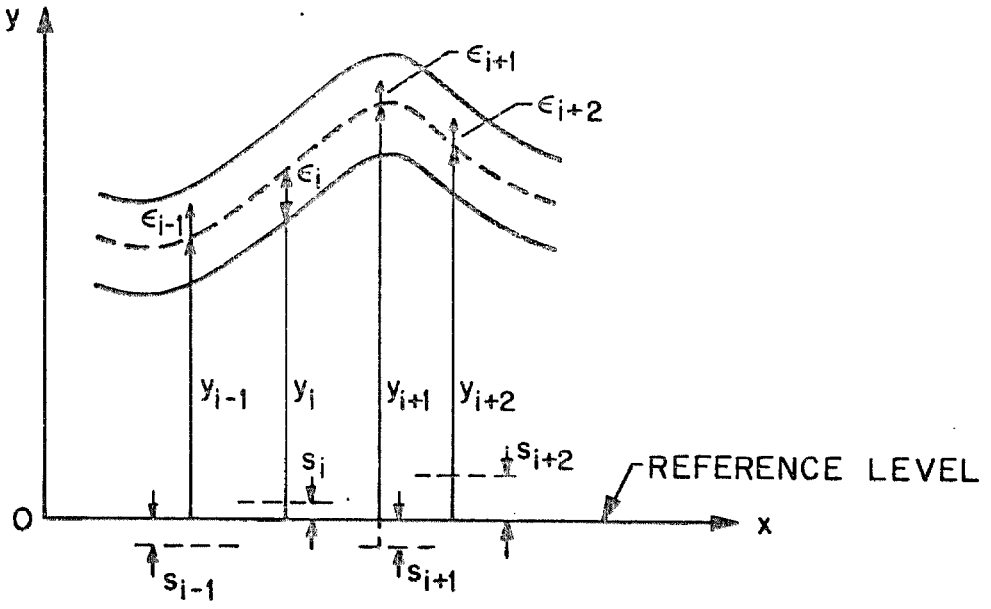

Figure A.7b Systematic error caused by a shift in the baseline with respect to a fixed reference level.

symmetric. For the case where n = 3 (which would correspond to a "thin" trace whose thickness is about 1/5 mm) the percentage change due to the presence of the discretization error is about 6%.

Next, we consider the case where y does not coincide with an exact digitization level, so that $\delta \neq 0$, as indicated in Fig. A. 6 (b).

The total error E, in the digitization process then becomes

$$E = N(\epsilon + \delta) - \delta$$

The probability density function $p(\delta)$ depends on the nature of the function being digitized. Assuming that the digitization is done at close enough intervals along the time axis, δ can be considered a random uniformly distributed variable for most accelerograms as shown in Fig. A.8. Knowing $p(\epsilon)$ and $p(\delta)$, $p[N(\epsilon + \delta)]$ can be calculated, and hence the distribution of the error E.

To illustrate the effect of the error δ, we again take $p(\epsilon)$ to be that shown in Fig. A.5 (a). The distribution of $p(N(\epsilon + \delta))$ is shown in Fig. A.9 (a) and that of the error E is shown in Fig. A.9 (b). From the figure for n = 2, the variance of the new distribution $\sigma^2_E = \frac{4}{3} + \frac{1}{6} + \frac{1}{12}$. Comparing this with the variance of the error in the case where $\delta \equiv 0$, $\sigma^2_{N(t)} = \frac{4}{3} + \frac{1}{6}$, we note that the presence of δ has increased the variance of the error by only a small amount.

This suggests that the discretizing error, herein represented by the parameter δ and the operator N is not as significant as the human error involved in the digitization process, even in cases where the trace is thin and well discernible by the eye. This indicates that errors involved in digitization are more a consequence of the human limitation

PROBABILITY DISTRIBUTION $p(\delta)$
δ = DIGITIZER TRUNCATION ERROR

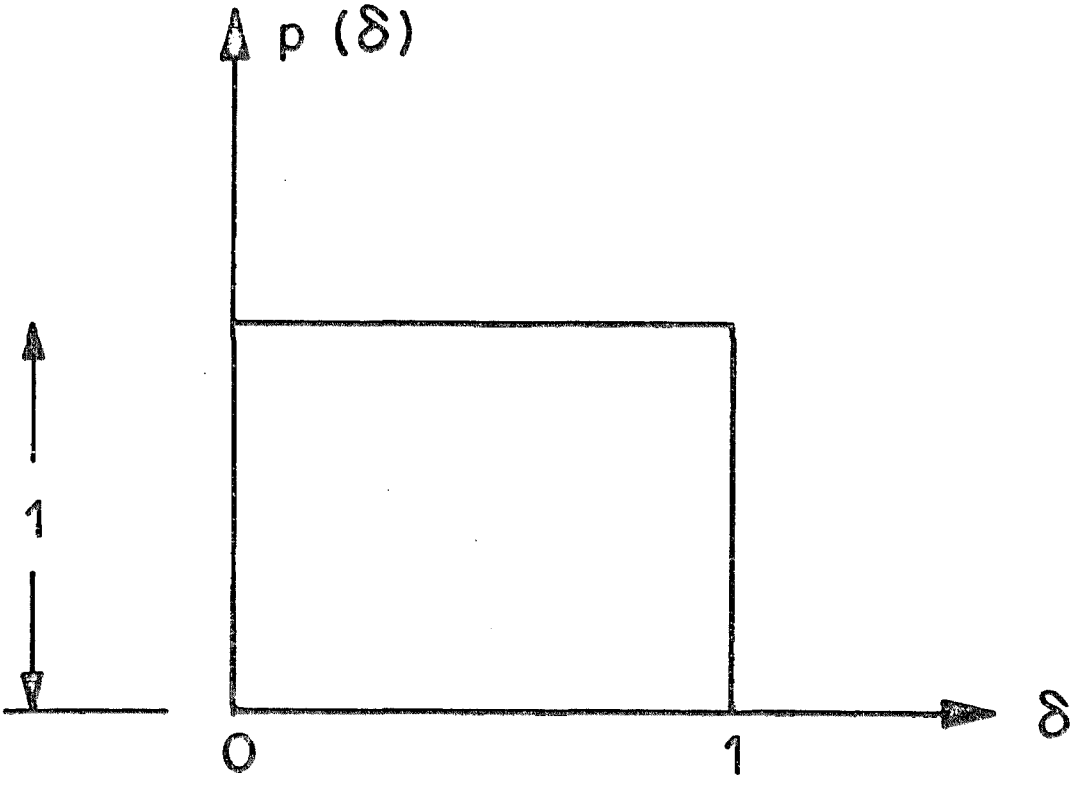

Figure A. 8

PROBABILITY DISTRIBUTION $p[N(\epsilon+\delta)]$

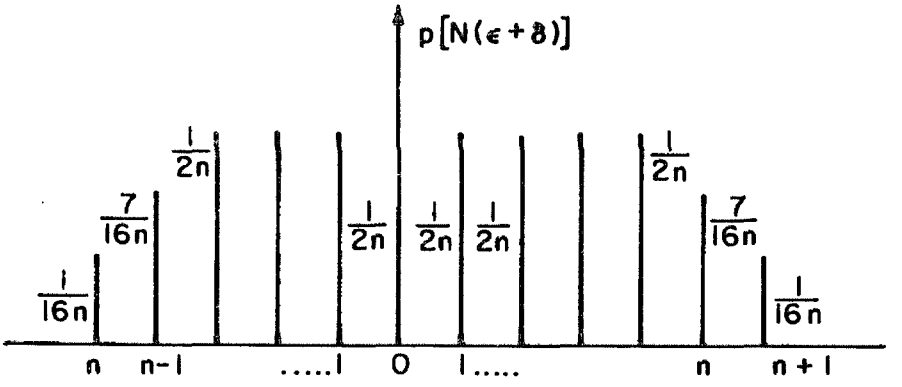

(a)

PROBABILITY DISTRIBUTION $p(E)$

$E=N(\epsilon+\delta)-\delta$

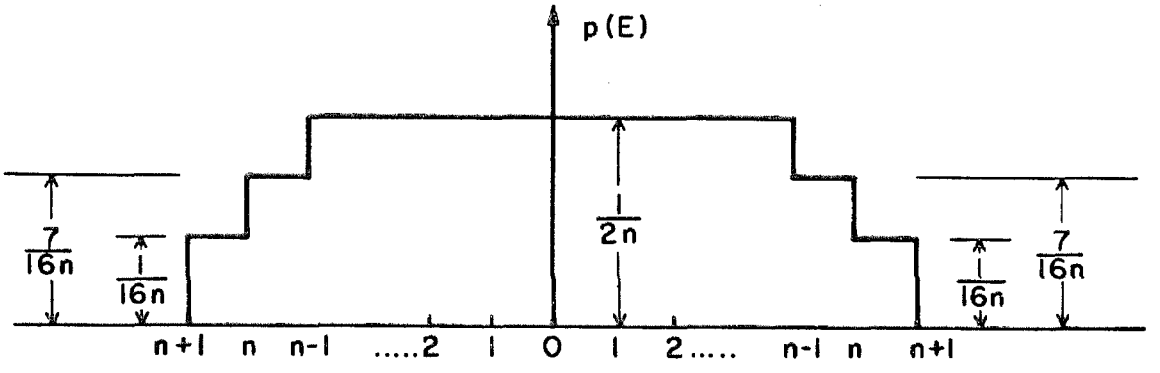

(b)

Figure A.9

in picking out the centerline of a trace rather than the instrumental limitations set up due to the limited resolution of the Benson-Lehner instrument currently being used.

(c) Systematic error: A systematic error is caused by imperfections in the mechanical carriage system of the vertical cross beam on the digitizer. Let us assume that the true ordinates of the centerline of the trace can be referred to a particular set of axes which we shall denote as the "reference axes" (Fig. A.7 (b)). A systematic error arises due to a shift in the base axis as the cross hair is moved horizontally across the digitizing table. These base axis locations at points x_{i-1}, x_i, x_{i+1}, x_{i+2} are indicated by dashed lines in Fig. A.7 (b). s_i denotes the shift in the base level at x_i. Referring the curve to be digitized to the reference axes, the digitized ordinate y_i' corresponding to x_i is given, as before, by

$$y_i' = y_i + \epsilon_i$$

where, y_i is the distance from the fixed reference level to the centerline of the trace and ϵ_i is the random digitizing error. However the shift in base level from point to point as one moves along the x-axis causes the digitizer output O_i to be represented as

$$O_i = N(y_i' - s_i)$$

Since the digitization operator is not a linear operator,

$$N(x+y) \neq N(x) + N(y).$$

However,

$$N(x+y) = N(x) + N(y) + \begin{Bmatrix} 0 \\ 1 \end{Bmatrix}.$$

Using this we have

$$O_i = N[(y+\epsilon)_i] + N(-s_i) + \begin{Bmatrix} 0 \\ 1 \end{Bmatrix}$$

where the vector $\{^0_1\}$ implies that either the value 0 or 1 will be picked up depending on the value of $(y+\epsilon)_i$.

As shown earlier,

$$N[(y+\epsilon)_i] = N\left\{\text{int}[y_i] + \epsilon_i + \delta_i\right\}.$$

Denoting by E_i the quantity given by

$$E_i = N[(y+\epsilon)_i] - y_i$$
$$= N[(\epsilon+\delta)_i] - \delta_i$$

we have,

$$N[(y+\epsilon)_i] = y_i + N[(\epsilon+\delta)_i] - \delta_i$$

so that,

$$O_i = y_i + N[(\epsilon+\delta)_i] - \delta_i + N(-s_i) + \gamma(0,1)$$

where γ can be assumed to be a random variable that acquires values 0 or 1 with equal probability.

Considering now in greater detail the procedure used in the error analysis in Part (a) of this section we have

$$^k z_i = {}^k O_i - \hat{}^k O$$

where the superscript denotes the k^{th} operator, and $\hat{}^k O$ denotes the least square fitted line to the data $^k O_i$ obtained at the points $i = 1, 2, \ldots$ by the k^{th} operator. Also, the expected value of z_i is

$$E[z_i] = y_i + E\left\{N[(\epsilon+\delta)_i] - \delta_i\right\} + N(-\delta_i) + E(\gamma) - E[\hat{O}].$$

But by assumption (Fig. A.9)

$$E\left\{N[(\epsilon+\delta)_i] - \delta_i\right\} \equiv 0$$

and

$$E[\gamma] \equiv 0$$

Hence

$$E\left[{}^{k}z_i\right] = y_i + N(-s_i) - E[\hat{O}]$$

and

$${}^{k}z_i - E\left[{}^{k}z_i\right] = N\left\{(\epsilon+\delta)_i - \delta_i\right\} + \gamma + E[\hat{O}] - \hat{k}_O$$

Since

$$E[\hat{O}] \approx \hat{k}_O$$

$${}^{k}z_i - E\left[{}^{k}z_i\right] = {}^{k}z_i - \bar{z}_i$$

$$= [N(\epsilon+\delta)_i - \delta_i] + \gamma$$

$$= E_i + \gamma$$

We observe then that the "systematic error" arising out of a systematic shift in base level from point to point in the horizontal traversal of the cross hair leads to an additional random error γ.

4. Low-Pass Filtering Effects of the Optical-Mechanical Digitization. During a typical optical digitization process the operator attempts to define a continuous function by a sequence of discrete points. Although the accuracy of the process depends on each individual operator and the purpose for which the record is to be used, some

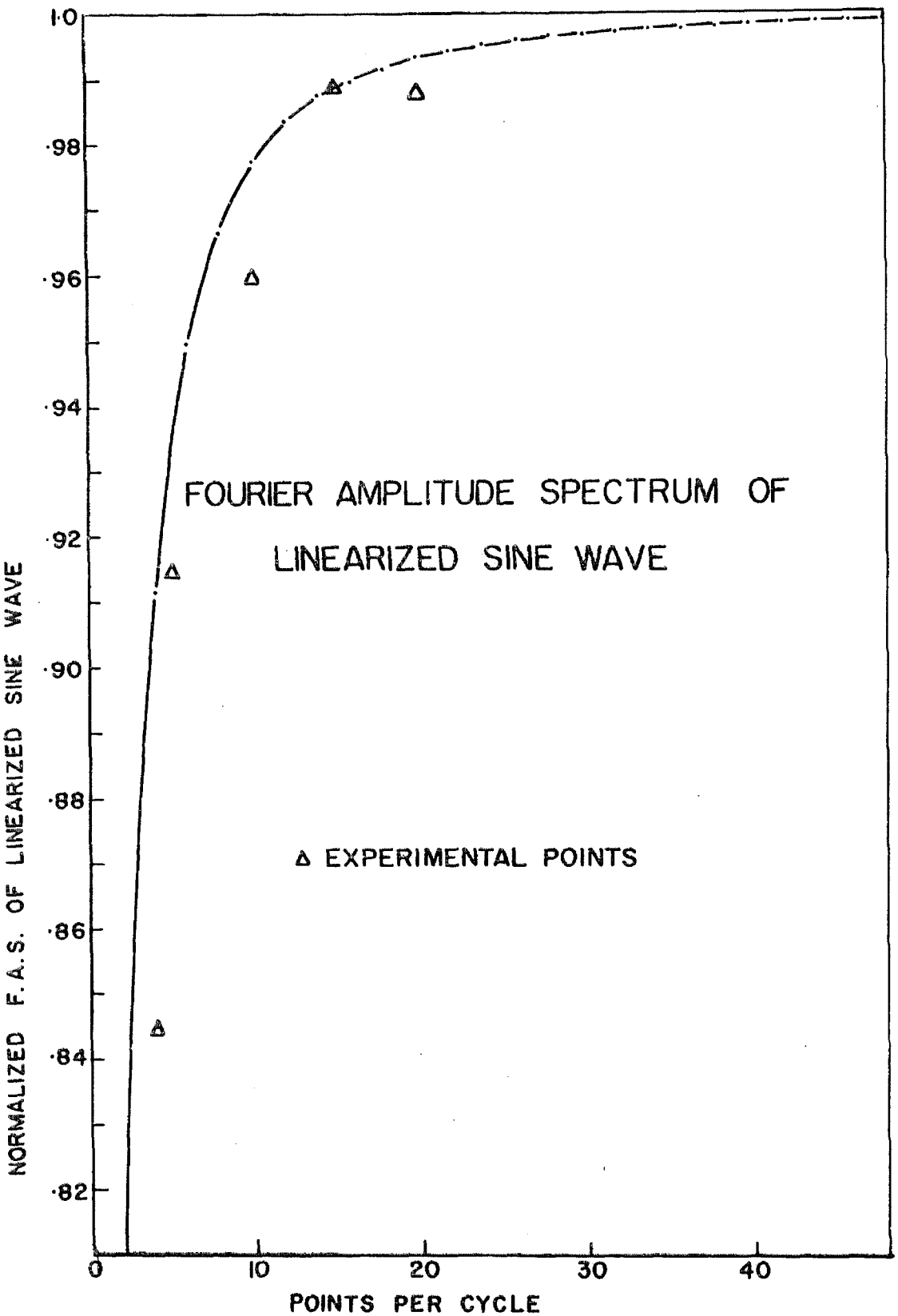

Figure A. 10 A comparison of the theoretically determined Fourier amplitude spectrum of a linearized sine wave (- - · - - ·) and the experimentally obtained spectrum (Δ).

general features particularly relevant to accelerogram digitization can be outlined as follows. While digitizing, the operator chooses points unequally spaced in time according to the frequency of the analog trace. Thus, for a typical strong-motion accelerogram the density of digitized points tends to increase in higher-frequency portions of the accelerogram and decrease towards the end of the record. The manner in which each digitized point is selected is such that the operator imagines a straight line connecting each point and the previous point. The distance between the two points then becomes a function of the frequency of the record. The operator chooses the next point so that a straight line will aptly approximate a section of the continuous analog trace.

Although most modern techniques of digital data analysis do not define the functional behavior between two digitized points, this has nevertheless become a common practice in earthquake engineering and related studies. The assumption of a straight line between the two successive points leads to filtering of some small-amplitude high-frequency components (frequencies higher than $1/2\ \Delta t$) that are too small to be detected by the operator, but on the other hand precisely defines the digitized record in the form of a continuous function. Since such digital data are not equally spaced, but are chosen by the operator on the basis of irregularities of the function digitized, fewer points give a better approximation to a continuous function than would equally spaced data of the same density.

To determine the transfer function properties of piecewise straight-line approximations, several cycles of a sine function were defined by equally spaced data interconnected with straight lines. The Fourier amplitude spectrum was then calculated theoretically for this continuous function and was divided by the Fourier amplitude spectrum for the exact truncated sine function [40]. This ratio, by definition, gives the modulus of the transfer function for the frequency in question. The result is given in Fig. A. 10, in which the transfer function is plotted versus the number of digitized points per one sine wave cycle. Thus, if the equally spaced digitized data are connected with straight-line segments, the continuous function so defined has essentially the same Fourier amplitudes as the original function up to the Nyquist frequency. Small differences on the order of a few percent for 5 to 10 points per cycle gradually increase to about 20 percent near the Nyquist frequency, corresponding to 2 points per cycle.

This experiment with equally spaced points was performed to approximately determine the shape of the transfer function that would correspond to the unequally spaced points [40] of the same average density. The validity of such an approximation was experimentally verified by optically digitizing several sine wave traces and using unequally spaced data of various densities. The transfer functions were calculated in the same way as for the equally spaced points, and the result is indicated in Fig. A. 10 by triangular

points. From the agreement of experimental points for digitized, unequally spaced data and the theoretical curve, we conclude that by assuming a straight line between points the transfer function for the unequally spaced optical digitization process may be described by the curve given in Fig. A. 10.

A.2 The Minimum Average Period in Hand Digitized Accelerograms

The density of digitized points naturally varies from operator to operator. It has been found [40] on analysis of 263 acceleration components that most of them have information on the frequencies near and above 20 cps. Fundamental frequencies of most instruments fall between 10 and 30 cps. Recorded signals with frequencies higher than 30 cps would have either a very low signal to noise ratio or be distorted by the higher modes of vibration of the instrument transducers or have both effects present. This high frequency limit is the consequence of presently available instruments and means of hand digitization. With future improvements in instrument design and in technology of data processing, this frequency will no doubt be further increased.

A. 3 Effect of Random Digitization Errors on the Accuracy of the Double Integrated Accelerograms

Since the acceleration data obtained during strong ground motions are used to compute the ground velocity and displacement, it is

necessary to determine the effect of random digitization errors on the reliability of such integration.

To study this, referring to Fig. A.7, the error in the once integrated acceleration can be computed as

$$e_v(t_0) = \int_0^{t_0} N(y+\varepsilon)dt - \int_0^{t_0} y\,dt$$

where $e_v(t_0)$ denotes the error in the velocity computed at time t_0 due to digitization errors

$$e_v(t_0) = \int_0^{t_0} \left\{ N\left[\text{int}[y] + \varepsilon + \delta\right] - \left[\text{int}[y] + \delta\right] \right\} dt$$

$$= \int_0^{t_0} \left\{ N[\varepsilon + \delta] - \delta \right\} dt$$

Using Reimann integration, we have

$$e_v(t_0) = \sum_{m=1}^{n} \left\{ N(\varepsilon + \delta) - \delta \right\}_m \Delta t$$

where Δt is the interval of digitization and $n\Delta t = t_0$.

Taking the expected values on both sides of the equation we have

$$E[e_v(t_0)] = 0$$

The variance becomes

$$\text{Var}[e_v(t_0)] = n\Delta t^2 \sigma_E^2$$

$$= (\Delta t)(t_0)(\sigma_E^2) \qquad \text{(A.3)}$$

Thus, the reliability of the estimated velocity at any time t_0 decreases linearly with increasing time. This reliability can be improved with more accurate digitization decreasing σ_E^2 and by decreasing the interval of digitization Δt.

The trend in the reliability of the error obtained by twice integrating the acceleration curve can be obtained by considering a simple integration scheme. Using the trapezoidal rule,

$$d_1 = \frac{y_1(\Delta t)^2}{2}$$

$$d_2 = d_1 + \frac{1}{2}(2y_1+y_2)(\Delta t)^2$$

$$\vdots$$

$$d_n = \frac{1}{2}\left[(2n-1)y_1 + (2n-3)y_2 + \ldots y_n\right](\Delta t)^2$$

Hence,

$$\text{Var}[d_n] = \frac{(\Delta t)^4}{4}\sigma_E^2\left[(2n-1)^2 + (2n-3)^2 + \ldots 1\right]$$

$$= \frac{(\Delta t)^4}{4}\sigma_E^2 \cdot \frac{(4n^3-n)}{3}$$

$$\propto (\Delta t)\cdot t_0^3\,\sigma_E^2 \qquad \text{(A.4)}$$

This result tells us that the trend in the uncertainty of the double integrated result as measured by the variance increases as the cube of the time t_0. It is therefore necessary to filter out these digitization errors so that they do not interfere with the computed results. It may be noted that even if the actual numerical algorithm used for integration were replaced by a more accurate one [59], the basic

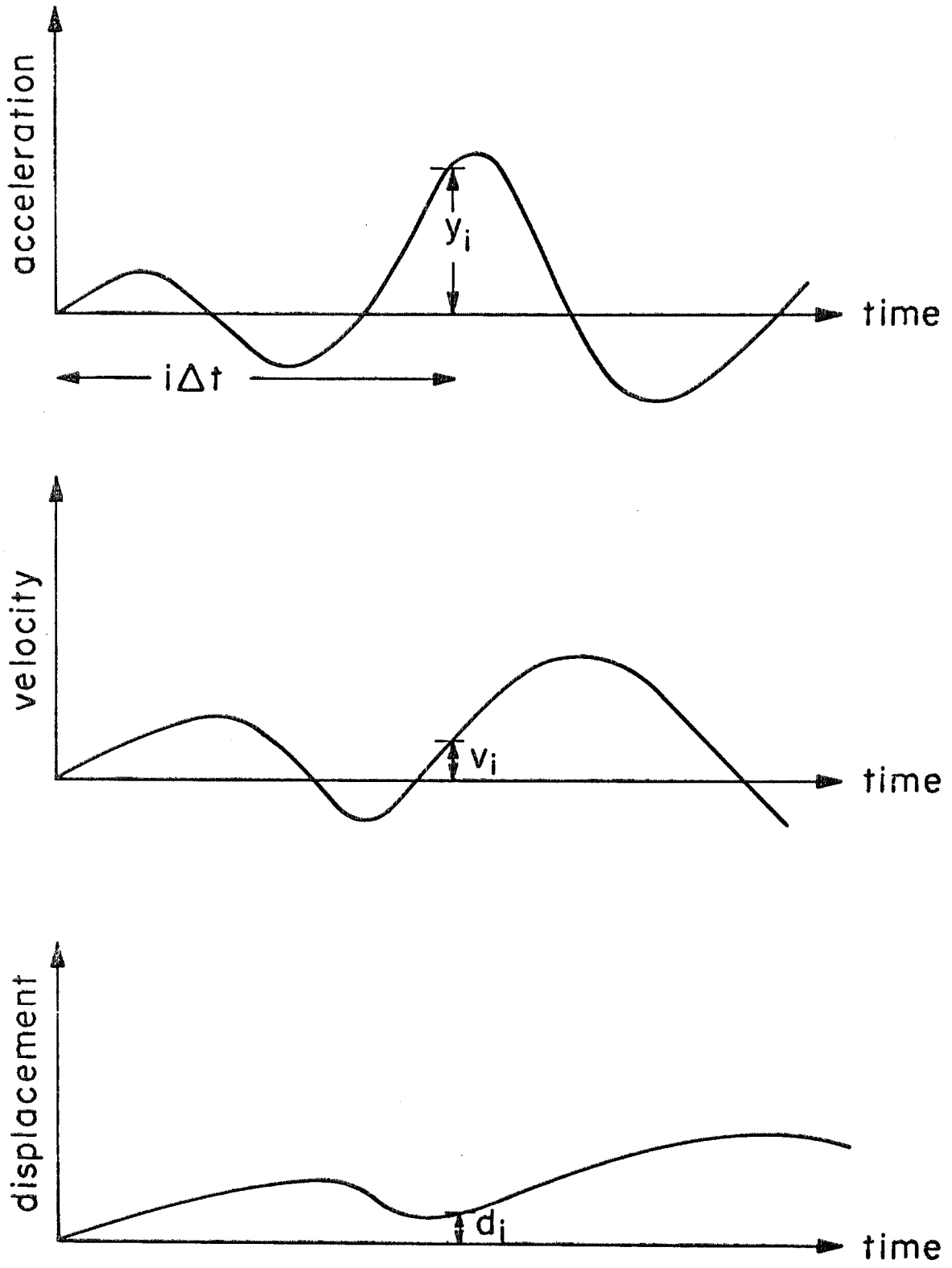
acceleration
y_i
time
$i\Delta t$
velocity
v_i
time
displacement
d_i
time

Figure A. 11

trend in estimating the reliability of the double integrated accelerogram would remain unchanged.

A.4 Errors in Automatic Digitization

The automatic analog to digital (A-D) converter used for the conversion of microtremor data to digital form leads to two main problems:

(1) The round-off error of the digitizer, and

(2) The truncation error.

(1) The Round-Off Error. If v is the voltage in counts, the relation between the input in volts and the output in counts is

$$v = \alpha + \beta$$

where α is always an integer and β is a random variable which can be assumed to be uniformly distributed over the interval $[-\frac{1}{2}, \frac{1}{2}]$. Therefore, if $E[\alpha] \equiv 0$, then $E[\text{output}] \equiv 0$ and the variance of the output obtained as

$$\text{Var}[\text{output}] = \int_{-1/2}^{1/2} \beta^2 \, d\beta = \frac{1}{12}$$

If the errors are uncorrelated, the autocorrelation function is

$$R(i\Delta t) = \begin{cases} 1/12 & i = 0 \\ 0 & i \neq 0 \end{cases}$$

Then the power spectral density S(f) is given by

$$S(f) = \frac{2\Delta t}{12} = \frac{\Delta t}{6} \; \frac{(\text{count})^2}{\text{cycle}}$$

If P volt $\equiv \delta$ counts, the spectral density becomes

$$S(f) = \frac{\Delta t}{6} P^2 \delta^{-2} (\text{volts})^2/\text{sec} \qquad (A.5)$$

We notice then that S(f) is much more affected by δ, the resolution of the converter, than by the interval, Δt, of sampling. Most converters have variable sampling rates. The sampling rate is generally fixed by the highest significant frequency present in the record. A reduction in S(f) can then be brought about economically through an increase in resolution of the instrument.

(2) Truncation Error. Most A-D converters have an upper bound beyond which the output-to-input relationship is no longer linear. Beyond a certain voltage level, a truncation occurs due to voltage overloading of the system. We can consider a simplified model of this process in the following way. Assume that the digitizer has an output such that

$$y(t) = \begin{cases} x(t) & ; \quad |x(t)| < c \\ c & ; \quad x(t) \geq c \\ -c & ; \quad x(t) \leq -c \end{cases}$$

This is the ideal case in which the digitizer merely acts as a "clipper", clipping off all voltages whose absolute magnitude exceeds c.

For

$$x(t) = A \cos 2\pi f_0 t \,,$$

$$S(f) = \frac{A^2}{2} \delta(f - f_0) \quad \text{if} \quad A < c \qquad (A.6)$$

and no clipping occurs. The extreme case of clipping would occur for $A >>> c$. The digitizer output, y, would then look like a square wave with amplitude c, whose spectral density would be

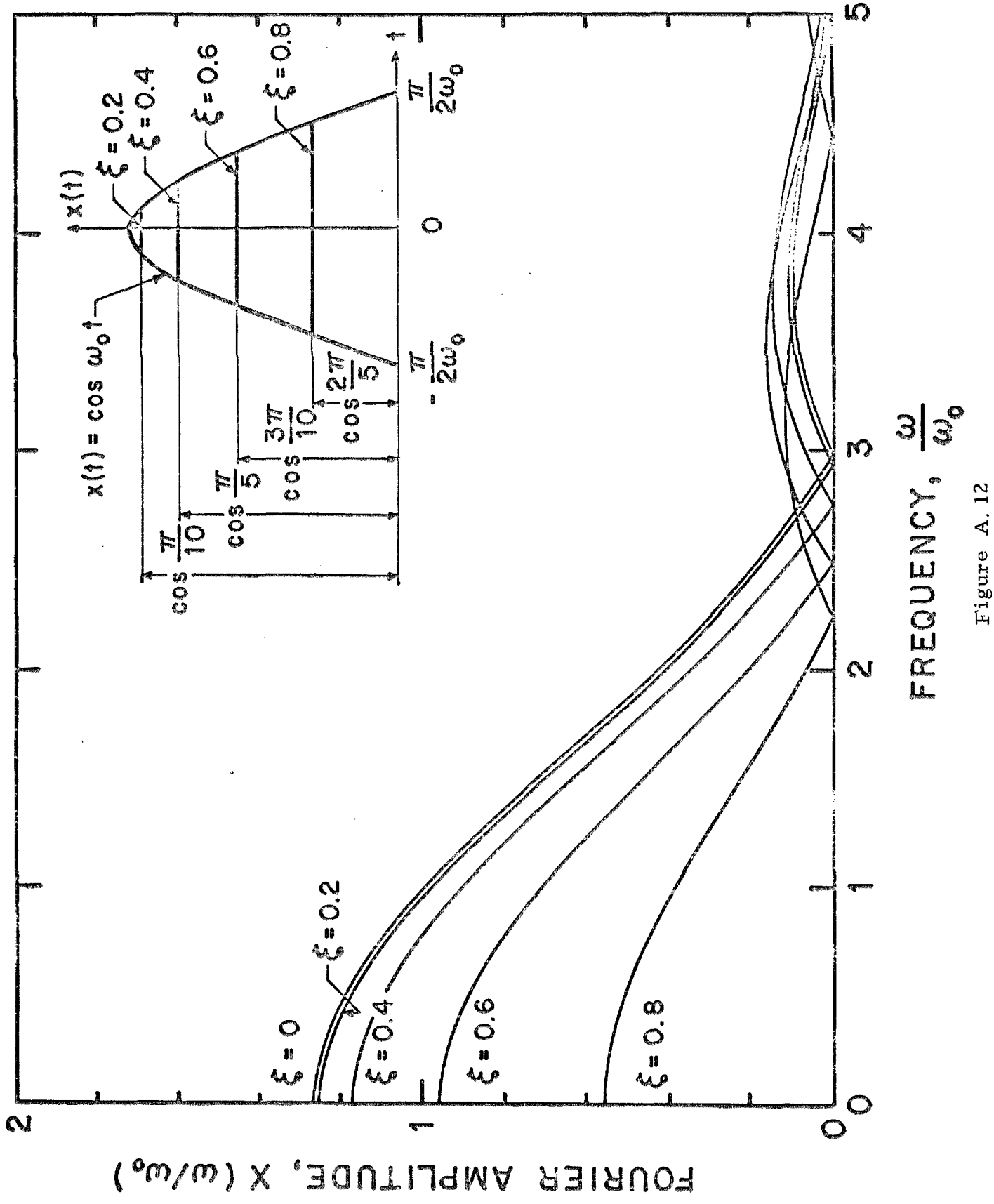
FOURIER AMPLITUDE, X (ω/ω₀)
FREQUENCY, ω/ω₀
ξ = 0
ξ = 0.2
ξ = 0.4
ξ = 0.6
ξ = 0.8
x(t) = cos ω₀t
x(t)
cos π/10
cos π/5
cos 3π/10
cos 2π/5
π/2ω₀
-π/2ω₀

Figure A. 12

$$S(f) = \frac{8c^2}{\pi^2} \sum_{i=1}^{h} \frac{1}{(2i-1)^2} \delta(f - (2i-1)f_0) \qquad (A.7)$$

Note that the spectral density at f_0 decreases proportionally to c^2/A^2, and that the energy originally concentrated at f_0 is spread away from f_0. Thus, the clipping represents a nonlinear mechanism for the spreading of input energy.

In a typical analog to digital conversion process, when the clipped analog signal is converted to digital data, usually only one or two extreme peaks of the analog signal get cut off. Although the effect of clipping one or several peaks cannot be modeled in general, since the shape of the peaks is not known, the effect on a part of the Fourier amplitude spectrum contributed by the peak can be qualitatively demonstrated. To this end, we analyze a peak which has a form $\cos \omega_0 t$ and is cut off at a level $\cos \xi \frac{\pi}{2}$ where $0 \le \xi \le 1$, as shown in Fig. A.12. The Fourier amplitude spectrum $X(\omega/\omega_0)$ corresponding to the cutoff peak $x(t)$ given by

$$x(t) = \begin{cases} \cos \omega_0 t & -\frac{\pi}{2\omega_0} \le t \le \xi \frac{\pi}{2} \\ \cos \xi \frac{\pi}{2} & -\xi \frac{\pi}{2} \le t \le \xi \frac{\pi}{2} \\ \cos \omega_0 t & \xi \frac{\pi}{2} \le t \le \frac{\pi}{2\omega_0} \end{cases}$$

as shown in Fig. A.12. As seen from the figure, the effect of clipping is at first small for small ξ. However, although it does not seriously affect the shape of the spectrum as ξ increases, the clipping creates a decrease in the amplitudes together with an increase in the bandwidth

— a behavior also observed in Eq. A.7. Since Fig. A.12 only models a small contribution to the spectrum of the general function, proportional to the contribution of a time interval π/ω, the effect of clipping of one peak on the overall spectrum of a function will be small for $\xi < 0.5$.

B. Instrument Correction of Accelerograms and Microtremor Data

Unlike the baseline correction of accelerograms [39], the instrument correction has not yet been intensively studied. McLennan [57] has derived an exact method of correcting for the accelerometer characteristics in the acceleration record. The disadvantage of the method is that it was designed to correct the response spectrum and not the actual recorded accelerogram, which serves as the basic input for all engineering calculations although it can be extended for that purpose. The more direct differentiation scheme [40] has been used in this study due to its computational economy.

For natural frequencies of acceleration transducers between 10 and 30 cps, the recorded instrument response may be taken to represent the ground accelerations up to frequencies of about 5 to 10 cps. To accurately recover higher frequencies, an instrument correction must be performed. In this work the errors resulting from imperfections in transducer design will be neglected. This is permissible because the routine optical digitization process does not resolve frequencies higher than 25 cps and higher modes in the transducer are significantly higher than this.

The highest frequency limit to which accurate accelerations may be recovered is determined by the lower of the two characteristic frequencies. The first is the frequency corresponding to that defined by the digitized data. This is the folding frequency if the data are equally spaced, or the equivalent highest frequency resolved by unequally spaced data. The other characteristic frequency is obtained by the intersection of the instrument response curve (Fig. A.1) and the chosen constant multiple of the digitization noise level. The latter level depends on the accuracy required of the corrected data and the response characteristics of the instrument. Since the natural frequency of most acceleration transducers is between 10 and 30 cps, the first frequency becomes important for all strong-motion accelerograms. The low pass filtered accelerograms thus need to be instrument corrected. For the data analyzed herein, the cutoff frequency chosen was 27 cps with a roll-off beginning at 25 cps. An Ormsby filter was used for the process.

The instrument correction procedure involves the assembling of the terms on the left-hand side of Eq. A.1, the transducer response being represented by 'x'. The process involves differentiation of the original signal. This could lead to problems arising from the amplification of the high frequency digitization errors. These errors cause a broad-banded spectrum and hence would be inherently present in the instrument corrected data.

It may be noted that the digitization process that leads to digitization errors can be thought of as a random stationary ergodic process having a certain spectral density, $S(\omega)$.

Since $S(\omega) = \underset{T\to\infty}{\mathcal{L}t} \frac{1}{T} E[|F(\omega)|^2]$ where T is the time length of the record and $F(\omega)$ is shown in Fig. A.5, an estimate of this could be obtained as

$$\hat{S}(\omega) = \frac{1}{T} E[|F(\omega)|^2]$$

Hence, the Fourier spectrum indicated in Fig. A.4 would have the same form for different time lengths of record, the actual amplitudes being proportional to the length of the record. The broad-band character of Fig. A.4 shows that the increased amount of digitization needed to enhance the knowledge of the high frequency compo nents of the ground motion introduces errors in the intermediate frequency range. Since the predominant frequencies of digitization errors are increased with a decrease in the average interval of digitization, it follows that one should try to digitize as many closely-spaced points as possible.

If the transducer used has an output signal proportional to the relative velocity $\dot{x}$, the numerical application of Eq. A.1 to recover 'a' needs to be done with a little more caution. The data obtained from the earthquakes are from accelerometers, and hence the problem does not arise here. However, the microtremor data obtained are from a velocity transducer. The method used for recovering the "true ground acceleration" from such a record is as follows:

1) Removal of a d. c. component from the microtremor velocity data.
2) Low pass filtering of the data with a cutoff frequency of 27 cps and a rolloff of 2 cps.

3) Differentiation of the data to get $\ddot{x}$.

4) Integration of the data to get an estimate of x.

5) Fitting a least squares fit straight line through the once integrated data in Step 4.

6) High pass filtering of the curve with a cutoff frequency of 0.07 cps.

7) The use of Eq. A.1 to get 'a'.

C. The Fourier Transform as Used in the Analysis of Microtremor Data

In this section some of the aspects of Fourier Analysis as applied to random signals will be studied. In general, for a random stationary process, the Fourier Transform $|X(f)|$ will not be a finite quantity, and one would need to employ a representation such as the power spectral density of the process defined as

$$S(f) = \underset{T\to\infty}{\mathcal{L}t} \frac{1}{T} E\left[|X(f)|^2 \right] \qquad (C.1)$$

However, due to the fact that only a finite length of sample record is available, the finite range Fourier Transform X(f, T) can be computed where

$$X(f,T) = \int_0^T x(t) e^{-2\pi i f t} dt$$

This leads to an estimate

$$\hat{S}(f) = \frac{1}{T} |X(f)|^2 \qquad (C.2)$$

Hence,

$$|X(f)|^2 = T\hat{S}(f)$$

The finite Fourier Transform will thus be used as an indication of the nature of the power density of the process and hence as a convenient way of revealing frequency peaks. Since in this study we are only interested in picking out the predominant peaks, this appraoch is quite valid provided a sufficiently long length of record is analyzed. As seen in Section IV the close similarity in the spectra of two forty second lengths of record indicates that a length of forty seconds gives a good representation of the short time (of the order of 2 - 3 minutes) micro-tremor process.

C.1 Analysis of Smoothing of the Energy Spectrum of Accelerograms

As seen from the spectra of Appendix II, the Fourier Spectral Amplitudes are rapidly fluctuating functions in the frequency ranges of interest. In order to study the general trends in the spectra, these spectra have been smoothed.

Consider a general weighting function s(i), $i = -n, \cdots 0, \cdots, n$. Then the smoothing process can be expressed as a convolution wherein $\overline{F}(\omega_i)$ the smoothed amplitude at $\omega = \omega_i$ is given by

$$\overline{F}(\omega_i) = \begin{cases} \sum_{k=-n}^{n} s(k)\, F(\omega_{k+i}) \,, & \text{for } n \le i \le N-n \\ F(\omega_i) & \text{otherwise} \end{cases}$$

where

$$\sum_{k=-n}^{n} s(k) = 1 \qquad (C.3)$$

Consider the symmetric smoothing window

$$s(k) = \frac{n+1-|k|}{(n+1)^2} \qquad k = -n, \ldots, 0, \ldots n$$

We can show that such a smoothing leaves the average value of the function unaltered for all practical purposes provided n is small compared to N and $F(\omega_i)$ is not excessive in the regions $i \leq 2n$ and $i \geq N-2n$. This can be shown by splitting the summation in Eq. (C. 3) into three parts arising from the three following ranges of i:

(1) $n \leq i \leq 2n$,

(2) $2n < i \leq N-2n$, and

(3) $N-2n < i \leq N-n$.

$$\frac{1}{N}\left[\sum_{1}^{N} \overline{F}(\omega_i)\right] = \frac{1}{N}\left[\sum_{1}^{N} F(\omega_i)\right] - \frac{1}{N}\left[\sum_{i=1}^{2n} F(\omega_i)\{1-A(i,n)\}\right]$$

$$- \frac{1}{N}\left[\sum_{i=N-2n+1}^{N} F(\omega_i)\{1-B(i,n)\}\right]$$

$$+ \frac{1}{N}\sum_{1}^{n} F(\omega_i) + \frac{1}{N}\sum_{N-n+1}^{N} F(\omega_i) \qquad \text{(C. 4)}$$

where,

$$A(i,n) = \left[\frac{i(i+1) - 2U(i-(n+1))(i-n)(i-n-1)}{2(n+1)^2}\right]$$

$$B(i,n) = \left[\frac{(N-i+1)(N-i+2) - 2U((N-n)-i)[(N-n-i)(N-n-i+1)]}{2(n+1)^2}\right]$$

and

$$U(i-\ell) = 0 \ , \quad \text{for } i \leq \ell$$

$$= 1 \ , \quad \text{for } i > \ell$$

The average values of the original and the smoothed functions are identical as $N \to \infty$ and $|F(\omega_i)| \leq M$ where M is a constant. Also the area under the two curves, given by $\sum F(\omega_i)\Delta\omega$ and $\sum \overline{F}(\omega_i)\Delta\omega$ would be almost identical except for the difference of

$$\left| \sum_{i=1}^{2n} F(\omega_i)\{1-A(i,n)\}\Delta\omega + \sum_{N-2n+1}^{N} F(\omega_i)\{1-B(i,n)\}\Delta\omega - \sum_{1}^{n} F(\omega_i)\Delta\omega - \sum_{N-n+1}^{N} F(\omega_i)\Delta\omega \right| \qquad (C.5)$$

$$\leq 2n \left| F(\omega_i) \right|_{\substack{\max \\ 1 \leq i \leq 2n \\ N-2n+1 \leq i \leq N}} (\Delta\omega)$$

C.2 Smoothing of Microtremor Spectra

Since we are constrained to study only a finite length of microtremor record, it is only possible to obtain an estimate of the true power spectral density of the microtremor process. A reasonable estimator of the true power spectrum density S(f), would then seem to be

$$\hat{S}(f,T) = \frac{1}{T} |X(f,T)|^2 \qquad (C.6)$$

Though it may seem intuitive that the longer the length of record chosen the better the estimate of the true power spectrum, it can be shown that for the estimator given by Eq. (C.6) this is not the case. The variance of the estimate does not decrease as the time length of record T increases, making such an estimator inconsistent.

To show this, consider a Gaussian white process x(t), with mean zero and variance σ^2, sampled at N+1 points $x(n\Delta t)$, n=0,1,2,$\cdots$, N. Equation (C.6) can then be written as

$$\hat{S}(f,T) = \frac{\Delta t}{N}\left[\left\{\sum_{n=0}^{N-1} x(n\Delta t)\cos 2\pi fn\Delta t\right\}^2 + \left\{\sum_{n=0}^{N-1} x(n\Delta t)\sin 2\pi fn\Delta t\right\}^2\right]$$

$$-\frac{1}{2\Delta t} < f < \frac{1}{2\Delta t} \qquad \text{(C. 7)}$$

Let

$$X_R(f) = \sum_{n=0}^{N-1} x(n\Delta t)\cos 2\pi fn\Delta t$$

$$X_I(f) = \sum_{n=0}^{N-1} x(n\Delta t)\sin 2\pi fn\Delta t$$

Then,

$$\hat{S}(f,T) = \frac{\Delta t}{N}\left[X_R^2(f) + X_I^2(f)\right] \qquad \text{(C. 8)}$$

At the harmonic frequencies $\frac{k}{T} = f_k$, the expected value of $X_R(f_k)$ is

$$E[X_R(f_k)] = \sum_{n=0}^{N-1} E[x(n\Delta t)\cos 2\pi fn\Delta t]$$

$$= 0 \text{ since the } E[x(n\Delta t)] = 0$$

Similarly

$$E[X_I(f_k)] = 0 \qquad \text{(C. 9)}$$

Also,

$$E\left[X_R^2(f_k)\right] = \sum_{n=0}^{N-1}\sum_{m=0}^{N-1} E[x(n\Delta t)x(m\Delta t)]\cos 2\pi f_k n\Delta t \cos 2\pi f_k m\Delta t$$

$$= \sum_{n=0}^{N-1}\sum_{m=0}^{N-1} \sigma^2 \delta[(n-m)\Delta t]\cos 2\pi f_k n\Delta t \cos 2\pi f_k m\Delta t$$

$$= \sum_{n=0}^{N-1} \sigma^2 \cos^2 2\pi f_k n\Delta t$$

$$= \sigma^2 \left[\frac{N}{2}\right] \qquad k = \pm 1, \pm 2, \cdots \qquad (C.10)$$

Similarly

$$E\left[X_I^2(f_k)\right] = \sigma^2 \frac{N}{2} \qquad k = \pm 1, \pm 2, \cdots$$

and

$$E[X_R(f_k)X_R(f_j)] = 0 \qquad k \neq j$$

Since $X_R(f_k)$ and $X_I(f_k)$ are linear functions of normal random variables, they are each normally distributed with a mean zero and variance $\sigma^2 \frac{N}{2}$. Further

$$E[X_R(f_k)X_I(f_k)] = 0 \qquad (C.11)$$

$X_R(f_k)$ and $X_I(f_k)$ are uncorrelated and hence independent since they are normal random variables.

The random variables $X_R^2(f_k)/(\sigma^2 N/2)$ and $X_I^2(f_k)/(\sigma^2 N/2)$ are each χ^2 distributed with one degree of freedom. Their sum $Y(f_k)$ is hence a χ^2 variable with two degrees of freedom with a mean of 2 and a variance of 4. From this we conclude that

$$E[\hat{S}(f_k,T)] = E\left[\frac{\Delta t}{N}\left\{X_R^2(f_k)+X_I^2(f_k)\right\}\right]$$

$$= \frac{\Delta t}{N} E\left[Y(f_k)\cdot\frac{\sigma^2 N}{2}\right]$$

$$= \frac{\Delta t}{N}\cdot\frac{\sigma^2 N}{2} E[Y(f_k)]$$

$$= \frac{\Delta t}{N}\frac{\sigma^2 N}{2}\cdot 2$$

$$= \Delta t\,\sigma^2 \qquad (C.12)$$

and,

$$Var[\hat{S}(f_k,T)] = Var\left[\frac{\Delta t}{N}\cdot\frac{N\sigma^2}{2}\cdot Y(f_k)\right]$$

$$= Var\left[\frac{\Delta t\sigma^2}{2} Y(f_k)\right]$$

$$= (\Delta t)^2\,\sigma^4 \qquad (C.13)$$

Equation (C.13) indicates that the variance of the estimator is a constant independent of the sample size N. This can be interpreted as meaning that the distribution of the estimator does not tend to cluster more closely about the true spectrum as the sample size increases.

It may be noted that even if the process x(t) is not normal, the random variables $X_R(f_k)$ and $X_I(f_k)$ will be very nearly normal by the central limit theorem so that the distribution of $Y(f_k)$ will be very nearly χ_2^2 regardless of the distribution of x(t).

To reduce the variance of the estimate $\hat{S}(f_k,T)$ a smoothing over an ensemble of estimates can be performed. This can be done by computing individual spectral estimates at the frequencies f_k for q independent sample records ${}^j x(t)$, $j = 1, 2, \cdots, q$ and then averaging

the q estimates for each frequency. The variance of the smoothed estimate $\bar{\hat{S}}(f_k, T)$ will then be $(\frac{1}{q})^{th}$ of the variance of any one of the estimates $^{i}\hat{S}(f_k, T)$. A second method of reducing the variance is to smooth the spectral estimates over frequency by averaging together the spectral estimates for p contiguous components from a single record. Then the smoothed estimate $\bar{\hat{S}}(f_k, T)$ becomes

$$\bar{\hat{S}}(f_k, T) = \sum \omega_h \hat{S}_{k-h}$$

where ω_h represents the symmetric smoothing window with

$$\sum_{-\infty}^{\infty} \omega_h = 1$$

Then,

$$E[\bar{\hat{S}}(f_k, T)] = \sum \omega_h E[\hat{S}_{k-h}]$$

$$= (\sigma^2 \Delta t) \sum \omega_h = \sigma^2 \Delta t$$

$$\mathrm{Var}[\bar{\hat{S}}(f_k, T)] = \sum\sum \omega_h \omega_p \, \mathrm{cov}[\hat{S}_{k-h} \hat{S}_{k-p}]$$

$$= \sum \omega_h^2 \sigma^4 \Delta t^2 = \sigma^4 \Delta t^2 \sum \omega_h^2$$

If as an example we take ω_h to be the hanning window $\frac{1}{4}, \frac{1}{2}, \frac{1}{4}$, then $\sum \omega_h^2 = \frac{3}{8}$. Hence the variance of the estimate is reduced by $\frac{3}{8}$ of its original value.

It may be pointed out that through this discussion has been limited to a Gaussian white process, it can be extended to any process with a given power spectrum by regarding it as having been generated by passing white noise through an appropriate filter.

Appendix II

FOURIER SPECTRA OF EARTHQUAKE ACCELEROGRAMS

The computed Fourier Amplitude Spectra of the ground accelerations recorded at El Centro from the events indicated in Table III. 1 together with their smoothed version are illustrated in Figs. FAS 1 through FAS 15. The effect of the smoothing process is clearly brought out. An interesting feature is brought out by the spectrum of the vertical component of event 38.4 (Fig. FAS 3). This component of ground motion produced a very small amplitude trace of more than average line width on the recording paper. Due to the difficulty in picking out the centerline of this trace, the signal to noise ratio was very low, and it can be assumed that a major contribution to the digitized record came from the digitization noise. The Fourier Amplitude Spectrum of this component shows that the amplitudes are below 1 cm/sec. This is compatible with the maximum error bound on the Fourier Amplitude Spectrum of about 0.6 cm/sec for frequencies higher than about 2 rad/sec calculated from the spectra of digitization noise. This low value of the error introduced by digitization noise and instrument correction indicates that higher frequency components included in the analysis can be extracted without adversely affecting the accuracy of the spectrum.

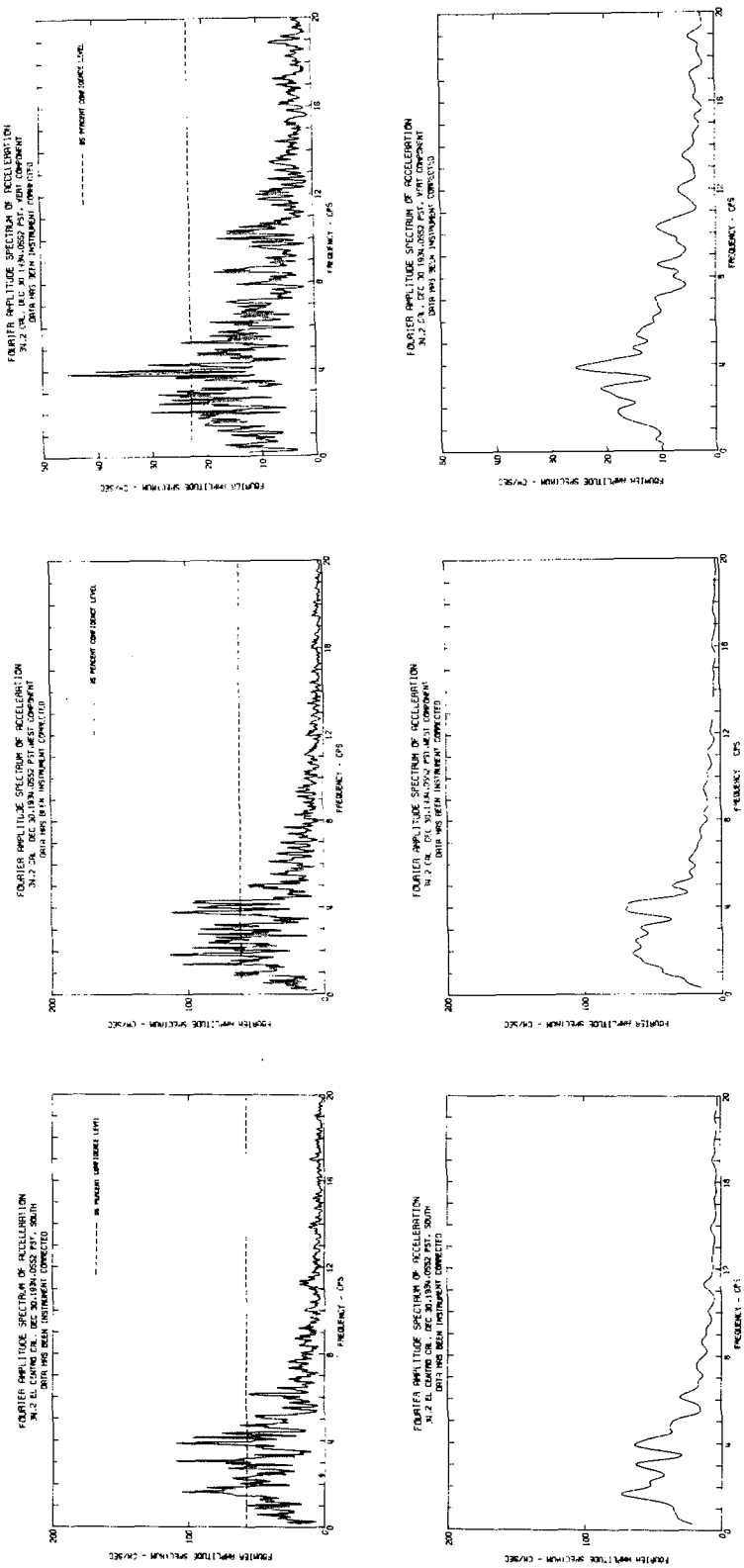

Figure FAS 1

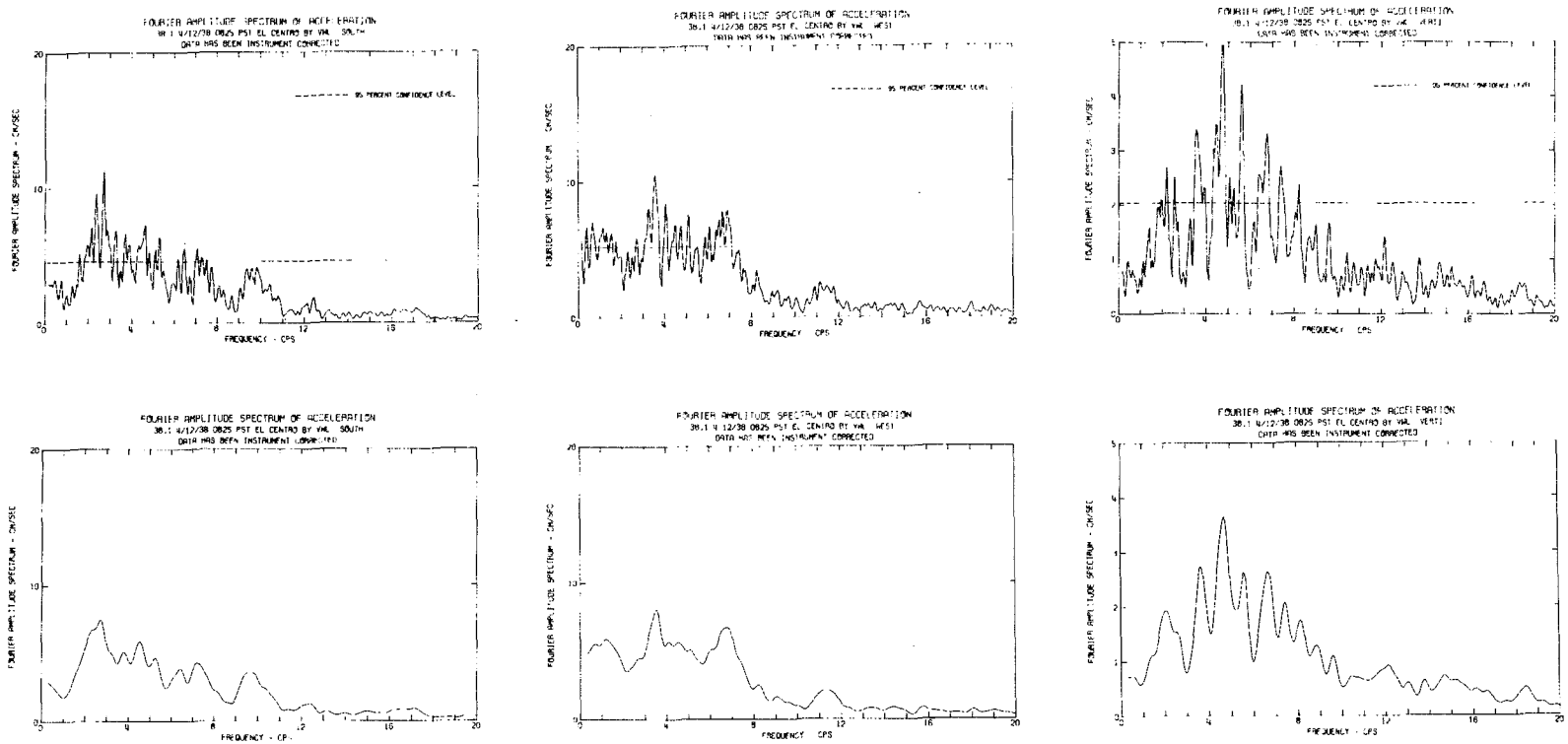
FOURIER AMPLITUDE SPECTRUM OF ACCELERATION
95 PERCENT CONFIDENCE LEVEL
FOURIER AMPLITUDE SPECTRUM - CM/SEC
FREQUENCY - CPS

Figure FAS 2

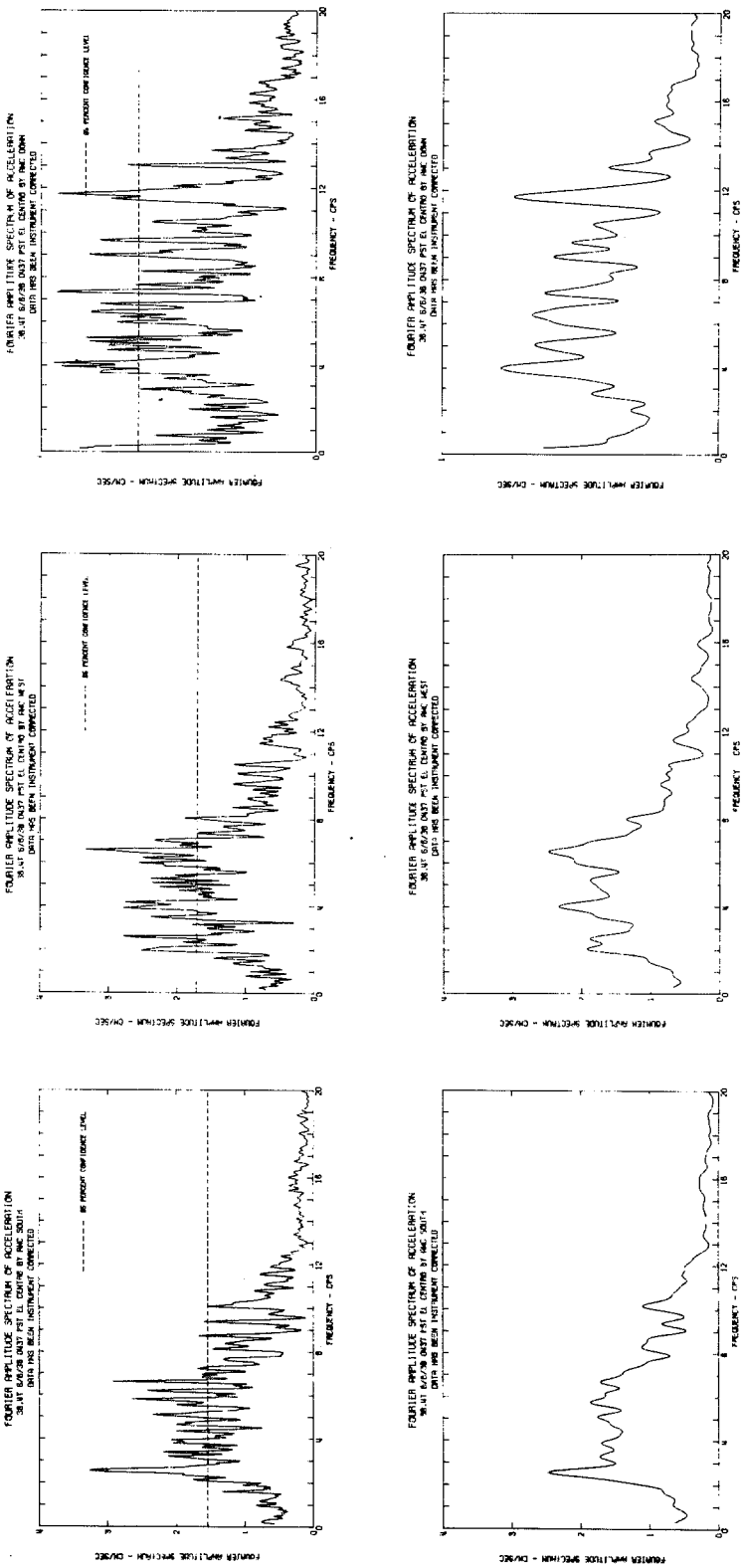

Figure FAS 3

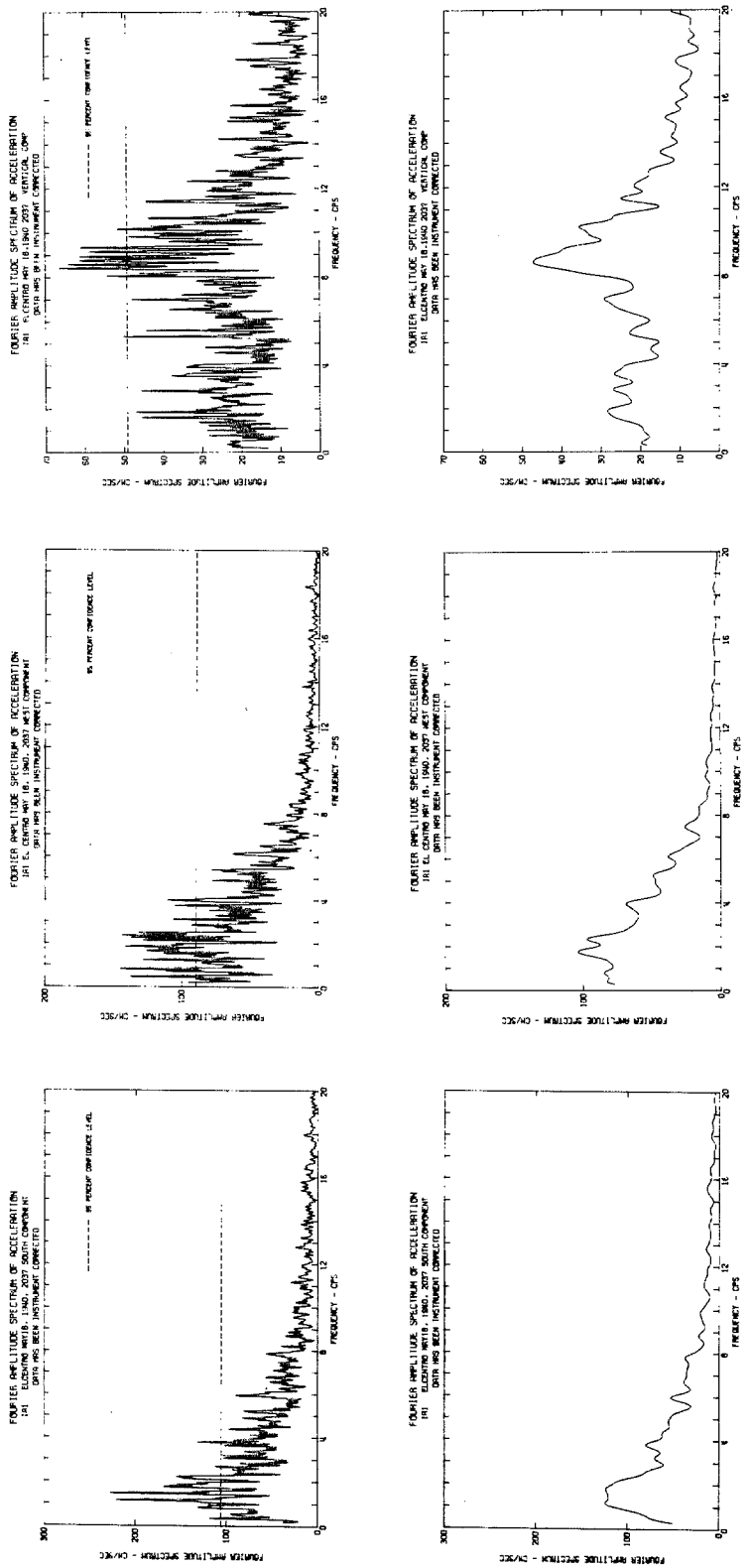

Figure FAS 4

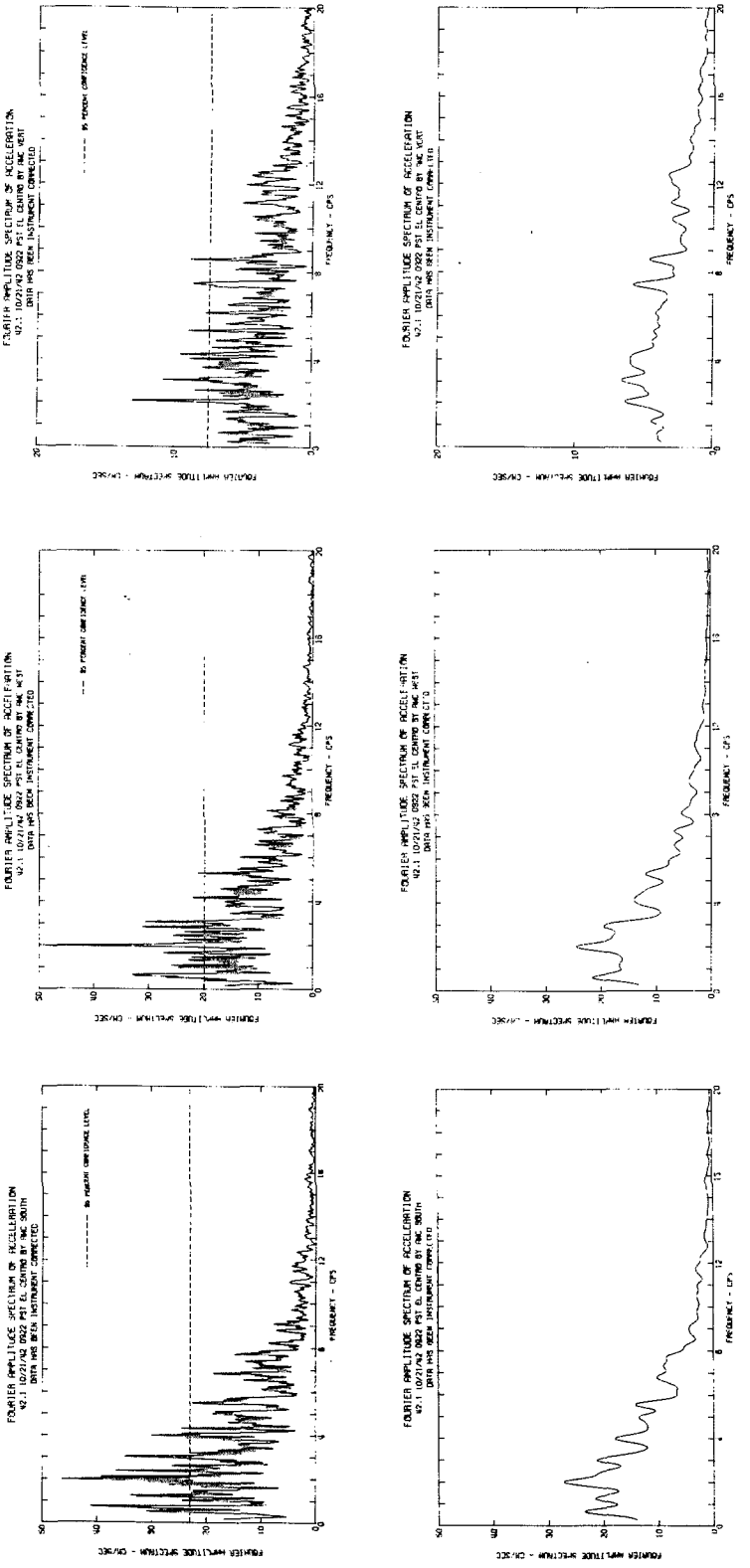

Figure FAS 5

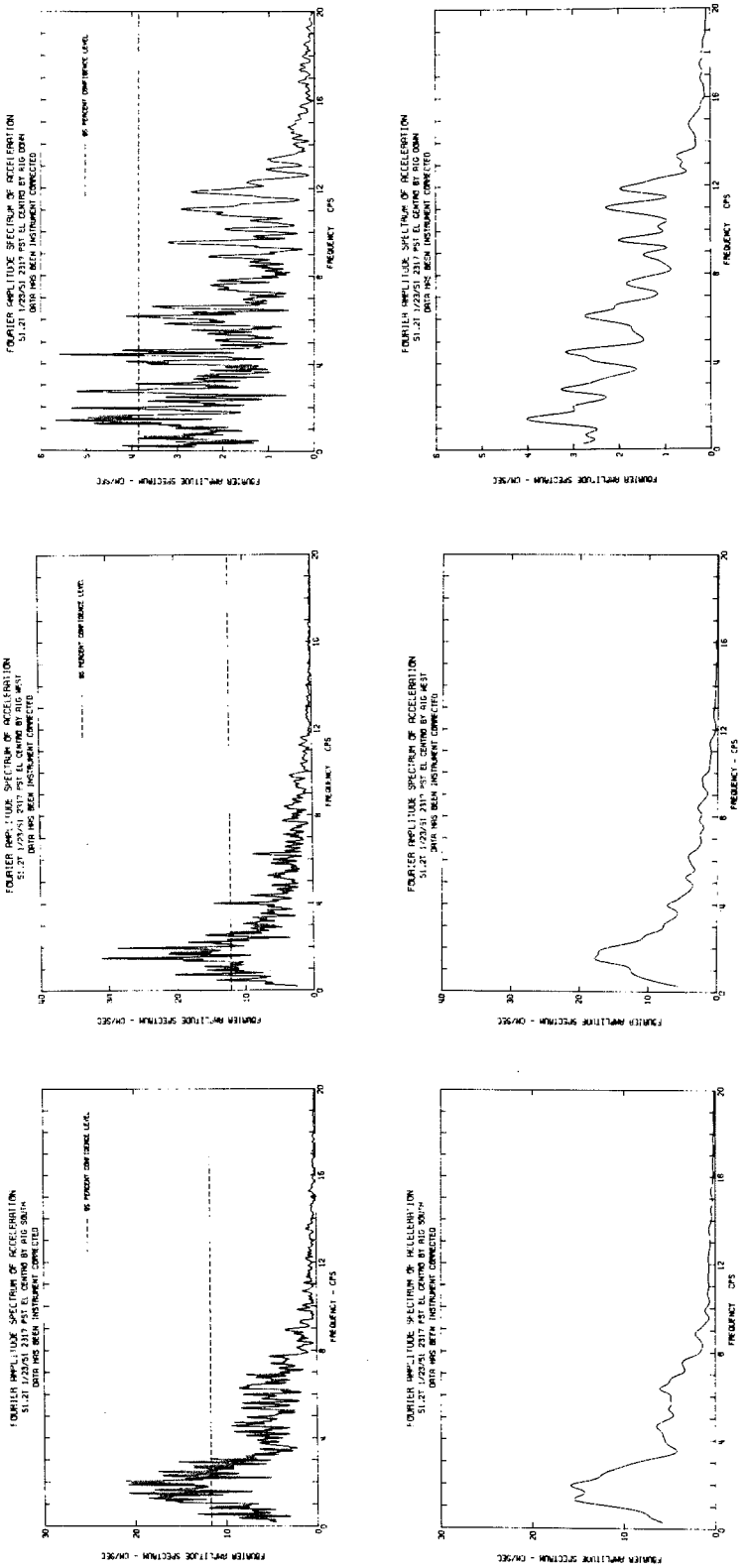

Figure FAS 6

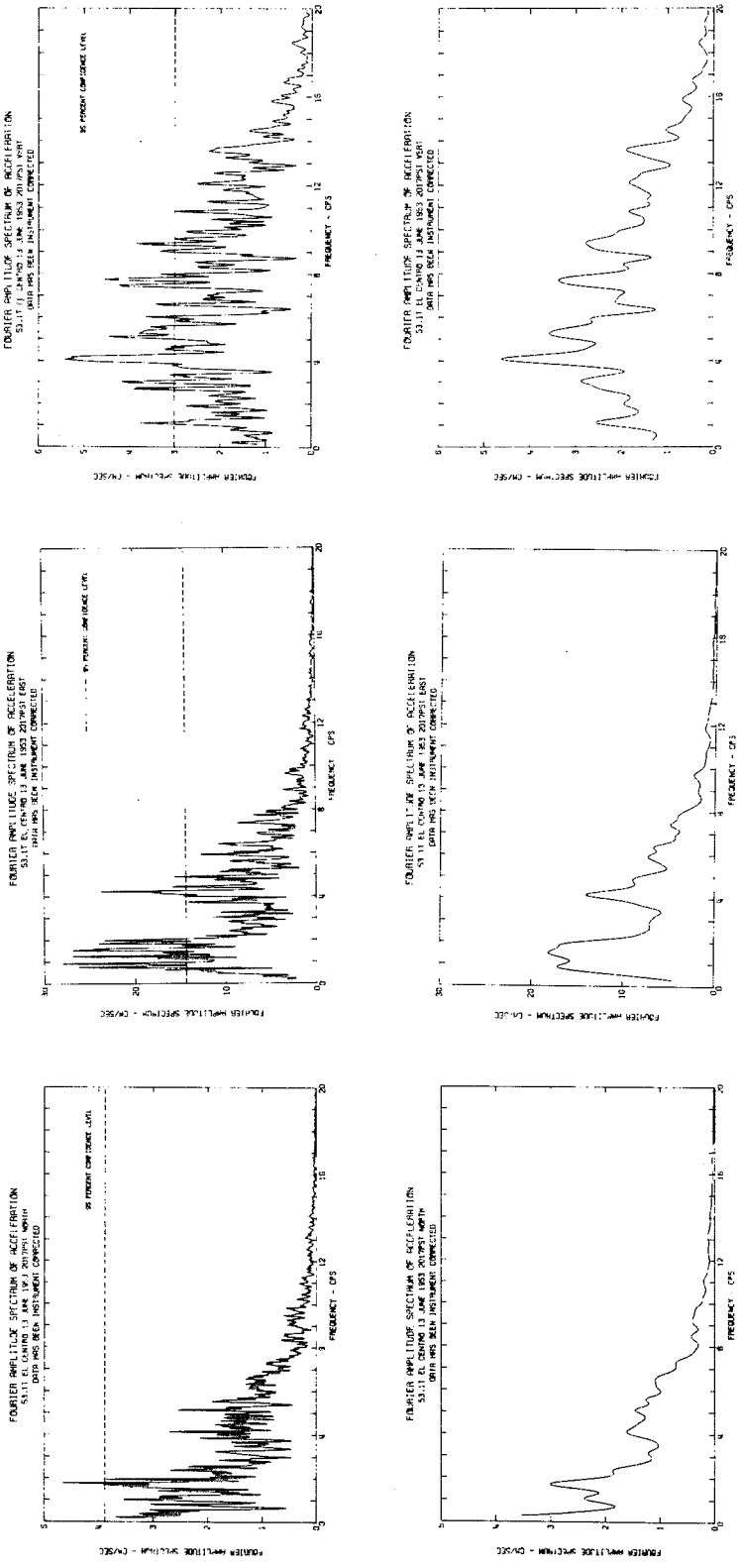

Figure FAS 7

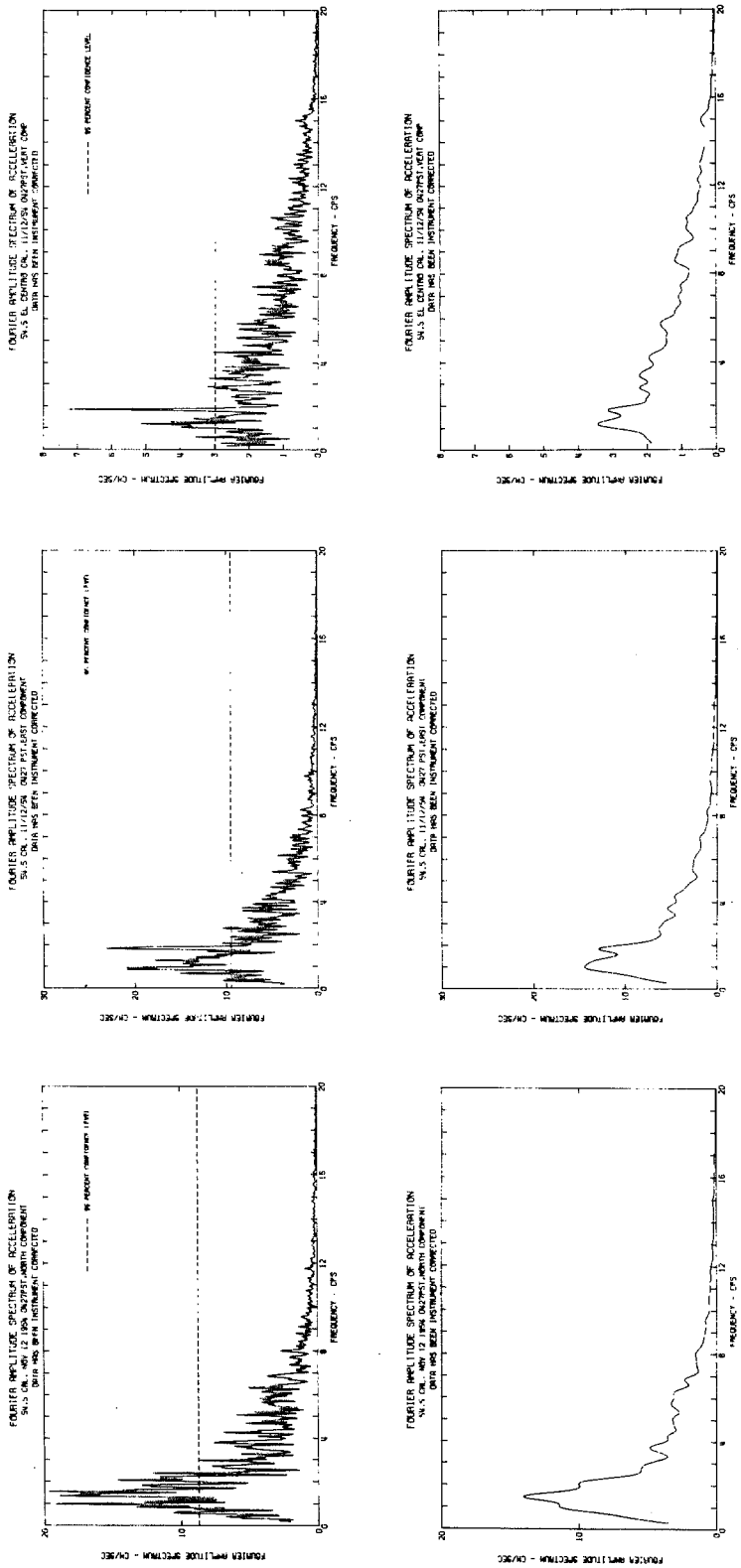

Figure FAS 8

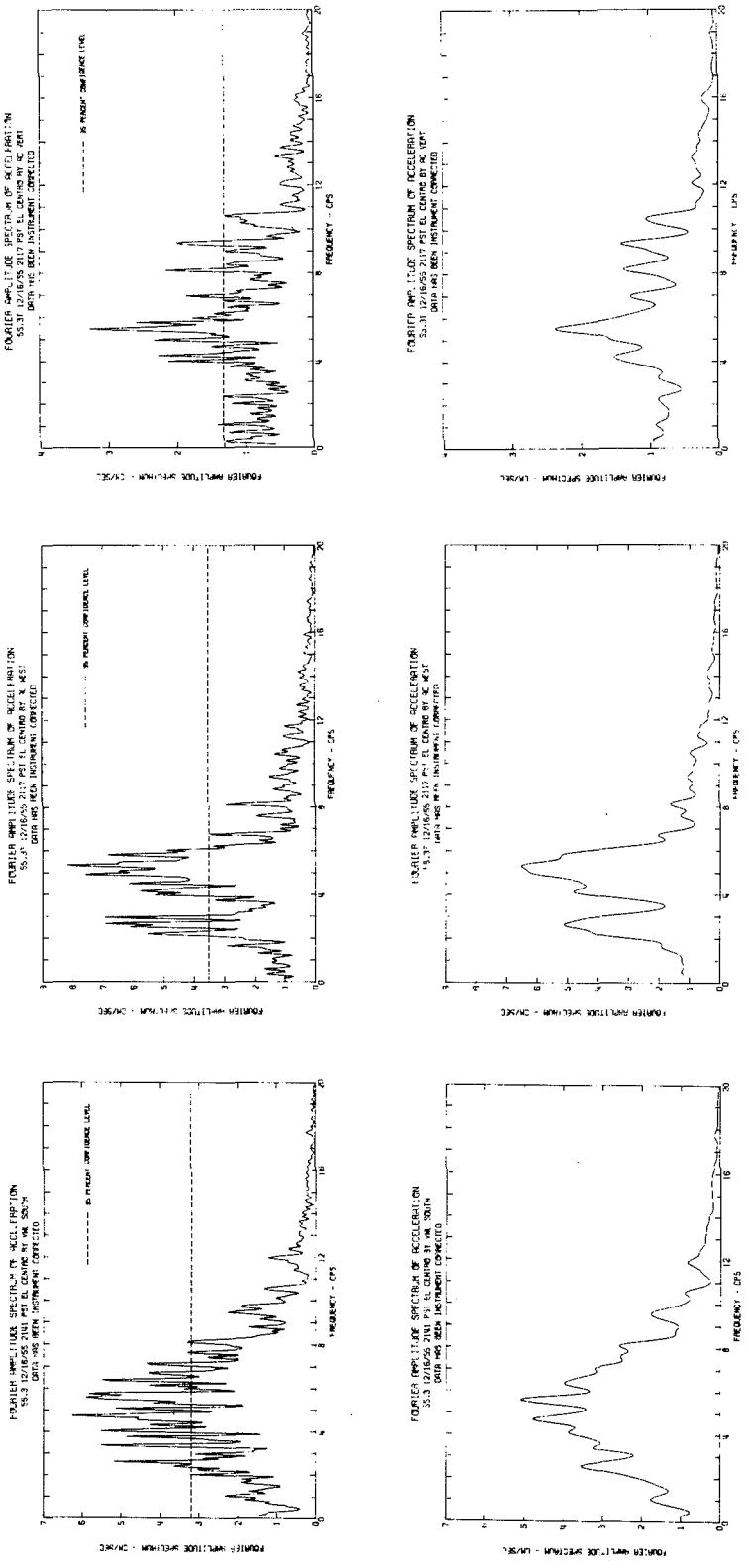

Figure FAS 9

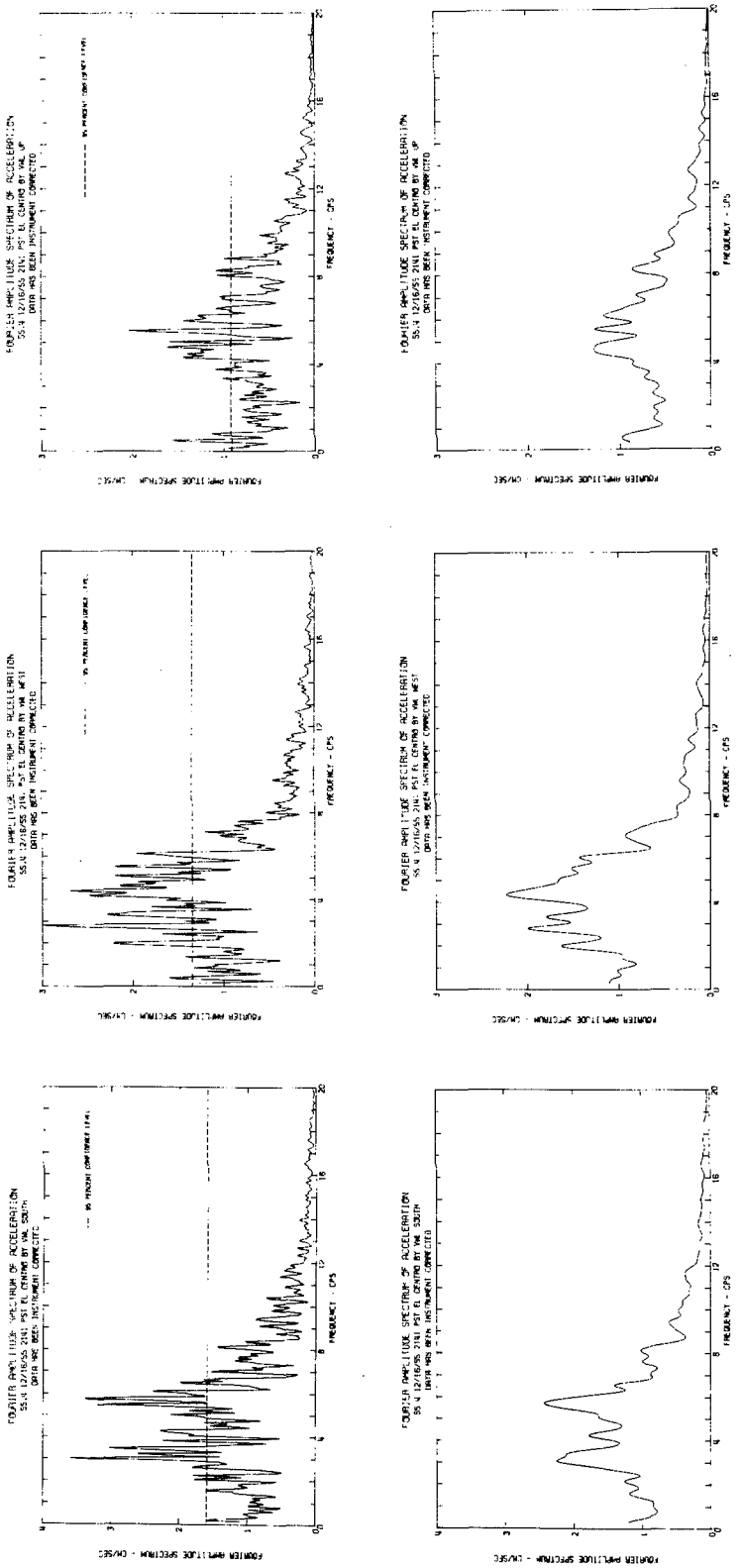

Figure FAS 10

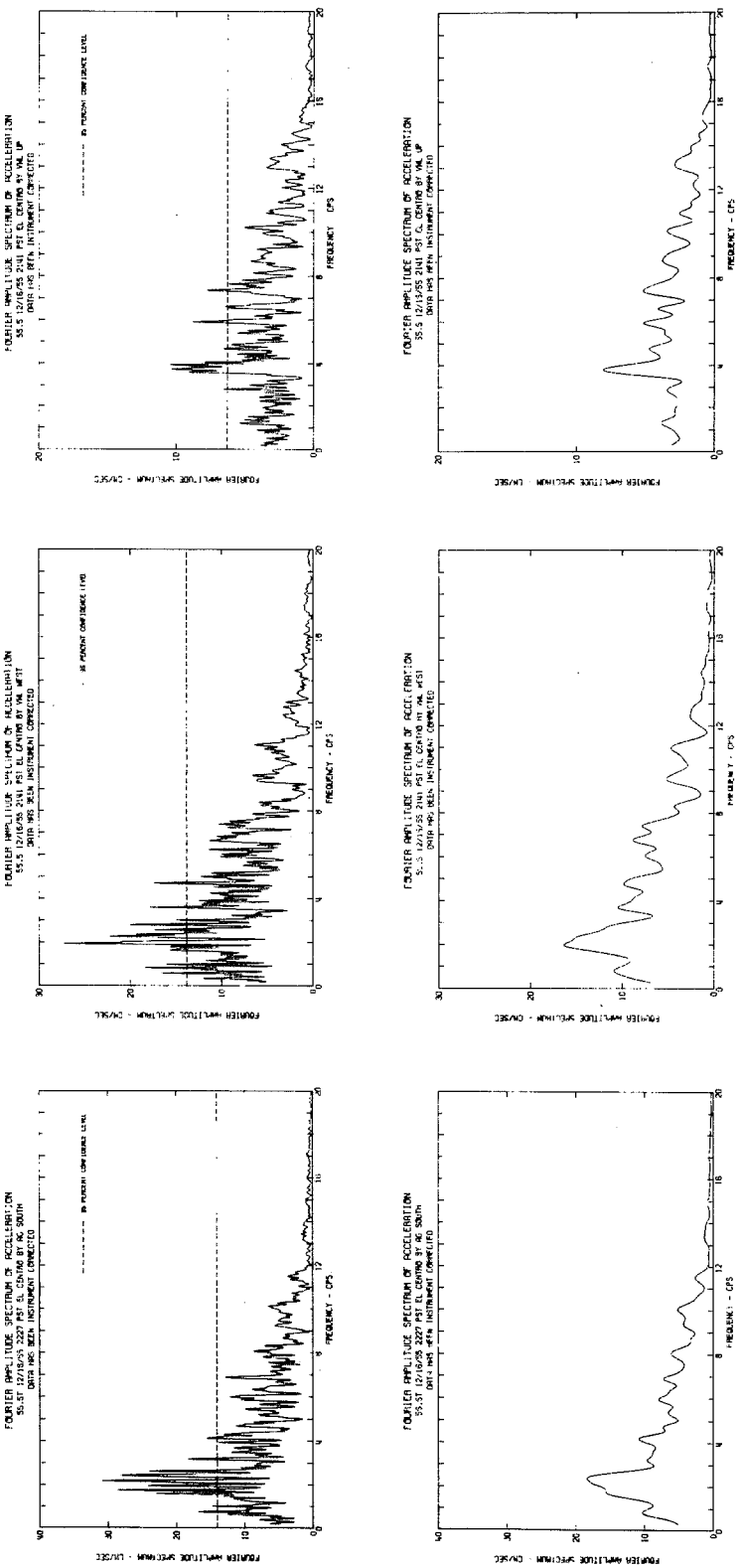

Figure FAS 11

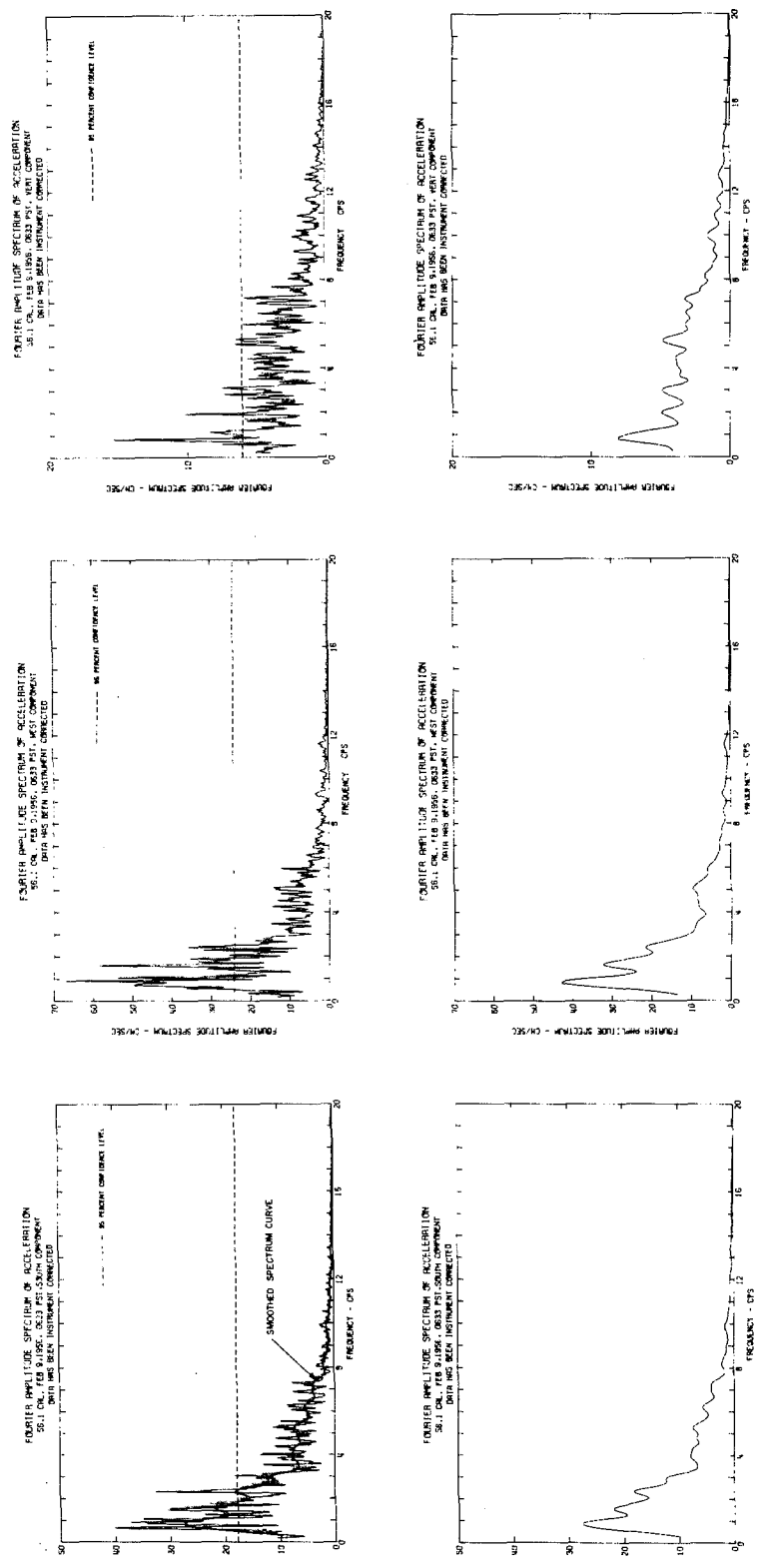

Figure FAS 12

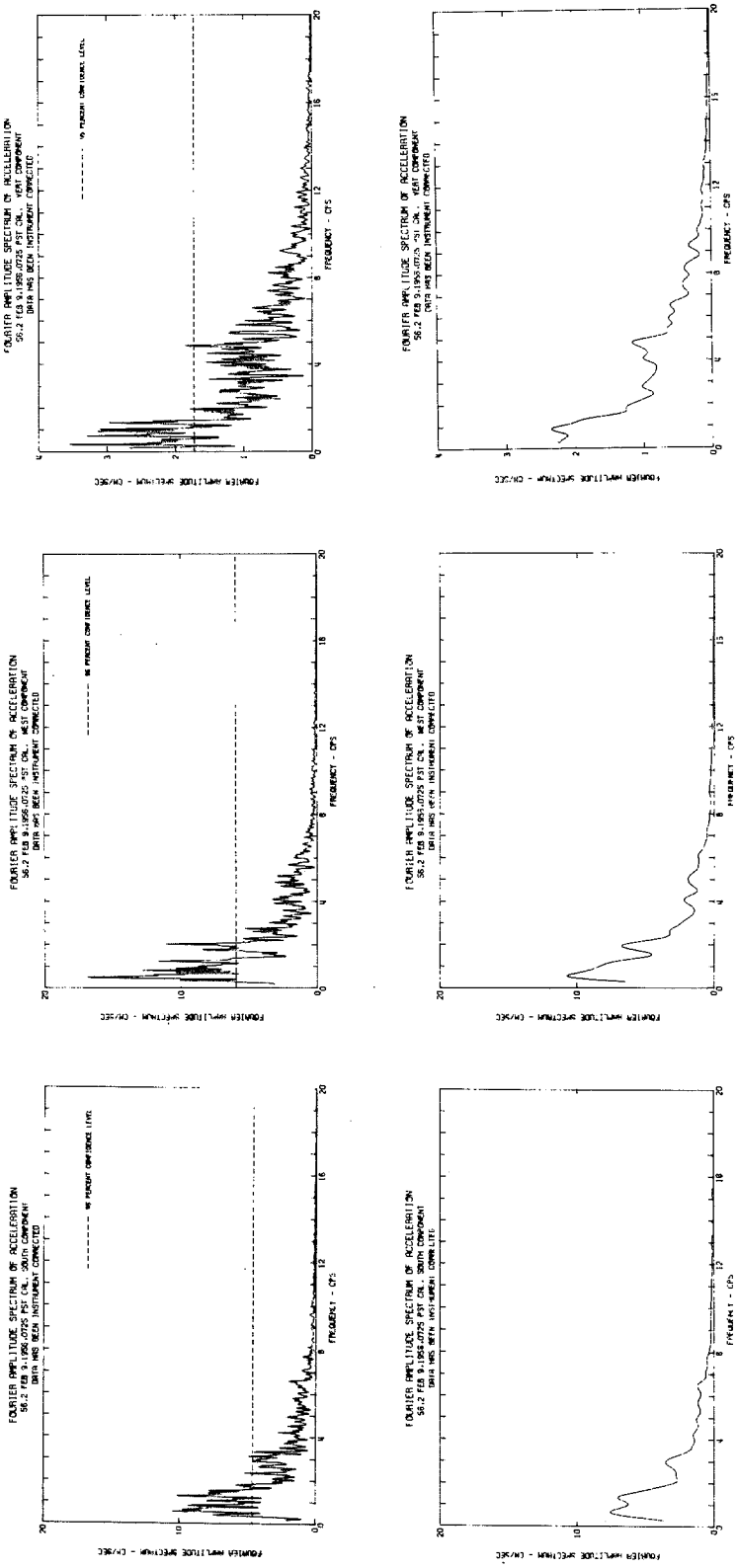

Figure FAS 13

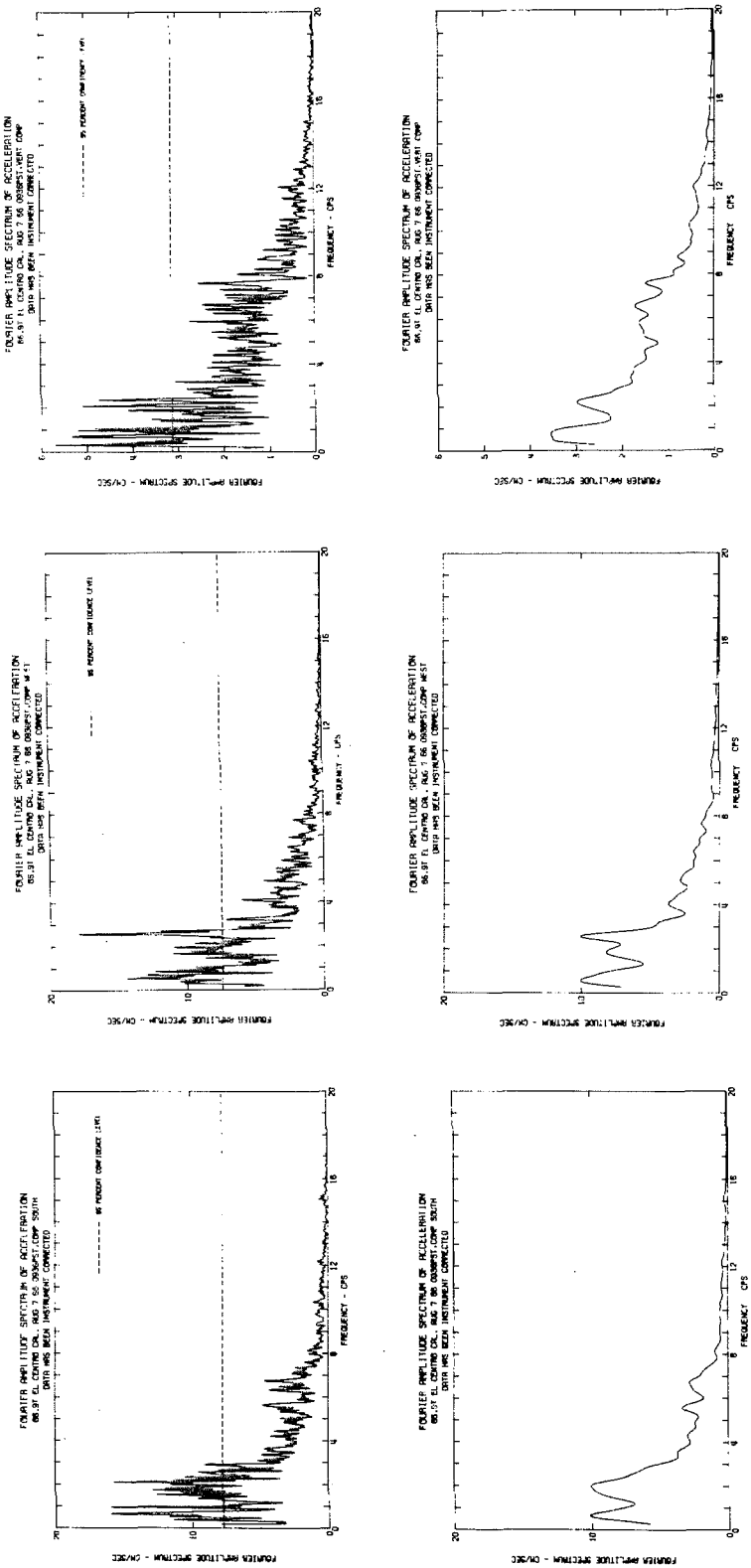

Figure FAS 14

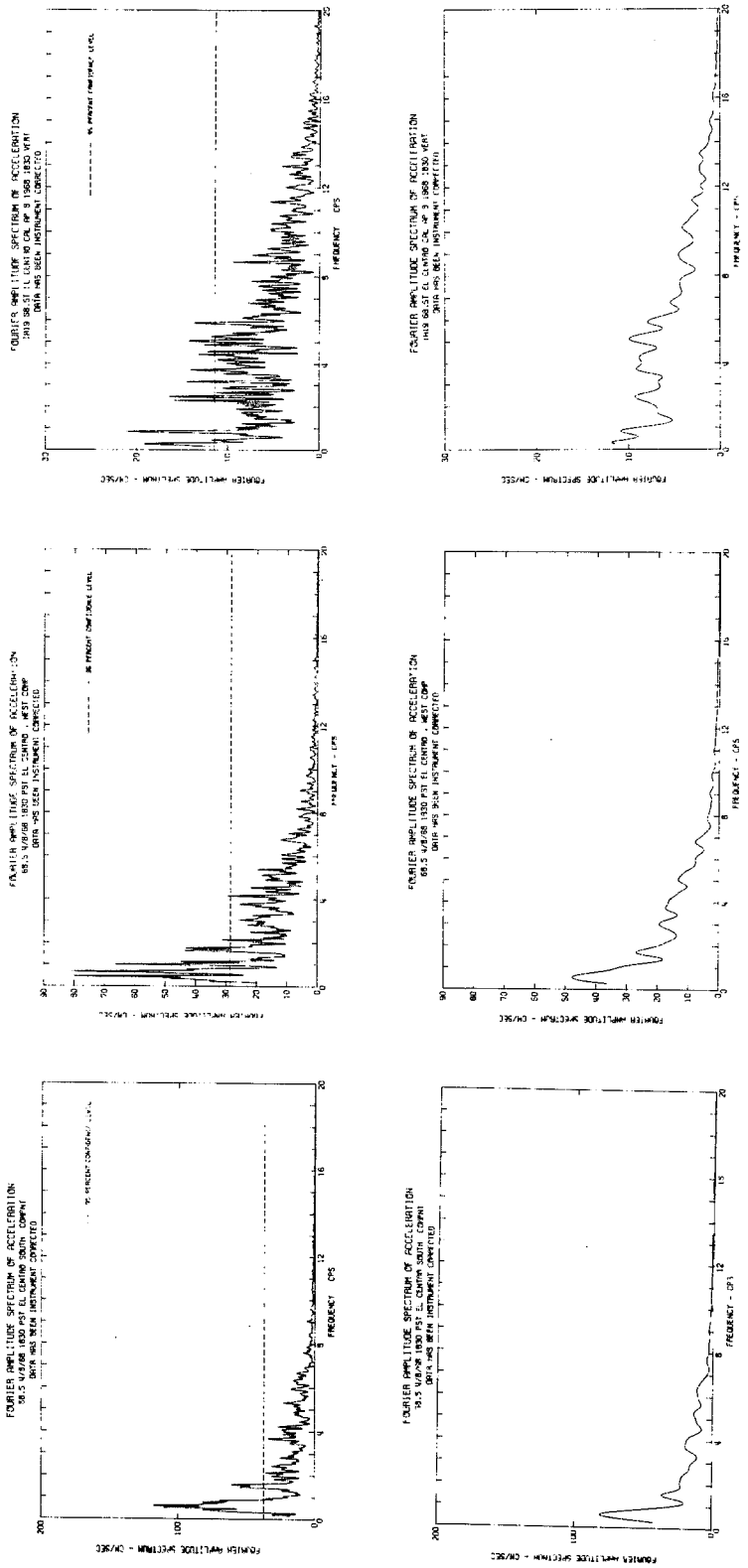

Figure FAS 15

Bibliography

1. Jennings, P. C. (Editor) (1971). San Fernando Earthquake of February 9, 1971, EERL-71-02, California Institute of Technology, Pasadena.

2. Waseda University Publication (1966). Special issue on Niigata Earthquake, Bull. of Seism. and Engg. Research Lab., Vol. 34.

3. Lee, K. L. and Monge, E. (1966). Effect of Soil Conditions on Damage in the Peru Earthquake of October 17, 1966, U. C. L. A.

4. Hudson, J. A. (1962). The Total Internal Reflection of SH Waves, Geophysical Journal, Royal Astr. Soc., 6, pp. 509.

5. Sezawa, K., and Kanai, K. (1930). Possibility of Free Oscillations of Strata Excited by Seismic Waves, Bull. Earthq. Research Inst., 8, pp. 1.

6. Herrera, I., Rosenblueth, E. and Rascón, D. A. (1965). Earthquake Spectrum Prediction, Proc. 3rd World Conference Earthq. Eng., New Zealand, Vol. I, pp. 1-61.

7. Trifunac, M. D. (1971). Response Envelope Spectrum and Interpretation of Strong Earthquake Ground Motion, Bull. Seism. Soc. of America, Vol. 61, pp. 343.

8. Gutenberg, B. (1957). Effects of Ground on Earthquake Motion, Bull. Seis. Soc. America, 47, pp. 221.

9. Byerly, P. (1940). The Periods of Local Earthquake Waves in Central California, Bull. of Seis. Soc. America, 30, pp. 129.

10. Wiggins, J. H. (1964). Effects of Site Conditions on Earthquake Intensity, J. Structural Div., A. S. C. E., ST2, pp. 279.

11. Kanai, K. (1957). The Requisite Conditions for Predominant Vibration of Ground, Bull. Earthq. Research Inst., 35, p. 457.

12. Kanai, K. Osada, K. and Yoshizawa, S. (1964). Observational Studies of Earthquake Motions in the Depth of the Ground, Part IV, Bull. Earthq. Research Inst., 33, pp. 363.

13. Kanai, K. and Tanaka, T. (1952). Relation Between Earthquake Damage and Nature of Ground, Bull. Earthq. Research Inst., 30, pp 57.

14. Herrera, I. and Rosenblueth, E. (1965). Response Spectra in Stratified Soil, Proc. 3rd World Conference Earthq. Eng. Vol. I, pp. I-41.

15. Idriss, I. M. and Seed, H. B. (1967). Response of Horizontal Soil Layers During Earthquakes, Soil Mech. and Bit. Matr. Research Lab., Univ. of Calif., Berkeley.

16. Tsai, N. C. (1969). Influence of Local Geology on Earthquake Ground Motion, Ph. D. Thesis, California Institute of Technology, Pasadena.

17. Brune, J. (1970). Tectonic Stress and the Spectra of Seismic Shear Waves from Earthquakes, Jour. Geophysical Research, Vol. 75, pp. 4997.

18. Aki, K. (1967). Scaling Law of Seismic Spectrums, Jour. Geophysical Research, Vol. 72, pp. 1217.

19. Haskell, N.A. (1969). Elastic Displacements in the Near Field of a Propagating Fault, Bull. Seism. Soc. America, 59, pp. 865.

20. Kanai, K., Relation Between the Nature of Surface Layer and the Amplitude of Earthquake Motions, Bull. Earthq. Research Inst., 30, pp. 31.

21. Haskell, N.A. (1962). Crustal Reflection of Plane P and SV Waves, Jour. Geophysical Research, Vol. 67, pp. 4751.

22. Gupta, R.N. (1966). Reflection of Plane Elastic Waves from Transition Layers with Arbitrary Variation of Velocity and Density, Bull. Seism. Soc. America, 56, pp. 633.

23. Isikawa, T. (1928). Journal Meteor. Soc., Japan, [ii] 6, No. 3.

24. Suzuki, T. (1932). On the Angle of Incidence of the Initial Motion Observed at Hongo and Mitaki, Bull. Earthq. Research Inst., 10, pp. 517.

25. Aki, K. and Larner, K. (1970). Surface Motions of a Layered Medium Having an Irregular Interface Due to Incident Plane SH Waves, Jour. Geophysical Research, Vol. 75, pp. 933.

26. Trifunac, M. D. (1971). Surface Motions of a Semicylindrical Alluvial Valley for Incident Plane SH Waves, Bull. Seismo. Soc. America, 61, pp. 1755.

27. Abubakar, I. (1962). Reflection and Refraction of Plane SH Waves at Irregular Interfaces I, II, Journ. Phys. Earth, 10, pp. 1-14 and 15-20.

28. Sato, R. (1963). Diffraction of SH Waves at an Obtuse Angled Corner, Journ. Phys. Earth, 11, pp. 1.

29. Alsop, L. (1966). Transmission and Reflection of Love Waves at a Vertical Discontinuity, Jour. Geophysical Research, Vol. 71, pp. 3969.

30. Trifunac, M. D. (in press). Scattering of Plane SH Waves by a Semicylindrical Canyon.

31. Boore, D. (1972). A Note on the Effect of Topography on Seismic Waves, Bull. Seism. Soc. of America, Vol. 62, pp. 275.

32. Biehler, S. (1964). Geophysical Study of the Salton Trough of Southern California, Ph. D. Thesis, California Institute of Technology, Pasadena.

33. Caltech Seismological Laboratory (Personal communication).

34. U.S. C. G.S. publications (1934 - 1967). United States Earthquakes.

35. Trifunac, M. D. (1969). Investigation of Strong Earthquake Ground Shaking, Ph. D. Thesis, California Institute of Technology, Pasadena.

36. Richter, C. F., Elementary Seismology, W. H. Freeman.

37. Crowell, J. C. (1962). Displacement Along the San Andreas Fault, California, Geol. Soc. America, Spec. Paper 71.

38. Hudson, D. E., Brady, A. and Trifunac, M. (1969). Strong Motion Earthquake Accelerograms, Digitized and Plotted Data, Vol. I, EERL 69-20, California Institute of Technology, Pasadena.

39. Trifunac, M. D. (1970). Low Frequency Digitization Errors and a New Method for Base-Line Correction of Strong Motion Accelerograms, EERL 70-07, California Institute of Technology, Pasadena.

40. Trifunac, M. D., Udwadia, F. E. and Brady, A. G. (1971). High Frequency Errors and Instrument Correction of Strong Motion Accelerograms, EERL 71-05, California Institute of Technology, Pasadena.

41.a Cooley, J. W. and Tukey, J. W. (1965). An Algorithm for the Machine Calculation of Complex Fourier Series, Math. of Comput., Vol. 19, pp. 297.

41.b Cochran, W. et al. (1967). What is the Fast Fourier Transform?, Proc. IEEE, Vol. 55, pp. 1664.

42. Trifunac, M. and Udwadia, F. (1972). Analysis of Strong Motion Earthquake Accelerograms, EERL 71-100 (in press), California Institute of Technology, Pasadena.

43. Blackman, R. B. and Tukey, J. W. (1958). The Measurement of Power Spectra, Dover, N. Y.

44. Nowroozi, A. A. (1965). Eigenvibrations of the Earth After the Alaskan Earthquake, J. Jeophys. Res., 70, pp. 5145.

45. Fisher, R. A. (1929). Test of Significance in Harmonic Analysis, Proc. R. Soc. A., 125, pp. 54.

46. Kanai, K., and Tanaka, T. (1961). On Microtremors VIII, Bull. Earthq. Research Inst., Vol. 39, pp. 97.

47. Tanaka, T. (1961). Some Equipment Used in Microtremor Measurement, Bull. Earthq. Research Inst., Vol. 40, pp. 533.

48. Kanai, K. (1962). On the Spectrum of Strong Earthquake Motions, Primeras Jornadas Argentinas De Ingenieria Antisismica, XXIV-1.

49. Allam, A. (1970). An Investigation into the Nature of Microtremors, Bull. Int. Inst. Seism. and Earthq. Eng., Vol. 7, pp. 1.

50. Kanai, K., (1960). Results of Microtremor Measurements in United States in 1960.

51. Wilson, C. D. V. (1953). The Origin and Nature of Microseisms in the Frequency Range 4 to 100 cps. Proc. Roy. Soc. A., 217, pp. 176.

52. Aki, K. (1957). Space and Time Spectra of Stationary Stochastic Waves, with Special Reference to Microtremors. Bull. Earthq. Research Inst., Vol. 35, pp. 415.

53. Akamatsu, K. (1961), On Microseisms in the Frequency Range from 1 cps to 200 cps, Bull. Earthq. Research Inst., Vol. 39, pp. 23.

54. Douze, E. J., (1964). Signal and Noise in Deep Wells, Geophysics, Vol. 29, pp. 721.

55. Allam, A. (1969). An Investigation into the Nature of Microtremors, Ph. D. Thesis, Tokyo University.

56. Matthiesen, R. B. (1964). Site Characteristics of Southern California Strong Motion Earthquake Stations, Report of the Department of Eng., Part II, U. C. L. A.

57. McLennan, G. A, (1969). An Exact Correction for Accelerometer Analysis Including Dynamic Instrumental Correction, Bull. Seism. Soc. Amer., 54, pp. 2087.

58. Tazime, K. (1956). Applicability of the Quarter Wave Length Law, Rep. Res. Inst. Mining Col., Akita Univ., 15, pp. 18.

59. Berg, G. V. and Housner, G. W. (1961). Integrated Velcotiy and Displacement of Strong Earthquake Ground Motion, Bull. Seis. Soc. Amer., 51, pp. 175.